SKB

TECHNICAL REPORT

92-41

Buoyancy flow in fractured rock with a salt gradient in the groundwater. A second study of coupled salt and thermal buoyancy

Johan Claesson, Göran Hellström, Thomas Probert

Depts. of Building Physics and Mathematical Physics,
Lund University, Sweden

November 1992

SVENSK KÄRNBRÄNSLEHANTERING AB

SWEDISH NUCLEAR FUEL AND WASTE MANAGEMENT CO

BOX 5864 S-102 48 STOCKHOLM

TEL 08-665 28 00 TELEX 13108 SKB S
TELEFAX 08-661 57 19

BUOYANCY FLOW IN FRACTURED ROCK WITH A SALT GRADIENT IN THE GROUNDWATER
A SECOND STUDY OF COUPLED SALT AND THERMAL BUOYANCY

Johan Claesson, Göran Hellström, Thomas Probert

Depts. of Building Physics and Mathematical Physics, Lund University, Sweden

November 1992

Information on SKB technical reports from 1977-1978 (TR 121), 1979 (TR 79-28), 1980 (TR 80-26), 1981 (TR 81-17), 1982 (TR 82-28), 1983 (TR 83-77), 1984 (TR 85-01), 1985 (TR 85-20), 1986 (TR 86-31), 1987 (TR 87-33), 1988 (TR 88-32), 1989 (TR 89-40), 1990 (TR 90-46) and 1991 (TR 91-64) is available through SKB.

BUOYANCY FLOW IN FRACTURED ROCK WITH A SALT GRADIENT IN THE GROUNDWATER

A second study of coupled salt and thermal buoyancy

JOHAN CLAESSON
GÖRAN HELLSTRÖM
THOMAS PROBERT

November 1992

Study for Swedish Nuclear Fuel and Waste Management Co.

Depts. of Building Physics and Mathematical Physics
Lund University, Sweden

Keywords: Nuclear waste repository, very deep boreholes, groundwater flow, coupled thermal and salt buoyancy, buoyancy barrier, analytical formulas for largest upward flow.

Abstract (English)

An underground nuclear waste repository produces heat that will induce a buoyancy flow of groundwater in fractures and other permeable regions in the surrounding rock. The radioactive material may then, in case of penetrated canisters, possibly reach the biosphere. Measurements of ground water in crystalline rock show an increasing salt content with depth. The resulting increase of water density counteracts the thermal buoyancy, and it may create a natural barrier for the groundwater flow between the repository and the biosphere.

The aim of the study is to analyse this barrier effect and to assess the maximum upward displacement of water starting from the vicinity of the repository. The coupled flow process for groundwater, salt and heat with buoyancy due to temperature and salt concentration differences is studied. The equations have been analysed in great detail, and a numerical model has been developed for the case of groundwater flow in a fracture plane.

The largest upward displacement from the repository has been determined with the model for any heat release. Approximate formulas, which are shown to be sufficiently accurate for assessments, have been derived. The main formula concerns the case, when the canisters are stacked on top of each other in a very deep borehole. There are no restrictions on the position of the fracture plane. The borehole may even lie directly in the fracture plane.

We find a strong barrier effect. In a reference case with a salt concentration increase of 2% per km downwards and with 300 canisters placed over a length of 2000 m in the borehole (the total amount of released heat is 0.32 TWh), the largest upward displacement from the top of canisters becomes, according to the formula, 60 m. The case, when the fractured rock is considered as a homogeneous porous medium, is also dealt with. The groundwater flow is then three-dimensional. The largest upward displacement now becomes 67 m for the reference case.

The main formula shows that the barrier effect is remarkably insensitive to variations of the involved parameters. A change of salt gradient, or total amount of released heat, by a factor 10 causes a change by $\sqrt{10} = 3.2$ of the upward displacement.

The parameters that do *not* enter into the formulas are noteworthy. The hydraulic conductivity of the flow plane, which is the most uncertain of all parameters, does not matter in the balance between thermal buoyancy and counteracting salt buoyancy.

Abstract (Swedish)

Ett djupförvar för använt kärnbränsle avger värme, vilket genom påverkan av vattnets densitet ger upphov till egenkonvektion i grundvattnet i sprickor och andra permeabla områden i omgivande berg. De radioaktiva ämnena kan då, vid läckage från defekta kapslar, möjligen nå biosfären. Mätningar i kristallint berg visar att grundvattnets salthalt ökar med djupet. Den resulterande ökningen av vattnets densitet motverkar densitetsminskningen p.g.a. ökande temperatur, och kan därigenom skapa en naturlig barriär för grundvattenflödet mellan djupförvaret och biosfären.

Avsikten med denna studie är att analysera barriäreffekten och att ange den maximala uppåtriktade förflyttningen för vatten som startar från djupförvarets närområde. Den kopplade flödesprocessen för grundvatten, salt och värme med egenkonvektion p.g.a. skillnader i temperatur och salthalt studeras. De styrande ekvationerna har detaljgranskats, och en numerisk modell har utvecklats för fallet med grundvattenflöde i ett sprickplan.

Den största uppåtriktade förflyttningen från ett djupförvar har bestämts med modellen för olika stor värmeutveckling. Approximativa formler, vilka visas vara tillräckligt noggranna för goda uppskattningar, har härletts. Huvudformeln avser fallet då kapslarna har placerats ovanpå varandra i ett borrhål med stort djup. Det finns inga restriktioner vad avser sprickplanets läge. Borrhålet kan således ligga direkt i sprickplanet.

Vi finner en stark barriäreffekt. För referensfallet med en salthaltsökning av 2% per km nedåt och med 300 kapslar placerade över längd av 2000 m i borrhålet (totalt avgiven värmemängd är 0.32 TWh), blir den största uppåtgående förflyttningen från den högst belägna kapseln 60 m enligt formeln. Fallet då det sprickiga berget behandlas som ett homogent poröst medium har också studerats. Grundvattenflödet är då tredimensionellt. Den största uppåtgående förflyttningen blir nu 67 m för referensfallet.

Huvudformlerna visar att barriäreffekten är anmärkingsvärt okänslig för variationer av de ingående parametrarna. En ändring av salthaltsgradienten, eller totalt avgiven värmemängd, med en faktor 10 medför en ändring på $\sqrt{10} = 3.2$ i uppåtgående förflyttning.

Det är även värt att notera att några viktiga parametrar *inte* ingår i formlerna. Den hydrauliska konduktiviteten i sprickplanet, vilken är den mest osäkra av alla parametrar, är betydelselös för balansen mellan termiskt inducerad konvektion och motverkande saltinducerad egenkonvektion.

Foreword

This study is made for the Swedish Nuclear Fuel and Waste Management Co (SKB). The particular cases to study and data for the heat release of the canisters have been determined in discussions with experts from SKB.

Johan Claesson

Dept. of Building Physics, Lund University, Sweden

Contents

Summary of first and second study

Nuclear waste, encapsulated in canisters in rock, produces heat that will induce a buoyancy flow of groundwater in fractures and other permeable regions in the surrounding rock. The radioactive material may then, in case of penetrated canisters, possibly reach the biosphere. Measurements of groundwater in crystalline rock show an increasing salt content with depth. The resulting increase in water density counteracts the thermal buoyancy, and it may create a natural barrier for the groundwater flow between the repository and the biosphere.

The aim of the study is to analyse this barrier effect and to assess the extent of upward displacement of wtaer starting from the vicinity of the repository. The coupled flow process for groundwater, salt and heat with buoyancy due to temperature and salt concentration differences is studied. The equations have been analysed in great detail, and a numerical model has been developed for the case of groundwater flow in a fracture or crack plane.

The largest upward displacement from the repository has been determined with the model for any heat release. Approximate formulas, which are shown to be sufficiently accurate for assessments, have been derived.

The main formula concerns the case, when the canisters are stacked on top of each other in a very deep borehole over a length H_o. The total amount of released heat is E_o (J), and the main decay time for the heat release is t_d. There are no restrictions on the position of the fracture plane. The borehole may even lie directly in the fracture plane. An assessment of the largest upward displacement, at any time, from the top of the canisters is:

$$z|_{\text{max upward}} \leq 0.31 \cdot \sqrt{\frac{\tilde{\alpha} E_o}{H_o \sqrt{4 a t_d}}} \qquad \tilde{\alpha} = \frac{\alpha_T}{\alpha_c c_z^o C} \tag{0.1}$$

Here, a is the thermal diffusivity and C the volumetric heat capacity of the rock. The buoyancy parameter $\tilde{\alpha}$ contains the salt gradient c_z^o and the relative density change of groundwater with temperature, α_T, and of salt concentration, α_c.

There is a strong barrier effect. In a reference case with a salt concentration increase of 2% per km downwards and with 300 canisters placed in the borehole ($E_o = 0.32$ TWh, $H_o = 2000$ m, $t_d = 46$ years), the largest upward displacement from the top of canisters becomes, according to the formula, 60 m.

The case, when the fractured rock is considered as a homogeneous porous medium, is also dealt with. The groundwater flow is then three-dimensional. The main formula for the largest upward displacement is:

$$z|_{\text{max upward}} \leq \sqrt[3]{\frac{\tilde{\alpha} E_o}{4\pi H_o}} \tag{0.2}$$

The reference case gives 67 m. The formula does not take into account the exponential decay of the heat release. A smaller value is obtained, if the more complicated formula for exponentially decreasing heat release were used.

There are two main limitations in the study this far. The fracture plane is assumed to have infinite extension in all directions. The second limitation concerns the water-filled pore volume of around 0.5% in the rock outside the fracture plane. The salt in the water-filled pores is initially in equilibrium with the downwards increasing salt concentration in

the fracture plane. The upward flow results in a difference in salt concentration between the fracture and the pores, which causes salt to diffuse from the fracture plane. This diffusion reduces the salt concentration in the region of upward flow in the fracture and will therefore diminish the barrier effect.

The main formula (0.1) shows that the barrier effect is remarkably insensitive to variations of the involved parameters. A change of salt gradient c_z^o (or E_o, α_T, $\sqrt{t_d}$ and so on) by a factor 10 causes a change by $\sqrt{10} = 3.2$ of the upward displacement.

The parameters that do *not* enter into the formulas are noteworthy. The hydraulic conductivity of the flow plane, which is the most uncertain of all parameters, does not matter in the balance between thermal buoyancy and counteracting salt buoyancy. The position of the fracture plane, which is the other main uncertainty, is arbitrary. The formulas are valid as an upper estimate for radioactive migration at any time. The influence between the boreholes of the repository is shown to be negligible for the design spacing of 500 m.

Chapter 1

Introduction

This study is a direct sequel of the first report [1], which should be read before this one. The same notations are used. The problem and, in particular, the different approximations of [1] are not restated in detail here.

The heat released from the canisters buried deep down in the rock induce an upward thermal buoyancy flow of groundwater in cracks and fissure zones. By assumption there is an increasing salt concentration and, hence, an increasing water density downwards. This will counteract the thermal buoyancy. The aim of [1] and this study is to analyse and quantify the potential barrier effect from the salt gradient. We have, in particular, endeavored to obtain simple formulas to *assess* the largest upward movement of groundwater from the repository region.

Figure 1.1 shows the studied SKB concept for final storage of nuclear waste. A number of very deep boreholes are to be used. The canisters are put in the boreholes over a vertical extension of some 2000 m starting at a depth of some 4000 m. The thermal process is driven by line heat sources from the canisters in the boreholes. The effect of the ground surface may here be neglected. The line sources may be considered to lie in an infinite surrounding rock region.

The first study [1] deals with the simplified case, when the heat is released at a single point. The exponential decrease of heat release is also neglected. All heat E_o is released at the initial time. (This is a worst case.) The groundwater flow was assumed to take place in a fracture plane ($y = 0$) at a distance y_o from the point heat source.

The time-scale of the groundwater flow due to differences in salt concentration is shown in Section 3.6 of [1] to be much smaller than the time-scale of the three-dimensional thermal process. Because of this, the temperature field is considered at a time t_o. This time-independent temperature field $T(x, 0, z, t_o)$ in the groundwater flow plane $y = 0$ causes a thermal buoyancy flow $\vec{v}_T(x, z)$, which is calculated analytically. The time-dependent buoyancy flow due to salt concentration differences is calculated by a numerical model. The formulas for the upward movement are obtained from an approximate balance between the upward thermal buoyancy and the downward force from water with a higher salt density.

The temperature and the strength of the thermal buoyancy will increase with t_o during a first period. Then it will decrease due to decreasing heat release and heat flow away from the warm fracture region. The upward displacement attains a maximum for a certain t_o. The formulas for largest upward displacement refer to this maximum. We do not solve the real problem with a slowly changing temperature field and a nearly steady-state salt concentration field, which changes slowly with the temperature field. Instead, we consider the much simpler problem of a time-independent temperature field and the salt flow process starting with the undisturbed salt concentration ($c = c_o(z)$). This means that we consider a worse case, in which the 'strongest' temperature field is used at all times.

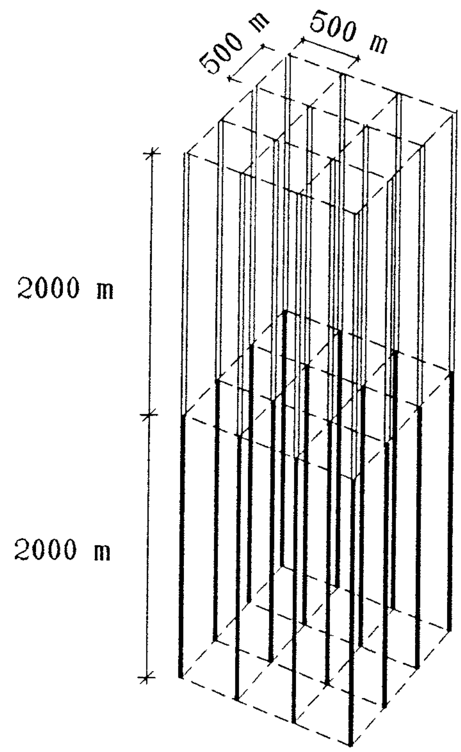

Figure 1.1. Repository using very deep boreholes. The canisters lie along the lower part of the holes.

In this second study, the case of a line heat source with all heat released at $t = 0$ is first considered in Chapter 2. This worst case is studied numerically in Chapter 3. The previous computer model for the point heat source is modified for the case of a line heat source. The case when the heat release rate decreases exponentially is studied in Chapter 4. Only the approximate formulas for the largest upward movement are dealt with.

An important assumption in the studies is that the groundwater flow is confined to the two-dimensional case of a fracture plane. Another extreme case is to consider the fractured rock as a homogeneous porous medium. The groundwater flow becomes three-dimensional. This case is dealt with in Chapter 5. This three-dimensional case without any salt effects has previously been studied by Hodgkinson [3] and Robinson [4]. The problem is then that there is no limit on the upward displacement.

A survey of formulas for the largest upward displacement and the application to the SKB concept are presented in Chapter 6. A reader who is mostly interested in the results and their application should read this chapter first.

This study and the first one contain quite a lot of material, and many different tools of analysis are used. Therefore, there is a rather detailed survey of the line of thought and the main results in the last chapter 7. The reader is advised to read this chapter first.

Chapter 2

Line heat source

The first study [1] considered the simplified case with the heat source concentrated to a single point $(0, y_o, 0)$. In the SKB concept considered here, the canisters are to be deposited in deep boreholes. They are put on top of each other over a length H_o along the borehole. See Figure 1.1.

The heat release from the canisters decreases exponentially with time. This was neglected in the first study [1], where all heat E_o (J) was released at $t = 0$. We will in this chapter consider this simplified case for the single finite line source, while the more complicated case of exponentially decreasing heat release is dealt with in Chapter 4.

We have a *line heat source* with the instantaneous heat release E_o/H_o (J/m) at $t = 0$:

$$E_o/H_o \quad \text{(J/m) released along} \quad (0, y_o, z), \quad 0 > z > -H_o, \quad \text{at} \quad t = 0 \tag{2.1}$$

The ground surface lies far (2000 m) above the top $(0, y_o, 0)$ of the line source, so we can consider the ground around the heat source as infinite in all directions.

The case of more than one line source, i.e. a repository consisting of several boreholes as in Figure 1.1, will also be considered.

2.1 Temperature field

The excess temperature above the undisturbed ground temperature $T_o(z)$ is denoted $T''(x, y, z, t)$. It is obtained from the point heat source, formula (4.4) in [1] on page 22, by integration along the line heat source:

$$T''(x,y,z,t) = \int_0^{H_o} \frac{E_o/H_o}{C\,(4\pi a t)^{3/2}} \cdot e^{-\left[x^2+(y-y_o)^2+(z+\zeta)^2\right]/(4at)} \cdot d\zeta \tag{2.2}$$

With the substitution $\zeta + z = s \cdot \sqrt{4at}$, we get

$$T''(x,y,z,t) = \frac{E_o}{C H_o 8\pi a t} \cdot e^{-\left[x^2+(y-y_o)^2\right]/(4at)} \cdot \left[\mathrm{erfc}\left(\frac{z}{\sqrt{4at}}\right) - \mathrm{erfc}\left(\frac{z+H_o}{\sqrt{4at}}\right)\right] \tag{2.3}$$

Here $\mathrm{erfc}(z')$ denotes the complementary error function:

$$\mathrm{erfc}(z') = \frac{2}{\sqrt{\pi}} \int_{z'}^{\infty} e^{-s^2}\, ds \tag{2.4}$$

The vertical extension of the line source, H_o, is typically 2000 m, while we are interested in the process in a region of some hundreds of meters around the top of the line source. It is then a good approximation to consider the line source as *semi-infinite*: $H_o = \infty$. (The heat release per meter, E_o/H_o, is kept constant.) The temperature field is then:

$$T''(x,y,z,t) = \frac{E_o}{CH_o 8\pi a t} \cdot e^{-[x^2+(y-y_o)^2]/(4at)} \cdot \operatorname{erfc}\left(\frac{z}{\sqrt{4at}}\right) \tag{2.5}$$

This corresponds to an instantaneous line heat source along $(0, y_o, z)$, $0 > z > -\infty$.

The finite line heat source along $(0, y_o, z)$, $0 > z > -H_o$, is obtained by superposition of two semi-infinite line sources:

$$\begin{aligned} &+E_o/H_o \quad \text{along} \quad (0, y_o, z) \quad 0 > z > -\infty \\ &-E_o/H_o \quad \text{along} \quad (0, y_o, z) \quad -H_o > z > -\infty \end{aligned} \tag{2.6}$$

This type of superposition is also valid for the ensuing groundwater flow field. Therefore, we can focus our attention on the case of a semi-infinite line source.

The groundwater flow in the fracture plane $y = 0$ is driven by the temperature field $T''(x, 0, z, t)$. As in [1], we consider this temperature field at any fixed time t_o:

$$T''(x,0,z,t_o) = \frac{E_o}{CH_o 8\pi a t_o} e^{-y_o^2/(4at_o)} \cdot e^{-x^2/(4at_o)} \cdot \operatorname{erfc}\left(\frac{z}{\sqrt{4at_o}}\right) \tag{2.7}$$

We use the same *dimensionless* formulation as in [1]. We have (see Sections 6.1 and 2.6 in [1]):

$$x' = \frac{x}{L_1} \qquad z' = \frac{z}{L_1} \qquad L_1 = \sqrt{4at_o} \tag{2.8}$$

$$T'(x', z') = \frac{1}{T_1} T''(x, 0, z, t_o) \qquad T_1 = \frac{L_1 \alpha_c c_z^o}{\alpha_T} \tag{2.9}$$

This gives:

$$T'(x', z') = A_1 \cdot e^{-(x')^2} \cdot \frac{\sqrt{\pi}}{2} \operatorname{erfc}(z') \tag{2.10}$$

The *dimensionless temperature amplitude* A_1 is given by

$$A_1 = \frac{\alpha_T E_o}{\pi\sqrt{\pi}\alpha_c c_z^o C H_o} \cdot \frac{1}{(4at_o)^{3/2}} e^{-y_o^2/(4at_o)} \tag{2.11}$$

We have, as an important first result of the analysis, that the dimensionless temperature field is determined by a *single* parameter A_1 (as in [1]). The dimensionless temperature amplitude A_o for the corresponding point source of [1], Eq. (1:6.5), is related to A_1 by:

$$A_1 = A_o \cdot \frac{\sqrt{4at_o}}{H_o} \tag{2.12}$$

The temperature field $T'(x',z')$, (2.10), has a rather simple structure. Below the top, z' less than, say, -2, it behaves as $A_1\sqrt{\pi}\cdot\exp\left[-(x')^2\right]$, and it decreases strongly as $\mathrm{erfc}(z')$ for positive z'. In the calculation of the groundwater flow we need the derivative of T' with respect to z'. We get from (2.10) and (2.4) the remarkably simple expression:

$$\frac{\partial T'}{\partial z'} = -A_1 e^{-(x')^2-(z')^2} \tag{2.13}$$

For the *finite* line source along $0 > z > -H_o$ we have with the superposition (2.6):

$$T(x',z') = A_1 \cdot e^{-(x')^2} \cdot \frac{\sqrt{\pi}}{2}\left[\mathrm{erfc}(z') - \mathrm{erfc}\left(z' + H_o'\right)\right] \tag{2.14}$$

where H_o' is the dimensionless length of the line source:

$$H_o' = \frac{H_o}{L_1} = \frac{H_o}{\sqrt{4at_o}} \tag{2.15}$$

The derivative with respect to z' becomes:

$$\frac{\partial T'}{\partial z'} = A_1 \cdot \left[e^{-(x')^2-(z')^2} - e^{-(x')^2-(z'+H_o')^2}\right] \tag{2.16}$$

2.2 Temperature-induced groundwater flow

The groundwater flow, which by assumption is confined to the plane $y = 0$, is driven by the buoyancy force of the water density $\rho(T,c)$, with one component $\vec{v}_T$ from the temperature and another component $\vec{v}_c$ from the salt concentration.

The dimensionless, temperature-induced groundwater flow $\vec{v}_T'$ is according to section 2.6 in [1] given by:

$$\vec{v}_T = v_{f1}\cdot\vec{v}_T' \qquad v_{f1} = \frac{L_1}{t_c} = \frac{\sqrt{4at_o}}{t_c} \qquad t_c = \frac{V_p^c \mu_{wo}}{k^c g \rho_{wo} \alpha_c c_z^o} \tag{2.17}$$

The dimensionless flow is determined by (1:3.40):

$$(\nabla')^2 P_T' - \frac{\partial T'}{\partial z'} = 0 \tag{2.18}$$

$$\vec{v}_T' = -\nabla' P_T' + T'\hat{z} \tag{2.19}$$

The source term $\partial T'/\partial z'$ in the Poisson equation for the dimensionless pressure P_T' is given by (2.13).

We will in the remaining part of this chapter, until Eq. (2.61), and in the whole next chapter consider the dimensionless problem only. Therefore, we *drop* the cumbersome prime ($'$) for all dimensionless variables.

2.2.1 Calculation of flow field

The dimensionless problem for the pressure P'_T or, dropping the prime, P_T is from (2.18) and (2.13):

$$\nabla^2 P_T + A_1 e^{-x^2-z^2} = 0 \tag{2.20}$$

The dimensionless velocity $\vec{v}'_T = \vec{v}_T$ is from (2.19) and (2.10):

$$\vec{v}_T = -\nabla P_T + A_1 e^{-x^2} \frac{\sqrt{\pi}}{2} \mathrm{erfc}(z)\hat{z} \tag{2.21}$$

The source term of (2.20), and hence the pressure P_T, depends on the radial distance only. This gives:

$$P_T = P_T(r) \qquad r = \sqrt{x^2 + z^2} \tag{2.22}$$

$$\frac{1}{r}\frac{d}{dr}\left(r\frac{dP_T}{dr}\right) + A_1 e^{-r^2} = 0 \tag{2.23}$$

The solution is straightforward:

$$\frac{d}{dr}\left(r\frac{dP_T}{dr} - \frac{A_1}{2}e^{-r^2}\right) = 0 \tag{2.24}$$

$$\frac{dP_T}{dr} = \frac{A_1}{2r}e^{-r^2} + \frac{B_1}{r} \tag{2.25}$$

The integration constant B_1 is determined by the condition that the flow from $r = 0$ vanishes:

$$\lim_{r\to 0} 2\pi r \frac{dP_T}{dr} = 0 \qquad \Rightarrow \qquad \frac{A_1}{2} + B_1 = 0 \tag{2.26}$$

The pressure becomes:

$$P_T(r) = B_2 - \frac{A_1}{2}\ln(r) - \frac{A_1}{4}\int_{r^2}^{\infty} \frac{1}{s}e^{-s} ds \tag{2.27}$$

Here, B_2 is an integration constant. The integral in the third term to the right is the so-called exponential integral $E_1(r^2)$. See [2A]. It behaves as $-\gamma - \ln(r^2)$, $\gamma = 0.5772$, for small r. This means that the pressure $P_T(r)$ is finite at $r = 0$.

The gradient of the pressure P_T becomes:

$$-\nabla P_T = -\frac{dP_T}{dr}\nabla(r) = \frac{A_1}{2} \cdot \frac{1 - e^{-r^2}}{r} \cdot \hat{r} \qquad \hat{r} = \frac{x}{r}\hat{x} + \frac{z}{r}\hat{z} \tag{2.28}$$

This gives with (2.21) the dimensionless velocity:

$$\vec{v}_T = \frac{A_1}{2}\left[\frac{1 - e^{-r^2}}{r}\hat{r} + \sqrt{\pi}e^{-x^2} \cdot \mathrm{erfc}(z)\hat{z}\right] \tag{2.29}$$

2.2.2 Stream function and character of flow field

The temperature-induced, dimensionless groundwater flow field is given by (2.29) for the *semi-infinite* line source. We will in this section discuss this field and the field from the finite line source.

The velocity field $\vec{v}_T$ is of the same character for all parameter values, since it is directly proportional to A_1. We have

$$\vec{v}_T^1 = \frac{2}{A_1} \cdot \vec{v}_T = \frac{1 - e^{-r^2}}{r} \hat{r} + \sqrt{\pi} e^{-x^2} \cdot \mathrm{erfc}(z) \hat{z} \tag{2.30}$$

The two components are:

$$v_{Tx}^1 = \frac{2}{A_1} v_{Tx} = \left(1 - e^{-x^2 - z^2}\right) \frac{x}{x^2 + z^2} \tag{2.31}$$

$$v_{Tz}^1 = \frac{2}{A_1} v_{Tz} = \left(1 - e^{-x^2 - z^2}\right) \frac{z}{x^2 + z^2} + 2e^{-x^2} \cdot \int_z^\infty e^{-s^2} ds \tag{2.32}$$

The flow field (2.30) consists of two parts. The first part is a radial, outward flow from $r = 0$, which behaves as $\hat{r}/r$ for large r:

$$\frac{1 - e^{-r^2}}{r} \cdot \hat{r} \longrightarrow \frac{1}{r} \hat{r} \qquad r \longrightarrow \infty \tag{2.33}$$

This flow is zero for $r = 0$. The second part is a vertical upward flow. For large negative z, we have

$$\sqrt{\pi} e^{-x^2} \cdot \mathrm{erfc}(z) \cdot \hat{z} \longrightarrow 2\sqrt{\pi} e^{-x^2} \cdot \hat{z} \quad z \longrightarrow -\infty \tag{2.34}$$

This is an upward flow along the negative z-axis. As this flow reaches the region near $r = 0$, around the top of the line source, it is spread out radially by the first radial part.

The flow field may be represented by a stream function $\psi(x, z)$ defined by:

$$\frac{\partial \psi}{\partial x} = v_{Tz}^1 \qquad \frac{\partial \psi}{\partial z} = -v_{Tx}^1 \tag{2.35}$$

The flow is perpendicular to the gradient of ψ, which means that the flow follows curves of constant ψ. The mathematical condition for the existence of a stream function is:

$$\frac{\partial}{\partial z} \left(\frac{\partial \psi}{\partial x} \right) = \frac{\partial}{\partial x} \left(\frac{\partial \psi}{\partial z} \right) \qquad \Leftrightarrow \qquad \frac{\partial v_{Tz}^1}{\partial z} = -\frac{\partial v_{Tx}^1}{\partial x} \tag{2.36}$$

This is automatically fulfilled since the divergence of the water flow fields is zero.

By solving (2.35), using (2.31-32), we obtain the following stream function:

$$\psi(x, z) = \int_z^\infty \frac{x}{x^2 + s^2} \left(1 - e^{-x^2 - s^2}\right) ds = \int_{z/x}^\infty \left(1 - e^{-x^2(1+t^2)}\right) \cdot \frac{dt}{1 + t^2} \tag{2.37}$$

The last expression is only valid for positive x-values. The stream function is an odd function of x. It is zero on the z-axis. The values of x lie between 0 and π for $x > 0$. The calculations to get $\psi(x, y)$ from (2.31-32) and (2.35) are somewhat lengthy, but it is quite straightforward to verify that the above expression for ψ indeed satisfies (2.35).

Figure 2.1 shows the stream function (2.37) for the semi-infinite line heat source. The curves are obtained by the numerical model used in Chapter 3. The formulas (2.31-32) are used for the moving particles, while the salt-concentration part is suppressed. (The small circle in the center indicates $(0,0)$ and the circle above represents the point $(0,1)$.)

The flow follows the curves of constant ψ, which means that the velocity $\vec{v}_T^1$ is a tangent to $\psi =$ constant. The magnitude of the velocity is from (2.35) given by the absolute value of the gradient of the stream function: $|\vec{v}_T^1| = |\nabla\psi|$. The velocity is inversely proportional to the distance between the ψ-curves. The highest velocities occur near the negative z-axis, which is the warmest region.

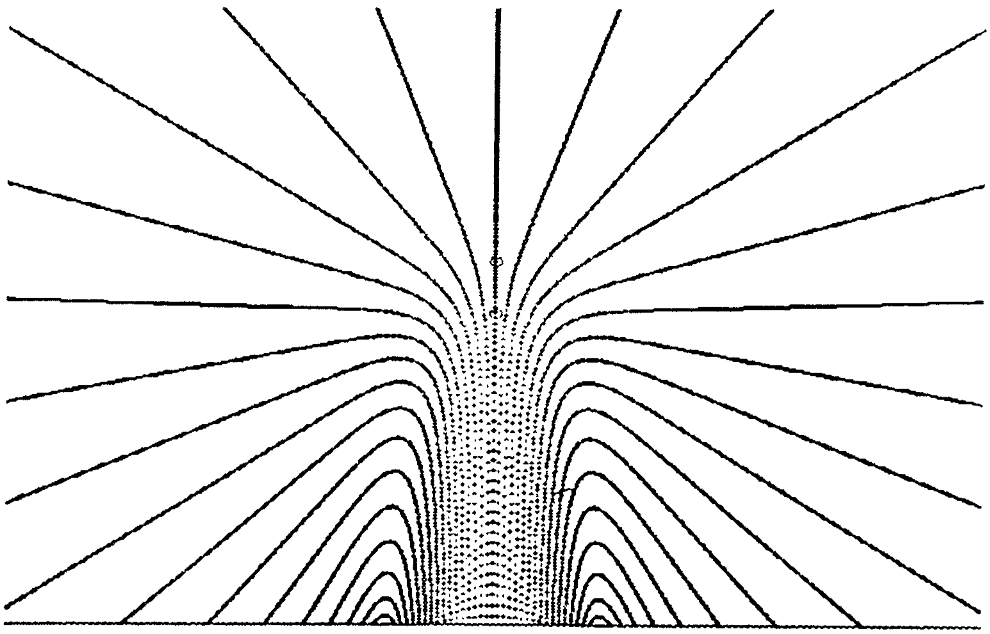

Figure 2.1. The stream function (2.37) for the semi-infinite line source.

Each curve $\psi =$ constant has two asymptotes. For $z = -\infty$, and for $x \to \infty$ with $z/x = \tan(\varphi)$, fixed we have:

$$\psi(x, -\infty) = \int_{-\infty}^{\infty} \frac{x}{x^2 + s^2}\left(1 - e^{-x^2 - s^2}\right) ds = \pi \cdot \mathrm{erf}(x)$$

$$\psi|_{\{z/x \text{ fixed }, x=\infty\}} = \int_{z/x}^{\infty} (1 - 0) \cdot \frac{dt}{1 + t^2} = \frac{\pi}{2} - \arctan\left(\frac{z}{x}\right) \qquad (x > 0) \quad (2.38)$$

Let x_- denote the asymptotic x-value for $z \to -\infty$ for a certain ψ, and φ_+ denote the angle of the radial asymptote. Then we have from the above two equations:

$$\psi = \pi \cdot \mathrm{erf}(x_-) = \frac{\pi}{2} - \varphi^+ \qquad (x > 0) \quad (2.39)$$

A few values are:

ψ	0	$\pi/4$	$\pi/2$	$3\pi/4$	π
φ_+	$\pi/2$	$\pi/4$	0	$-\pi/4$	$-\pi/2$
$\text{erfc}(x_-)$	0	1/4	1/2	3/4	1
x_-	0	0.22	0.48	0.81	∞

The above results concern the semi-infinite line heat source. The corresponding results for a *finite* line heat source are directly obtained from a superposition of the type (2.6). From the solution with the coordinates x and z, we just subtract the same solution with the coordinates x and $z+H_o'$. (Note that x and z are dimensionless, and that $H_o' = H_o/L_1$ is the dimensionless length of the line heat source.)

The dimensionless temperature-induced groundwater flow is then in accordance with (2.31-32):

$$v_{Tx} = \frac{A_1}{2} \cdot \left[\left(1 - e^{-x^2-z^2}\right) \frac{x}{x^2+z^2} - \left(1 - e^{-x^2-(z+H_o')^2}\right) \frac{x}{x^2+(z+H_o')^2} \right] \tag{2.40}$$

$$\begin{aligned} v_{Tz} = \frac{A_1}{2} \cdot \Bigg[& \left(1 - e^{-x^2-z^2}\right) \frac{z}{x^2+z^2} + \sqrt{\pi} e^{-x^2} \cdot \text{erfc}(z) - \\ & - \left(1 - e^{-x^2-(z+H_o')^2}\right) \frac{z+H_o'}{x^2+(z+H_o')^2} - \sqrt{\pi} e^{-x^2} \text{erfc}(z+H_o') \Bigg] \end{aligned} \tag{2.41}$$

The stream function for the finite line heat source has quite a simple form (compare with (2.37)):

$$\psi(x,z) = \int_z^{z+H_o'} \frac{x}{x^2+s^2} \left(1 - e^{-x^2-s^2}\right) ds = \int_{z/x}^{(z+H_o')/x} \left(1 - e^{-x^2(1+t^2)}\right) \frac{dt}{1+t^2} \tag{2.42}$$

The last integral is only valid for positive x-values.

2.2.3 Upward flow along the z'-axis

The upward displacement is analysed in section 6.4 in [1]. An analytical solution is obtained, when the pressure field P_c due to the salt is neglected, Eq. (1:6.13). The analysis in [1] is directly applicable. The only change is that the velocity field $\vec{v}_T$ for the line source, Eq. (2.29), is used instead.

Let $z_m(t', z_o)$ denote the motion along the z'-axis of a salt-water 'particle' that starts at $(0, z_o)$ at $t' = 0$. Here, z_m, z_o and t' are dimensionless quantities. Eq. (1:6.16) is valid. The dimensionless velocity along the z-axis is according to (2.32):

$$v_{Tz}(0,z) = \frac{A_1}{2} v_{Tz}^1(0,z) = \frac{A_1}{2} \left[\frac{1-e^{-z^2}}{z} + \sqrt{\pi} \cdot \text{erfc}(z) \right] \tag{2.43}$$

Eq. (1:6.16) for $z_m(t', z_o)$ becomes:

$$\frac{dz_m}{dt'} = \frac{A_1}{2} \left[\frac{1-e^{-z_m^2}}{z_m} + \sqrt{\pi} \cdot \text{erfc}(z_m) \right] - z_m + z_o \tag{2.44}$$

This equation may be integrated directly to give t' as a function of z_m. The integral (1:6.19) is here replaced by:

$$t' = \int_{z_o}^{z_m} \frac{ds}{A_1\left[\left(1-e^{-s^2}\right)/s + \sqrt{\pi}\cdot \mathrm{erfc}(s)\right]/2 - s + z_o} \tag{2.45}$$

For the finite line heat source, the velocity field (2.41) is to be used instead of (2.43). The integral (2.45) is quite easy to calculate numerically.

In our application A_1 is quite small ($A_1 \simeq 0.2$). A particle that starts at $z = z_o$ will then move upwards only a short distance. The linear approximation (2.49) for $v^1_{Tz}(0,z)$ may be used as long as $z = z_m$ is smaller than 0.75. The integral becomes then for $z_o = 0$:

$$t' \simeq \int_0^{z_m} \frac{ds}{A_1\left[\sqrt{\pi} - s\right]/2 - s} \qquad (z_o = 0,\ z_m < 0.75) \tag{2.46}$$

The solution is simple. The time t' depends on a logarithm in z_m. This means that z_m depends exponentially on time. We get:

$$z_m(t',0) = \frac{A_1\sqrt{\pi}}{2+A_1}\left(1 - e^{-(1+A_1/2)t'}\right) \quad (A_1 < 1.5) \tag{2.47}$$

This approximate solution is valid for $z_m < 3/4$, which is satisfied for all z_m when $A_1 < 1.5$.

2.2.4 Largest upward displacement

The largest upward displacement, which is of particular interest to us, is obtained for $t' = \infty$. This occurs, when the velocity $v_{Tz}(0, z_m)$ becomes equal to the counteracting weight $z_m - z_o$. See Eq. (2.44). The denominator of the integrand of (2.45) is then zero. We have in analogy with (1:6.23) for the largest dimensionless upward displacement $z'_{max}(z_o)$:

$$\frac{2}{A_1}(z_m - z_o) = \frac{1 - e^{-z_m^2}}{z_m} + \sqrt{\pi}\,\mathrm{erfc}(z_m) = v^1_{Tz}(0, z_m) \quad z_m = z'_{max}(z_o) \tag{2.48}$$

This formula concerns the semi-infinite line heat source. The equation is illustrated in Figure 2.2. The right-hand side, which gives the velocity, intersects the straight line with the slope $2/A_1$ at $z_m = z'_{max}$. The straight lines start at the initial position z_o. The two dashed lines show the approximation (2.49) and (2.50).

The velocity $v^1_{Tz}(0,z)$ is with good approximation linear for small $|z|$. We have:

$$v^1_{Tz}(0,z) \simeq \sqrt{\pi} - z \qquad |z| < 0.75 \tag{2.49}$$

The error in the given interval is less than 6%. For $|z| < 0.5$ the error is less than 2%. The approximation is shown by the dashed straight line in Figure 2.2. For large (positive) z, the following approximation is valid:

$$v^1_{Tz}(0,z) \simeq \frac{1}{z} \qquad z > 1 \tag{2.50}$$

The error for $z > 1$ is at most 9%. For $z > 1.5$ the error is below 2%. The approximation lies above the velocity $v^1_{Tz}(0,z)$ for all z. See Figure 2.2. It may therefore be used as a conservative approximation for all positive z-values.

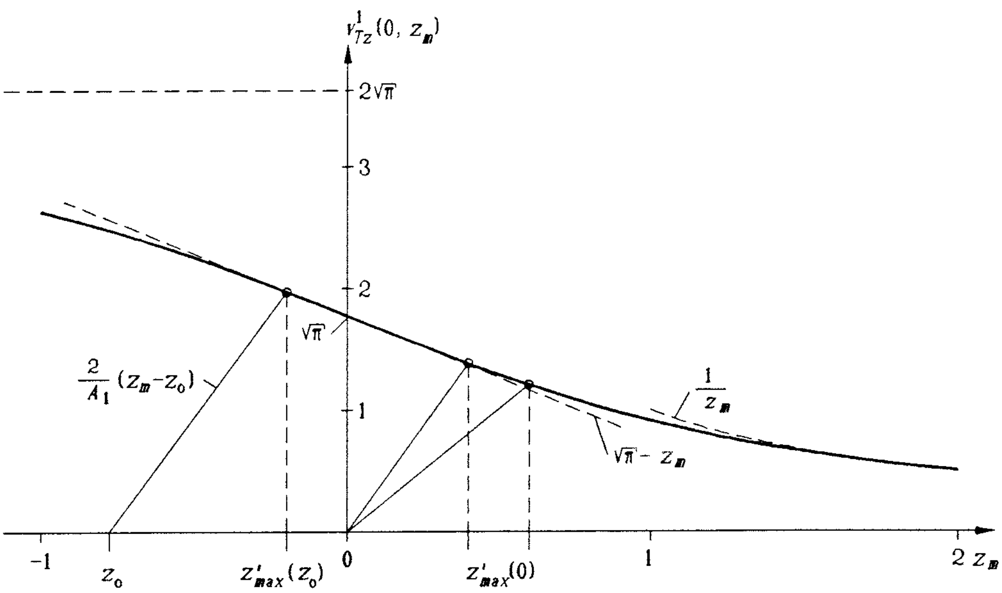

Figure 2.2. Figure to illustrate Eq. (2.48), which gives z'_{max} for given z_o and A_1.

Our main interest is z'_{max} for $z_o = 0$. The balance equation (2.48) gives with the approximation (2.50):

$$\frac{2}{A_1}(z_m - 0) \simeq \frac{1}{z_m} \qquad z_m = z'_{max}(0) \tag{2.51}$$

This gives our *main* formula for the largest upward displacement from a semi-infinite line heat source:

$$z'_{max}(0) = \sqrt{A_1/2} \tag{2.52}$$

The approximation (2.50) gives an error of at most 9% for $z'_{max}(0) > 1$, i.e. for $A_1 > 2$. For $z'_{max}(0) > 1.5$, i.e. for $A_1 > 4.5$, the error is less than 2%. The formula always overestimates the upward flow.

The overestimation is larger for small A_1. In this case, approximation (2.49) is to be used. The balance equation (2.48) is then:

$$\frac{2}{A_1}(z_m - 0) \simeq \sqrt{\pi} - z_m \quad (z_m < 0.75) \tag{2.53}$$

or

$$z'_{max}(0) = \frac{A_1\sqrt{\pi}}{2 + A_1} \qquad (A_1 < 1.5) \tag{2.54}$$

This formula also follows directly from Eq. (2.47). The validity of the formula is tested against the numerical model in Chapter 3. A conservative estimate is to neglect A_1 in the denominator. Then we get the simple estimate

$$z'_{max}(0) = \frac{\sqrt{\pi} A_1}{2} \qquad (A_1 < 0.5) \tag{2.55}$$

A comparison of this formula with the general estimate (2.52) shows that the general formula overestimates $z'_{max}(0)$ by 20% for $A_1 = 1$ and by 96% for $A_1 = 0.2$.

The above formulas concern the infinite line source. The upward velocity $v_{Tz}(0, z)$ for the case of a *finite* line heat source is given by (2.41). The dimensionless length H'_o of the line source is for our application around 20. We can neglect the exponential term and the erfc term with the argument $z + H'_o$. Then we have:

$$v_{Tz}(0, z) = \frac{A_1}{2} \left[\frac{1 - e^{-z^2}}{z} + \sqrt{\pi}\, \mathrm{erfc}(z) - \frac{1}{z + H'_o} \right] \qquad (z + H'_o > 3) \tag{2.56}$$

The approximation (2.50) becomes:

$$\frac{2}{A_1} v_{Tz}(0, z) \simeq \frac{1}{z} - \frac{1}{z + H'_o} \tag{2.57}$$

Equation (2.51) for the largest upward displacement for $z_o = 0$ is then:

$$\frac{2}{A_1} z_m \simeq \frac{1}{z_m} - \frac{1}{z_m + H'_o} \tag{2.58}$$

This is a cubic equation in z_m. We have:

$$z_m^2 = \frac{A_1}{2} \cdot \frac{H'_o}{z_m + H'_o} \qquad z_m = z'_{max}(0) \tag{2.59}$$

A good approximation is:

$$z'_{max}(0) = \sqrt{\frac{A_1}{2} \cdot \frac{H'_o}{\sqrt{A_1/2} + H'_o}} \qquad \left(H'_o > \sqrt{2A_1} \right) \tag{2.60}$$

This correction for the finite length of the line heat source decreases $z'_{max}(0)$. In our applications the correction is quite small. We can safely use the infinite line source to estimate the largest upward displacement.

The above results concern the ***dimensionless*** variables. Let $z_{max}(z_o)$ denote the real upward displacement. We have in accordance with (2.8):

$$z_{max}(0) = L_1 \cdot z'_{max}(0) = \sqrt{4at_o} \cdot z'_{max}(0) \tag{2.61}$$

Eqs. (2.52) and (2.11) give

$$z_{max}(0) = \sqrt{\frac{1}{2\pi\sqrt{\pi}} \cdot \frac{\alpha_T E_o}{\alpha_c c_z^o C H_o} \cdot \frac{1}{\sqrt{4at_o}} e^{-v_o^2/(4at_o)}} \tag{2.62}$$

The above formula overestimates $z_{max}(0)$ for small values of A_1. The estimate (2.55), which is valid for $A_1 < 0.5$, then gives:

$$z_{max}(0) = \frac{\sqrt{\pi}A_1}{2} \cdot \sqrt{4at_o} = \frac{1}{2\pi} \cdot \frac{\alpha_T E_o}{\alpha_c c_z^o C H_o} \cdot \frac{1}{4at_o} e^{-y_o^2/(4at_o)} \quad (A_1 < 0.5) \quad (2.63)$$

Formula (2.62) corresponds to (1:6.34). The time t_o, at which the temperature field was taken, may be chosen at will. As in section 6.5 of [1], we will consider the largest upward displacement, when t_o varies. In formula (2.62), the following function is to be maximized:

$$\sqrt{\frac{1}{\sqrt{\tau}} e^{-1/\tau}} \qquad \tau = \frac{4at_o}{y_o^2} \tag{2.64}$$

The maximum occurs for $\tau = 2$. Then $\sqrt{4at_o}$ is replaced by $y_o\sqrt{2}$ in (2.62). This gives the following largest upward displacement for any chosen time t_o:

$$z_{max}(0)\big|_{\max\, t_o} = \frac{1}{\sqrt[4]{e} \cdot (2\pi)^{3/4}} \cdot \sqrt{\frac{\alpha_T}{\alpha_c c_z^o C} \cdot \frac{E_o}{H_o y_o}} \tag{2.65}$$

The numerical factor is:

$$\frac{1}{\sqrt[4]{e} \cdot (2\pi)^{3/4}} = 0.20 \tag{2.66}$$

The corresponding maximum for formula (2.63) is obtained from the maximum of

$$\frac{1}{\tau} e^{-1/\tau} \qquad \tau = \frac{4at_o}{y_o^2} \tag{2.67}$$

The maximum occurs for $\tau = 1$. Insertion of $4at_o = y_o^2$ in (2.63) gives

$$z_{max}(0)\big|_{\max\, t_o} = \frac{1}{2\pi e} \cdot \frac{\alpha_T}{\alpha_c c_z^o C} \cdot \frac{E_o}{H_o y_o^2} \qquad (A_1 < 0.5) \tag{2.68}$$

The condition $A_1 < 0.5$ is equivalent to:

$$A_1 < 0.5 \quad \Leftrightarrow \quad z_{max}(0)\big|_{\max\, t_o} < \frac{y_o\sqrt{\pi}}{4} \simeq y_o/2 \tag{2.69}$$

2.2.5 Several line heat sources

We have until now considered a single line heat source. In the SKB-concept, the canisters are to be deposited in some twenty boreholes (rod consolidation case). The canisters lie over a length H_o of some 2000 meters, with the top at a depth of some 2000 meters. See Figure 1.1.

We now consider N line heat sources. Source j lies along (x_j, y_j, z), $0 > z > -H_o$. Here, $z = 0$ is the plane of the top of the heat sources. The ground surface lies far above ($z \simeq +2000$ m).

The temperature-induced groundwater flow field is obtained by superposition of the flow field for each line source. The dimensionless flow field for a single source is given by (2.29). It refers to a line source with $x_j = 0$ and $y_j = y_o$. In the formula, x is to be replaced by $x' - x'_j$ and z by z'. In formula (2.11) for A_1, y_o is to be replaced by y_j. We have from (2.11) for the case of semi-infinite line sources:

$$\vec{v}_T' = \sum_{j=1}^{N} \frac{1}{2} A_{1,j} \left(\frac{1 - e^{-(x'-x_j')^2-(z')^2}}{\sqrt{\left(x' - x_j'\right)^2 + (z')^2}} \cdot \hat{r}_j + \sqrt{\pi} e^{-\left(x'-x_j'\right)^2} \operatorname{erfc}(z') \cdot \hat{z} \right) \tag{2.70}$$

$$A_{1,j} = A_1 \cdot e^{(y_o^2 - y_j^2)/(4at_o)} \tag{2.71}$$

$$\hat{r}_j = \frac{1}{\sqrt{\left(x' - x_j'\right)^2 + (z')^2}} \left[\left(x' - x_j'\right) \hat{x} + z'\hat{z} \right] \tag{2.72}$$

In the case of finite line sources, the solution consists of two terms of the above type. The first term is exactly the same as (2.70-72). From this, the same expression but with $z' = z' + H_o'$ is to be subtracted:

$$\vec{v}_T'|_{\text{finite line source}} = \vec{v}_T'|_{z'} - \vec{v}_T'|_{z'+H_o'} \tag{2.73}$$

The largest dimensionless upward displacement was given by the solution $z_m = z'_{max}(z_0)$ of (2.48) for the single line heat source. For several line sources, the z-component of the velocity (2.70-72) is to be used on the right-hand side of (2.48). This gives the equation:

$$\frac{2}{A_1} (z_m - z_o) = \sum_{j=1}^{N} e^{(y_o^2 - y_j^2)/(4at_o)} \tag{2.74}$$

$$\times \left\{ \left[1 - e^{-(x'-x_j')^2 - z_m^2}\right] \frac{z_m}{(x' - x_j')^2 + z_m^2} + \sqrt{\pi} e^{-(x'-x_j')^2} \operatorname{erfc}(z_m) \right\}$$

The solution $z_m = z'_{max}(z_0)$ will depend on the choice of x'. The equation must be solved for different x'. The largest upward displacement $z'_{max}(z_0)$ is given by the maximum:

$$z'_{max}(z_0) = z'_m|_{\max x'} \tag{2.75}$$

Equation (2.74) will be solved numerically in Section 6.4. For simplicity we will consider cases with symmetry with respect to $x' = 0$, which means that the maximum (2.75) must occur for $x' = 0$.

Chapter 3

Numerical model and calculations

The numerical model for the groundwater flow and the development of the salt concentration distribution with heating from a point source is presented in Chapter 5 of [1]. Results of calculations are presented in Chapter 6 of [1]. The corresponding studies for the semi-infinite line heat source will be reported in this chapter. A user's manual for the model is given in [5].

The dimensionless formulation is used throughout this chapter. The dimensionless problem contains one parameter A_1 only. The flow process will be calculated for different A_1-values. We are interested in the largest upward displacement, in particular near the top of the line heat source. The motion along the z-axis will be compared to the approximate analytical formulas of Section 2.2.3-4.

3.1 Governing equations

The time-dependent groundwater and salt flow process takes place in the (x, z)-plane with $y = 0$. The dimensionless excess salt concentration is denoted $c' = c(x, z, t)$. The total dimensionless salt concentration with a linear component $-z$ is:

$$\tilde{c}(x, z, t) = -z + c'(x, z, t) \tag{3.1}$$

It satisfies the salt balance equation (1:5.1):

$$\frac{\partial \tilde{c}}{\partial t} + \nabla \cdot [\tilde{c}\,(\vec{v}_T + \vec{v}_c)] = 0 \tag{3.2}$$

The initial excess salt concentration c' is zero:

$$\tilde{c}(x, z, 0) = -z \tag{3.3}$$

The temperature-induced groundwater flow field from the semi-infinite line heat source $\vec{v}_T$ is given by (2.29):

$$\vec{v}_T(x, z) = \frac{A_1}{2} \cdot \left[\frac{1 - e^{-r^2}}{r} \cdot \hat{r} + \sqrt{\pi} e^{-x^2} \operatorname{erfc}(z) \cdot \hat{z} \right] \tag{3.4}$$

$$r = \sqrt{x^2 + z^2} \qquad \hat{r} = \frac{x}{r} \cdot \hat{x} + \frac{z}{r} \cdot \hat{z}$$

This flow field is time-independent, since the temperature field is taken at a time t_o. The dimensionless flow intensity factor A_1 is given by (2.11).

The groundwater flow $\vec{v}_c$ due to the salt distribution is given by (1:5.3):

$$\vec{v}_c(x,z,t) = -c(x,z,t)\hat{z} - \frac{1}{2\pi}\int_{-\infty}^{\infty} dx' \int_{-\infty}^{\infty} dz' \frac{(x'-x, z'-z)}{(x'-x)^2+(z'-z)^2} \cdot \frac{\partial c}{\partial z'}(x',z',t) \quad (3.5)$$

The solution of Eqs. (3.2) and (3.5) with $\vec{v}_T$ given by (3.4) involves moving 'salt particles' and a particular technique to evaluate the double integral at each time-step. This is described in Sections 5.1-3 in [1].

3.2 Numerical results

The flow process for the salt, Eqs. (3.1-5), has been calculated with the numerical model for values of A_1 from 0.1 to 30. The model is described in Chapter 5 in [1].

The dimensionless temperature amplitude A_1, (2.11), depends on the chosen time t_o:

$$A_1 = \frac{\alpha_T E_o}{\pi\sqrt{\pi}\alpha_c c_z^o C H_o y_o^3} \cdot \frac{e^{-1/\tau}}{\tau^{3/2}} \qquad \tau = \frac{4at_o}{y_o^2} \quad (3.6)$$

Derivation with respect for τ gives the maximum, which occurs for $\tau = 2/3$ or $y_o = \sqrt{6at_o}$:

$$A_{1,\max t_o} = \frac{e^{-1.5}}{\pi\sqrt{\pi}(2/3)^{3/2}} \cdot \frac{\alpha_T E_o}{\alpha_c c_z^o C H_o y_o^3} \quad (3.7)$$

For the data (1:3.55) and (1:6.53-55) we have:

$$A_{1,\max t_o} = 0.074 \cdot \frac{6.43 \cdot 10^{-6} \cdot 1.16 \cdot 10^{15}}{2000 \cdot 100^3} = 0.27 \quad (3.8)$$

So in the SKB applications, we are interested in the solution for rather small values of A_1.

3.2.1 Temperature flow component $\vec{v}_T$

The dimensionless groundwater flow has two components $\vec{v}_T$ and $\vec{v}_c$. The process (3.2) is initiated by the temperature component (3.4), which is at work all the time, while the salt component $\vec{v}_c$ changes as the salt distribution changes, Eq. (3.5).

There is an option in the program to completely suppress $\vec{v}_c$. Then the moving particles follows $\vec{v}_T$. This is not our physical situation but the flow pattern provides a good insight into the character of the driving flow.

Figure 2.1 shows the streamlines. The small circle in the center is the point $x = 0, z = 0$, where the top of the line heat source lies. The stream lines follow the line source along the negative z-axis. They are deflected as they approach the top, and they end following a radial asymptote. See Section 2.2.2.

Figures 3.1 and 3.2 show the particle motions in greater detail. The value of A_1 is 1. The considered particles start at $t = 0$ on the line $z = -4$ with a spacing of 0.1 in the x-direction. See Figure 3.1. The particles near the z-axis move upwards, while particles further out will move downwards out of sight. The time between two consecutive positions of the same particle is $\Delta t' = 0.1$. The positions are joined to a full curve, an isochrone, for $\Delta t' = 1$. The six isochrones for $t = 1, 2, \ldots 6$ show the position of particles that started on $z = -4$ at $t = 0$. Figure 3.2 shows the motion of the same particles during a much longer time. The shown region is $-4 < x < 4$ and $-4 < z < 2$. The distance between isochrones is here $\Delta t' = 0.5$.

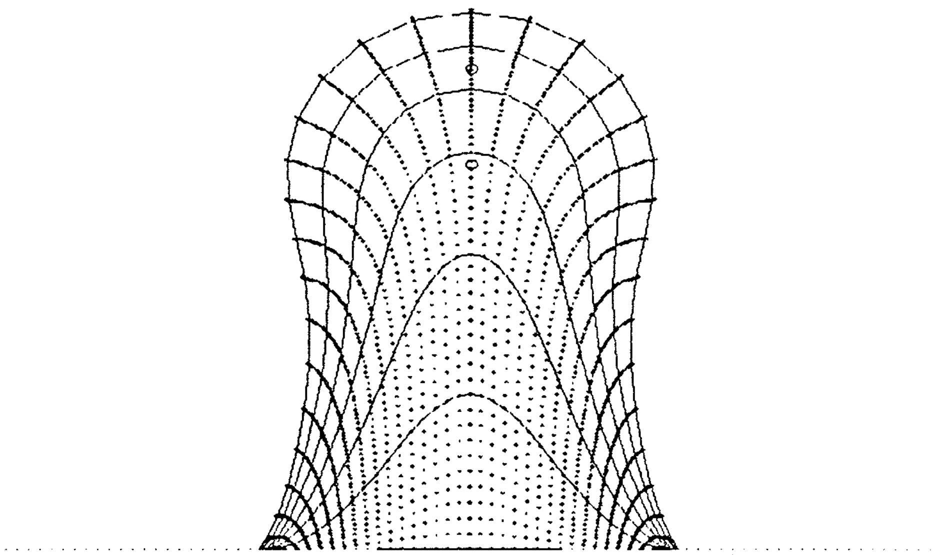

Figure 3.1. Motion of particles due to $\vec{v}_T$ only for $A_1 = 1$.
The time between two isochrones is 1.

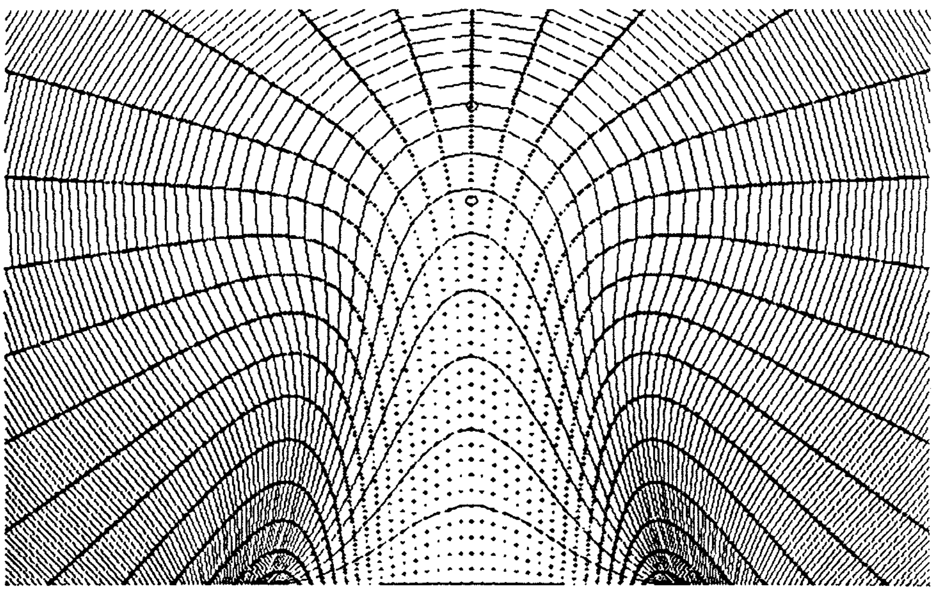

Figure 3.2. Motion of particles due to $\vec{v}_T$ only for $A_1 = 1$.
The time between two isochrones is 0.5.

Figures 3.1 and 3.2 correspond to Figure 6.1 in [1]. The isochrones are curves of constant salt concentration $\tilde{c}$, since the particles all start at the same z-level. There is a considerable difference between the point source of [1] and the line source. The circular motion around two stagnation points in Figure 6.1 in [1] does not occur for the semi-infinite line heat source. The temperature-induced flow $\vec{v}_T$ has a somewhat simpler structure for the line source.

It should be noted that there are two stagnation points for the *finite* line heat source. These points (one on each side) lie at middepth ($z = -H_o'/2$) at a certain distance from the line source. The circular motion around the stagnation points will occur far away from the top of the line source, and this motion will not influence the upward flow near the top region.

3.2.2 Results for different A_1

Figures 3.3 to 3.6 show the results for $A_1 = 0.1$, 1, 10 and 30. Curves of constant dimensionless total salt concentration $\tilde{c}$ are shown for different dimensionless times t'. The $\tilde{c}$-curves are horizontal lines at $t' = 0$ in accordance with (3.3). The point $(x', z') = (0, 0)$, where the top of the line source lies, is indicated in all figures by a full dot. The point $(x', z') = (0, 1)$ is also indicated by a full dot. The shown region is $-4 \leq x' \leq 4$ and $-1.5 \leq z' \leq 4$.

Figure 3.3 shows for $A_1 = 0.1$ the $\tilde{c}$-curves for the times $t' = 0.4$, 0.8, 1.6, 3.2, 6.4 and 12.8. The displacements after $t' = 0.8$ are quite small. The largest upward displacement for $(0, 0)$, $z'_{max}(0)$, is equal to 0.08. The calculations are continued to $t' = 12.8$. Nothing happens in the central region, but errors from the boundaries become visible in particular at the top of the shown region for $t' = 12.8$. This is discussed in Section 3.3.

Figure 3.4 shows the $\tilde{c}$-curves for $A_1 = 1$ for the times $t' = 0.2$, 0.6, 1.0, 1.4, 1.8 and 2.6. The largest upward displacement $z'_{max}(0)$ becomes 0.55.

Figure 3.5 shows the $\tilde{c}$-curves for $A_1 = 10$ for the times $t' = 0.1$, 0.2, 0.4, 0.7, 1.1 and 1.2. The largest upward displacement $z'_{max}(0)$ becomes 1.7. The flow is now much stronger and the numerical problems increase. The $\tilde{c}$-curves lie very close to each other above the center for $t' > 0.7$, and a numerical instability makes itself noticeable at the bottom for $t' = 1.2$. The numerical problems are discussed in Section 3.3.

Figure 3.6 shows the $\tilde{c}$-curves for $A_1 = 30$ for the times $t' = 0.05$, 0.1, 0.15, 0.25, 0.35 and 0.45. The largest upward displacement $z'_{max}(0)$ becomes 2.6. The same numerical instability as in Figure 3.5 is seen at the bottom for $t' = 0.45$.

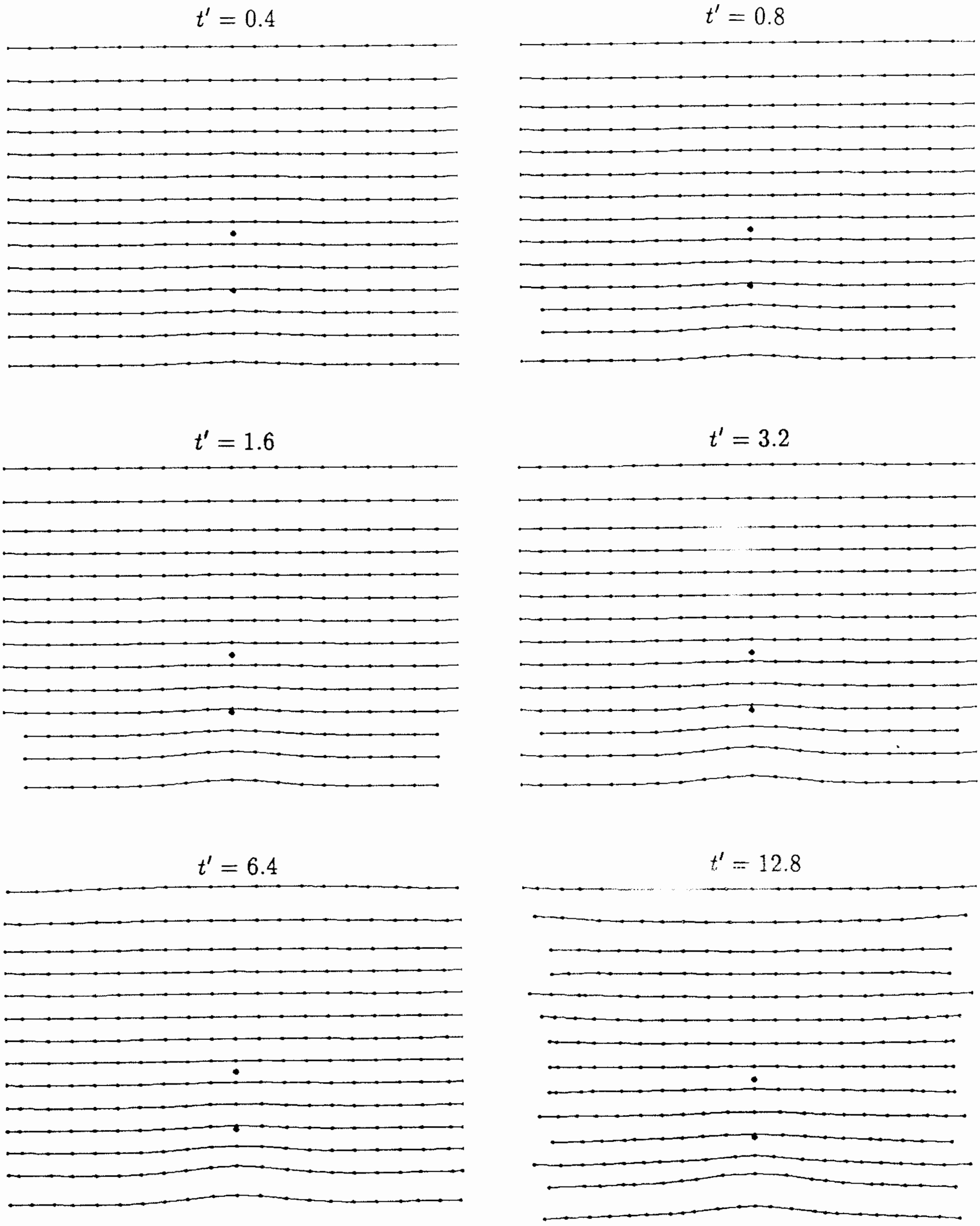

Figure 3.3. Curves of constant $\tilde{c}$ for $A_1 = 0.1$ for different times t'.

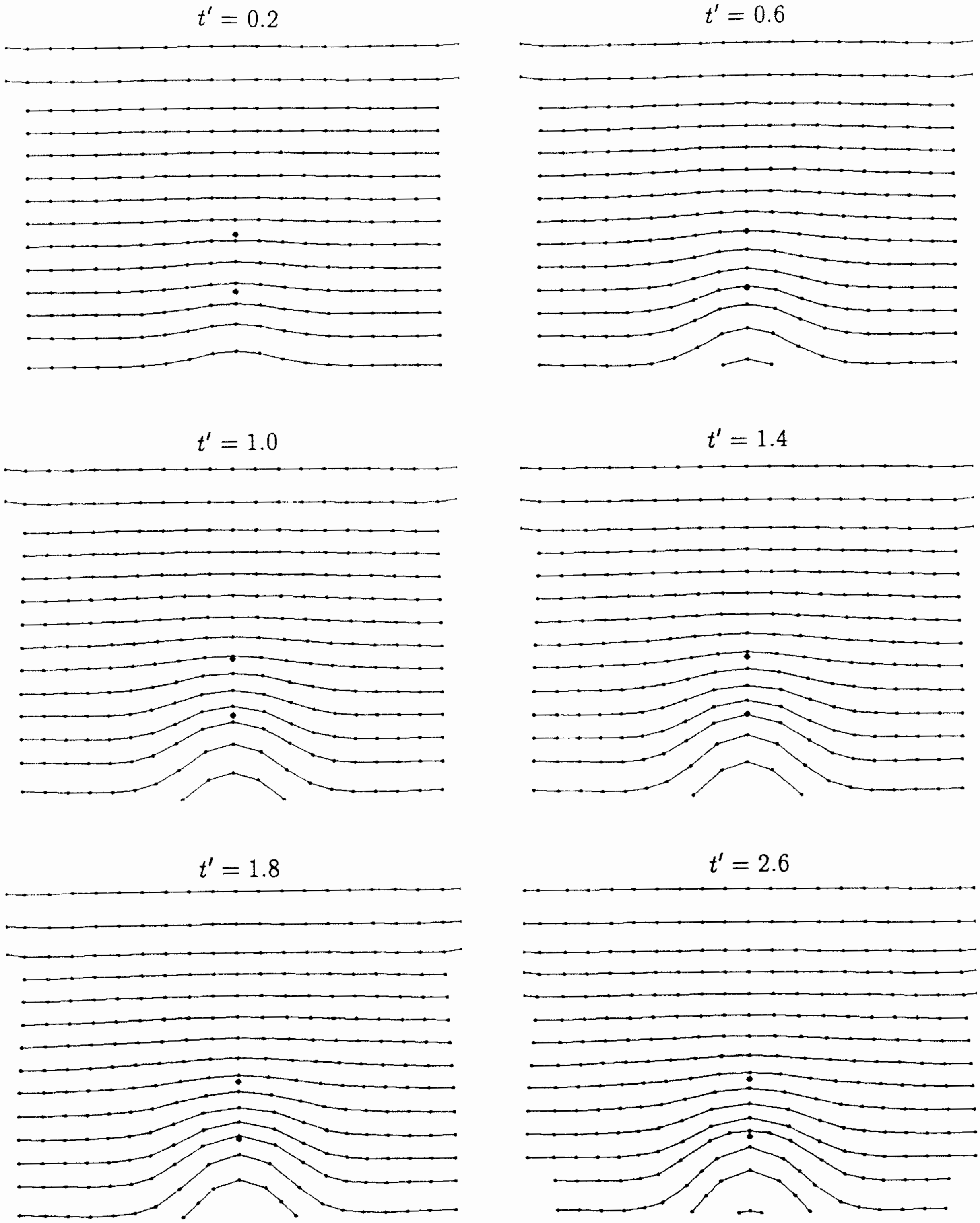

Figure 3.4. Curves of constant $\tilde{c}$ for $A_1 = 1$.

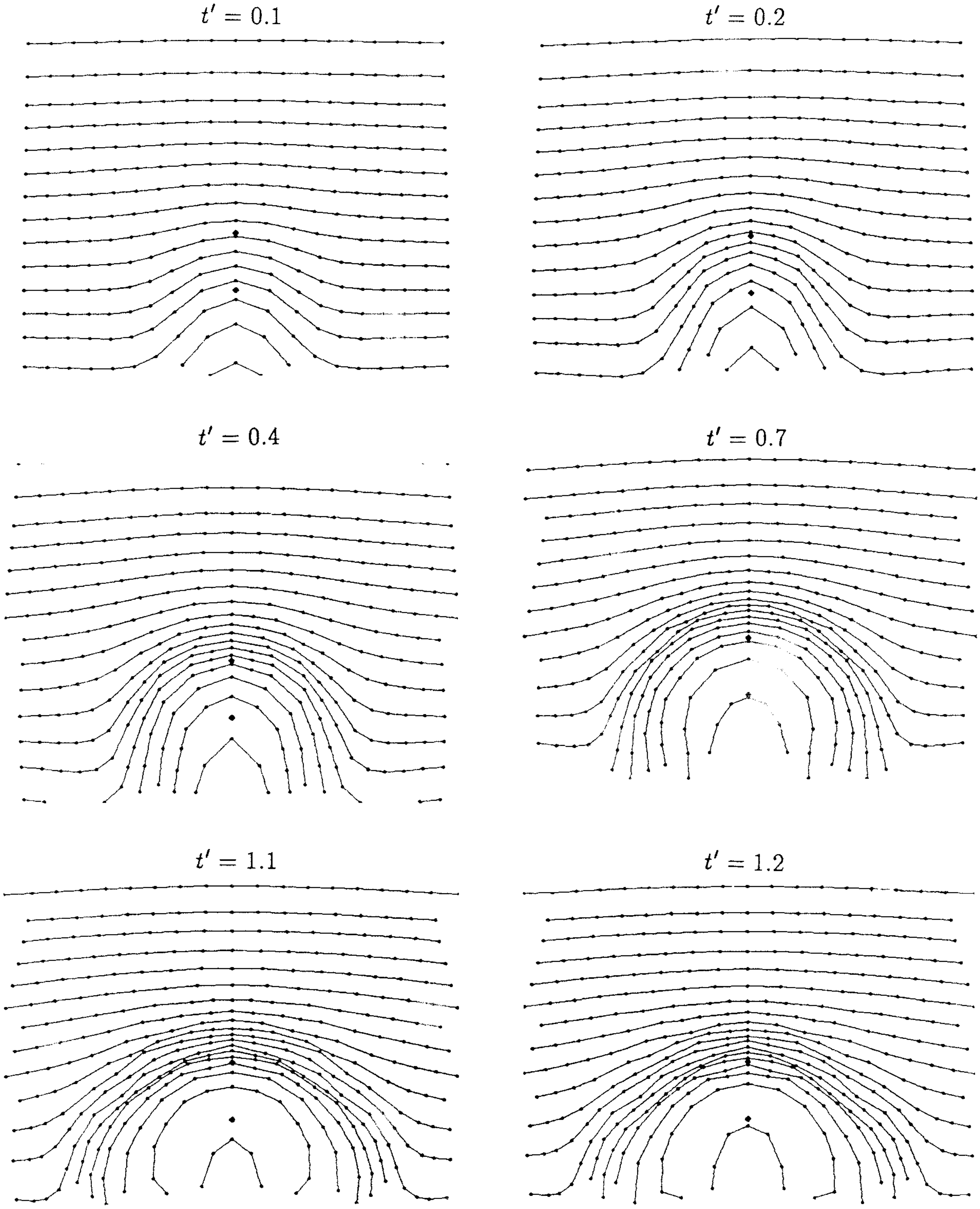

Figure 3.5. Curves of constant $\tilde{c}$ for $A_1 = 10$.

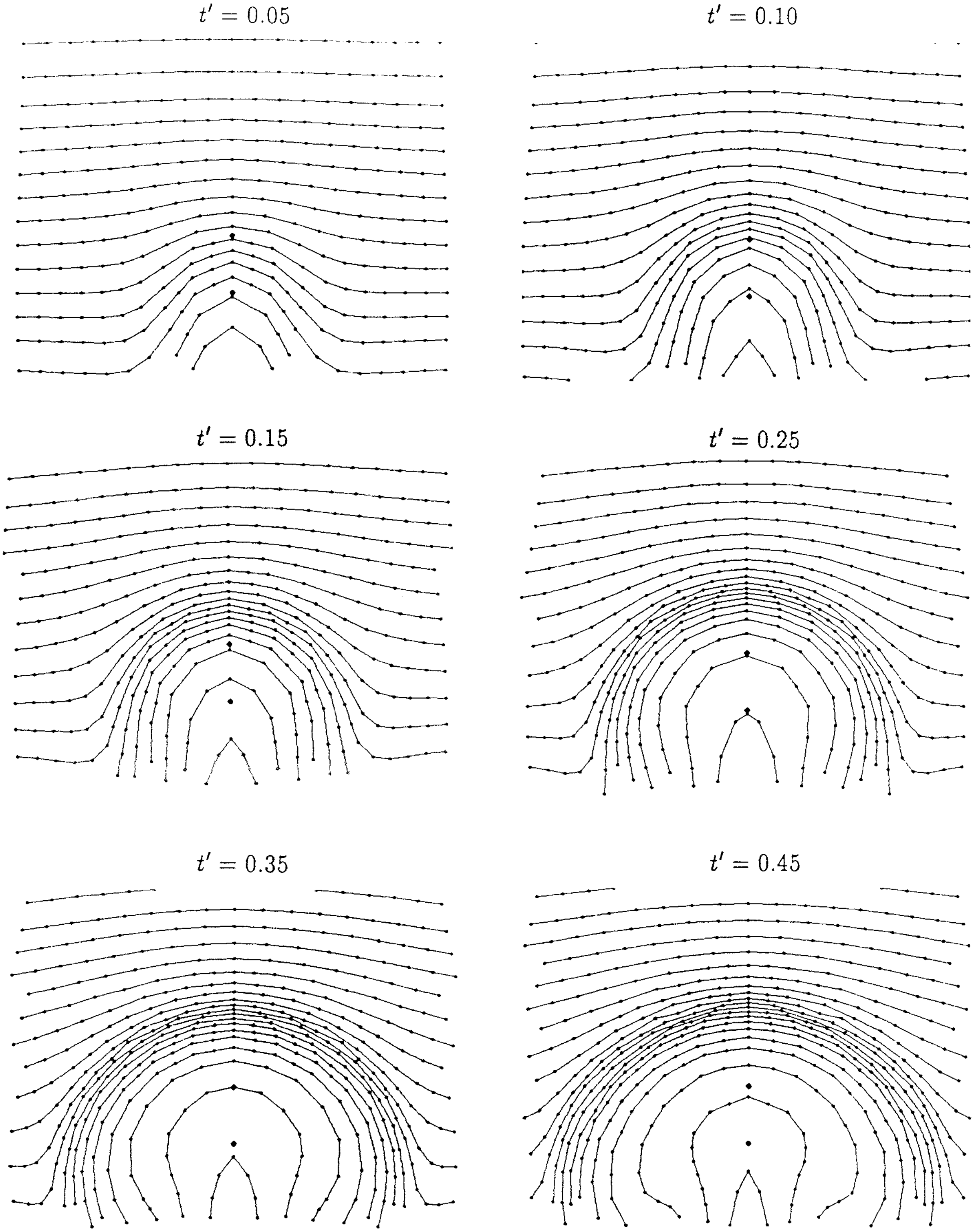

Figure 3.6. Curves of constant $\tilde{c}$ for $A_1 = 30$.

3.2.3 Largest upward displacement

One of the main goals in this study is to estimate the largest upward displacement, in particular for a particle that starts at the top of the line source. Table 3.1 gives $z'_{max}(0)$ from the above calculations for different A_1.

A_1	0.1	0.2	0.5	1	3	10	30
$z'_{max}(0)$	0.08	0.14	0.31	0.55	1.0	1.7	2.6
$\sqrt{A_1/2}$	(0.22)	(0.32)	(0.50)	(0.71)	1.2	2.2	3.9
$A_1\sqrt{\pi}/(2+A_1)$	0.084	0.16	0.35	0.59	-	-	-

Table 3.1. Numerically calculated $z'_{max}(0)$ and the two approximations (3.9) and (3.10).

It is of great interest to compare the numerical values with the values from the approximate analytical formulas (2.52) and (2.54):

$$z'_{max}(0) = \sqrt{A_1/2} \qquad (A_1 \text{ not too small}) \tag{3.9}$$

$$z'_{max}(0) = \frac{A_1\sqrt{\pi}}{2+A_1} \qquad (A_1 < 1.5) \tag{3.10}$$

The first formula may be used for any A_1, but it will overestimate $z'_{max}(0)$ for small A_1 (i.e. for $A_1 < 1.5$).

The numerically calculated values of $z'_{max}(0)$ are somewhat uncertain for small A_1. See Section 3.3. But the agreement between the numerical values and the approximate analytical formulas in Table 3.1 is quite satisfactory and certainly sufficient for our purpose.

3.2.4 Further comparison with analytical formulas

We have seen that the analytical formulas to estimate the largest flow from the top of the line source give quite acceptable results. The value of A_1 is rather small in our SKB application. Then the approximate formula (2.47) gives the whole upward motion for a particle that starts from $x = 0, z = 0$:

$$z_m(t', 0) = \frac{A_1\sqrt{\pi}}{2+A_1}\left(1 - e^{-(1+A_1/2)t'}\right) \qquad (A_1 < 1.5) \tag{3.11}$$

This upward motion is shown in Figure 3.7 for a few small values of A_1. The result for $A_1 = 3$ is also included although it exceeds the limit $A_1 = 1.5$. We see again that there is a good agreement between the numerical results and the analytical formula (3.11).

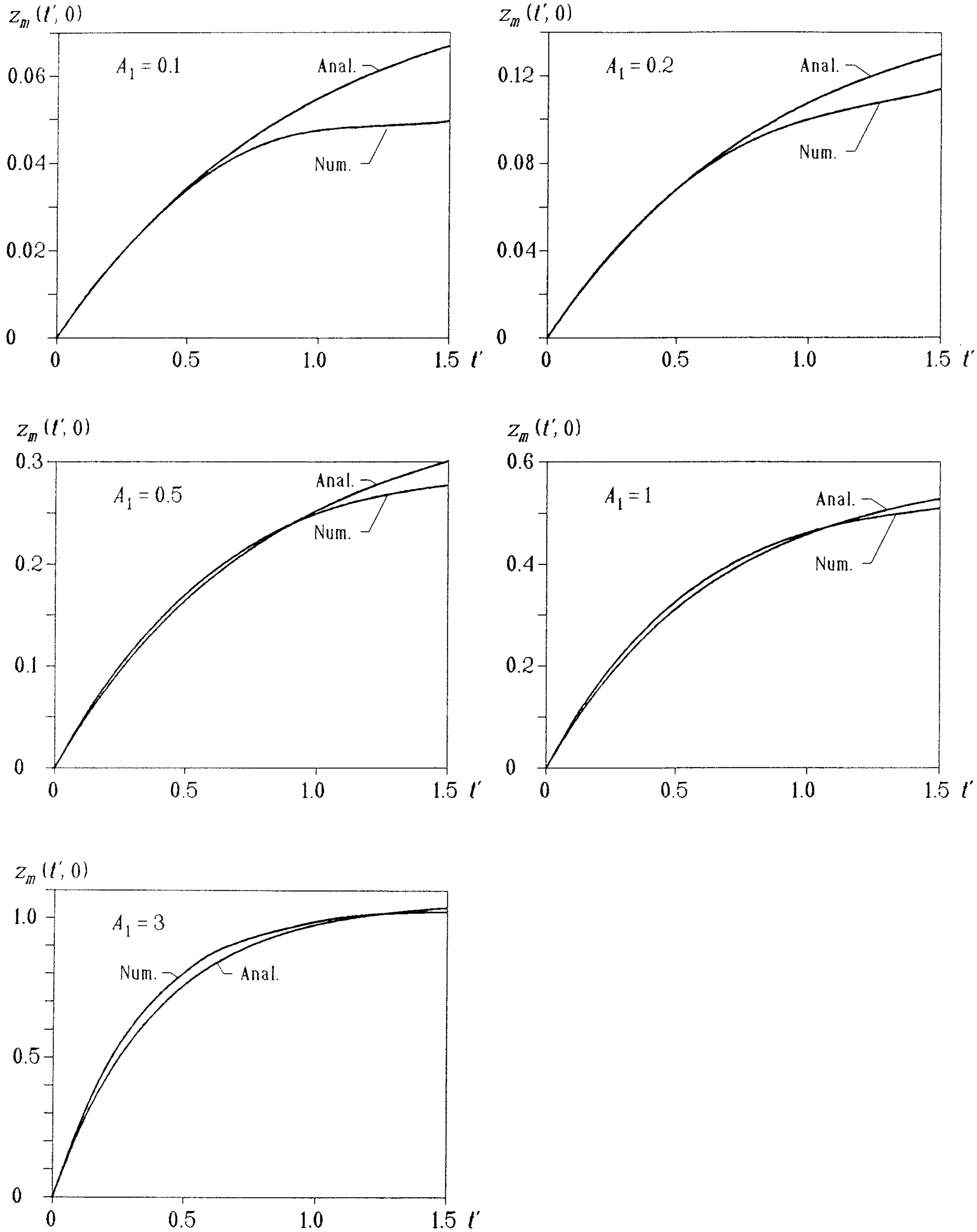

Figure 3.7. Comparison of analytical (Eq. 3.11) and numerical result for the upward motion $z_m(t', 0)$ along the z'-axis.

3.2.5 Accuracy of Riemann sums

A method for numerically evaluating the concentration-flow integral (Eq. 3.5) was presented in Section 5.2 of the first study. Riemann sums were used to calculate both integrals in (1:5.11) even though the second integral had an analytical solution. In this section we will derive this analytical solution and compare it with the corresponding numerical Riemann sum in order to test the accuracy of the numerical procedure.

The second integral in (1:5.11) with its x and z components is:

$$(I_x, I_z) = -\frac{1}{2\pi}\int_{x_-}^{x_+} dx' \int_{z_-}^{z_+} dz' \frac{(x'-x, z'-z)}{(x'-x)^2 + (z'-z)^2} \tag{3.12}$$

It can be calculated analytically as stated above. (It should be noted that in this section x' and z' are variables of integration, while the dimensionless coordinates are x and z. This notational inconsistency is a heritage from the previous study.) The second component of this integral is:

$$I_z = -\frac{1}{2\pi}\int_{x_-}^{x_+} dx' \int_{z_-}^{z_+} dz' \frac{z'-z}{(x'-x)^2 + (z'-z)^2} \tag{3.13}$$

By substituting x' with $\tilde{x} + x$ and z' with $\tilde{z} + z$, the integral is transformed into:

$$I_z = -\frac{1}{2\pi}\int_{x_- - x}^{x_+ - x} d\tilde{x} \int_{z_- - z}^{z_+ - z} d\tilde{z} \frac{\tilde{z}}{\tilde{x}^2 + \tilde{z}^2}. \tag{3.14}$$

It is then easy to verify that:

$$\frac{\tilde{z}}{\tilde{x}^2 + \tilde{z}^2} = \frac{\partial^2}{\partial\tilde{x}\partial\tilde{z}}\left(F(\tilde{x},\tilde{z})\right) \qquad F(\tilde{x},\tilde{z}) = \frac{\tilde{x}}{2}\ln(\tilde{x}^2 + \tilde{z}^2) + \tilde{z}\arctan\left(\frac{\tilde{x}}{\tilde{z}}\right) \tag{3.15}$$

By using this primitive function $F(\tilde{x},\tilde{z})$ the integral becomes:

$$I_z = -\frac{1}{2\pi}\left[F(x_+ - x, z_+ - z) - F(x_+ - x, z_- - z) - \right. \tag{3.16}$$

$$\left. - F(x_- - x, z_+ - z) + F(x_- - x, z_- - z)\right]$$

The first component I_x can be calculated in a similar way.

The double integral is evaluated numerically by using simple Riemann sums as discussed in Section 5.2 of the first study. A comparison of the analytical values with the approximate values of I_z is made for some points in Table 3.2. The constants x_+ and x_- define the right and left boundary of the initial mesh. Furthermore the constants z_+ and z_- define the upper and lower boundary of the initial mesh. The initial mesh used here is the initial mesh that is used in all our calculations. It is described in the last paragraph of Section 3.3 and shown in Figure 3.9. In Table 3.2 we find that the larger discrepancies are found along the mesh boundary as is expected. The largest errors are found along the lower boundary, where the largest initial particle spacings are situated. We see that the numerical Riemann sums give sufficiently accurate results.

		$x = -4$	$x = -0.8$	$x = 0$
$z = 8.1$	Num.	3.2814	4.0129	4.0380
	Anal.	3.4011	4.2526	4.2780
$z = 2.0$	Num.	2.0310	2.1956	2.2032
	Anal.	2.0213	2.1812	2.1885
$z = 0.0$	Num.	1.6931	1.8079	1.8128
	Anal.	1.6807	1.7838	1.7885
$z = -18.2$	Num.	-0.5975	-0.6153	-0.6166
	Anal.	-0.6024	-0.6237	-0.6246
$z = -34.2$	Num.	-2.9258	-3.3669	-3.3869
	Anal.	-3.4011	-4.2526	-4.2780

Table 3.2. The numerical Riemann sum for I_z compared with its analytical value, Eqs. (3.15) and (3.16), for some (x, z)-values.

3.3 Numerical problems

In the first study we had a number of problems with the numerical model. These problems were solved there (in Section 6.3.3) and since we are more or less using the same numerical model, these initial problems are still present and they are solved in the same manner as before.

Some new problems arise when we use the temperature velocity $\vec{v}_T$ of the line source. The particles near the line source will move much faster than before and this results in new problems.

We specify the time-step $\Delta t'$ as an input variable instead of the largest displacement $(= (A_0/2) \cdot \Delta t')$ as stated in the second last paragraph of Section 6.3.3 in the first study. This is the only alteration in the numerical model.

Our main interest is focused on the upward motion of particles that start in the area around the top of the line source, where the potentially defect canisters are assumed to be situated. We are particularly interested in the particle that starts right at the top of the line source (at $(x, z) = (0, 0)$) since this particle is the one that attains the highest z-value (for all times t'). We also want to look at curves of constant $\tilde{c}$ in an area around the top of the line source. This *area of interest* is roughly from $z = -1$ to $z = 3$. The width of this area is about 8 ($|x| < 4$). This area should be kept free of *numerical instabilities.*

Numerical instabilities occur mainly in three different forms. The first form is a *boundary effect* and it is always present at the mesh boundary though its influence isn't noticed at first in the area of interest. This effect makes itself noticeable after the process has reached quasi steady-state. This error is visible at the top of the region shown for $t' = 12.8$ in Figure 3.3. Notice how the curves of constant $\tilde{c}$ curve downwards. Large initial particle spacings in the z-direction at the upper and lower boundary of the mesh diminish this form of instability.

The second form is caused by large changes in initial particle spacing (a relative change of 40 percent or more). This disorder causes something that resembles *convection.* The first stages of this instability are shown in Figure 3.10. Notice how the curves of constant $\tilde{c}$ move around $(x', z') = (0, 0)$, and how they gradually fold back onto themselves from below. Different curves of constant $\tilde{c}$ cross each other for $t' = 1.7$. This is an error but the particle tracking method does not break down. To remedy this problem one has to choose the mesh with care, avoiding large relative changes in particle spacing. It is suitable to use a mesh with expansive particle spacing.

The third form of numerical instability is *oscillations* where a certain point in the mesh starts to move back and forth perpendicular to the $\tilde{c}$-curves. These oscillations are shown in Figure 3.8 for $A_1 = 0.1$. The upward motion $z_m(t', 0)$ along the z'-axis, calculated for different $\Delta t'$, is compared to the analytical solution given by Eq. (3.11). As can be seen in Figure 3.8 the oscillations in the upward motion $z_m(t', 0)$ are damped by choosing a smaller time-step. This phenomenon occurs when the process approaches a virtual steady-state though it can be present much earlier. These oscillations can be damped by choosing shorter time-steps which in turn prolongs execution times, unfortunately.

These instabilities may be suppressed at the time when they start to occur by applying the above recipes. But they always seem to occur sooner or later. We have not pursued this further since our main interest is the process up to the time for virtual steady-state above the centre.

Another problem, that did not exist in the first study, is the rapid motion of the particles, which lie on or near the line source ($x = 0$ and $z < 0$), due to the large temperature velocity in the z-direction. This causes a *large upward displacement* which is especially pronounced for particles that pass close to the line source. Either the lower boundary of the mesh interferes with the area of interest (boundary effect) or, more severe, the particles that start at the lower boundary of the initial mesh pass the area of interest leaving it empty of particles. To avoid this problem, the initial mesh must extend down to at least $z = -20$ (for $A_1 \leq 30$). This gives the salt concentration enough time to stop the upward motion before the area of interest is influenced.

The initial particle spacings in the z-direction may be expanded from say 0.5 in the area of interest to 4.0 at the lower boundary. It is then more appropriate for the initial mesh to go down to $z = -30$ instead of $z = -20$, in order to avoid numerical instabilities caused by too large relative changes in the spacings of adjacent particles.

It is sufficient to use one initial mesh for all the different A_1-values when a large A_1-value is compensated by a small $\Delta t'$-value. The mesh must at least cover the area $-4 \leq x \leq 4$ and $-20 \leq z \leq 8$. The left and right boundaries lie sufficiently far out to ascertain that contributions to the displacement velocity from the temperature field are small. The initial particle spacing at the top of the mesh must be about 1 to 2, and at the bottom 3 to 4. The area of interest must have a resolution (high resolution-small spacing, low resolution-large spacing) that is able to properly represent the movement of the particles. If the resolution is too low, then information is lost, and on the other hand, if the resolution is too high, execution times will be unnecessarily long. A very small A_1-value (less than 0.1) requires high resolution in order to see the finer details of the movement. The particle spacing in the x-direction is of lesser importance but it is kept at around 0.3 to 2. The smaller values (even values less than 0.3) should be used for small A_1-values, and the larger values should be used at the left and right boundaries.

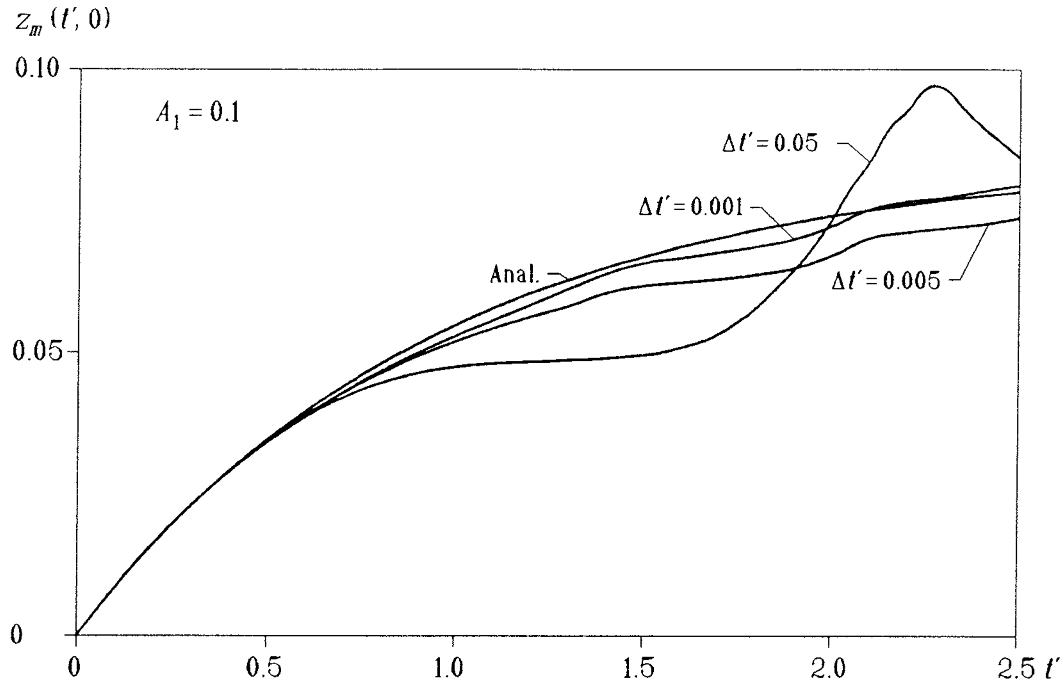

Figure 3.8. Oscillating behavior when the time-step is too large.

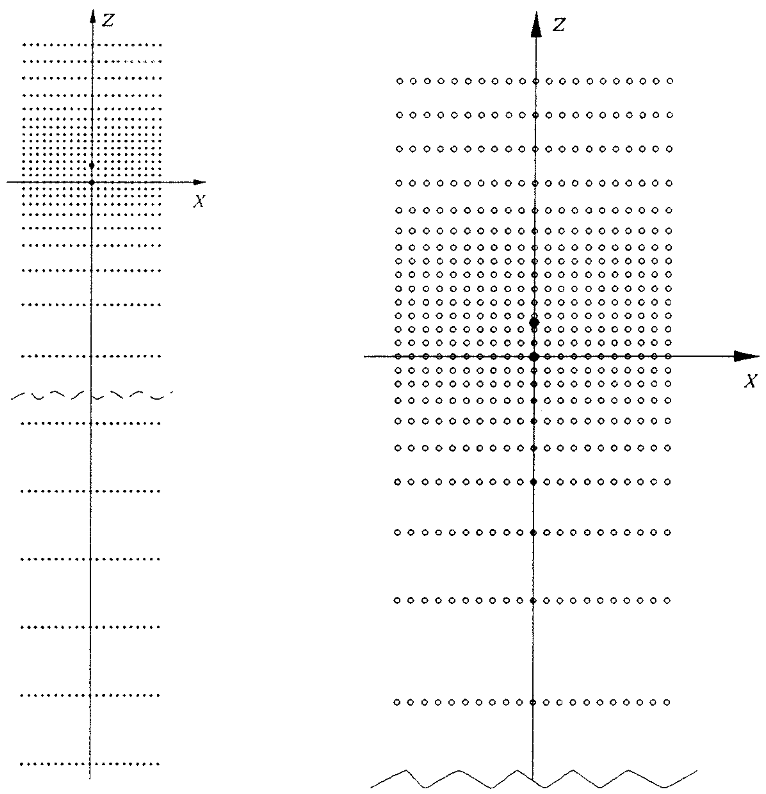

Figure 3.9. The initial mesh that is used in all calculations.

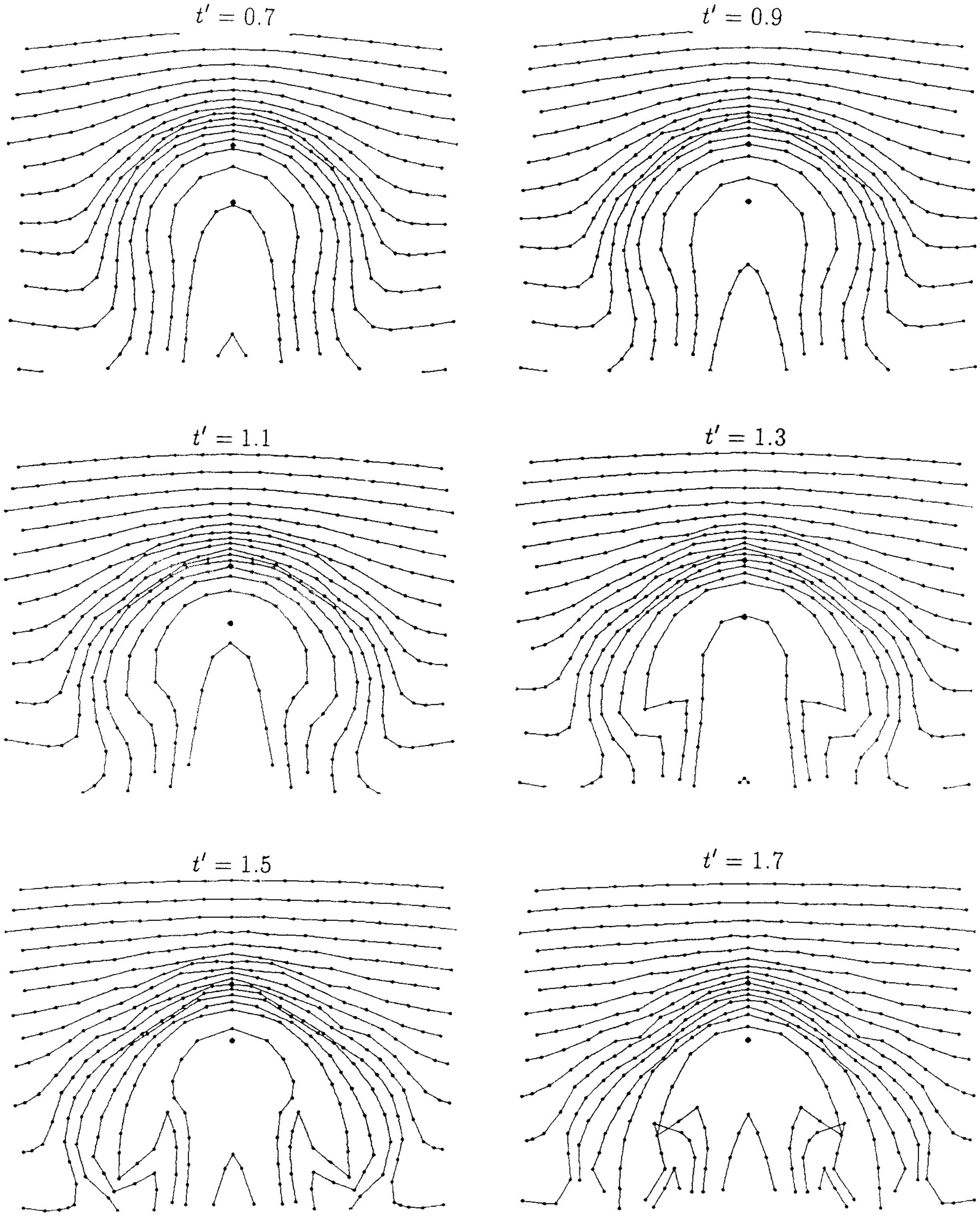

Figure 3.10. The initial stages of numerical instability called 'convection' ($A_1 = 10$).

The above considerations have led to the use of the following initial mesh. The initial mesh used in all the calculations presented in this study covers an area defined by $-4 \leq x \leq 4$ and $-34.2 \leq z \leq 8.1$. The number of initial particles is $21 \times 29 = 609$. The particle spacings in the z-direction vary from 1.0 at the upper boundary down to 0.4 at $z = 3.2$, and from 0.4 at $z = -0.8$ to 4.0 at the lower boundary. The particle spacings in the central region ($-0.8 \leq z \leq 3.2$) have the height 0.4. The particle spacings in the x-direction is kept at 0.4 (constant). The initial particle spacings used in the area of interest is 0.4×0.4. The initial mesh is shown in Figure 3.9. The small circles represent the initial positions of the particles at $t' = 0$. The initial mesh structure is deformed for $t' > 0$, when the particles move. The removal and insertion of particles during execution (see Section 6.3.3 in the first study) also deforms the initial mesh structure. The positions of the particles change with time, but we still refer to these as a mesh.

The choice of $\Delta t'$ needs consideration. This time-step $\Delta t'$ along with the initial mesh are the only means we have to control the numerical model in terms of tolerances and sensitivity. Some trial and error has been used to find appropriate $\Delta t'$-values. A value that is too small results in very long execution times whereas a value that is too large leads to numerical instabilities. One rule of thumb that is valid for this mesh is to keep the product $A_1 \cdot \Delta t'$ in the interval $0.005 \leq A_1 \cdot \Delta t \leq 0.01$.

Chapter 4

Exponentially decreasing heat release

The heat release from the canisters decreases exponentially. The point heat source in [1] and the line heat source in Chapters 2 and 3 were assumed to release all heat instantaneously at $t = 0$. This simplification means that the solutions are not valid during an initial time period. We will now remove this limitation.

A main interest in this study is the largest upward displacement from the canister region. The formulas for $z_{max}(0)$ are of particular interest. We will here confine ourselves to extend the previous formulas to the case of exponentially decreasing heat release.

In section 4.1, the formulas to determine the largest upward displacement are established. The point source case of [1] is treated in Section 4.2, and the line heat source with exponentially decreasing heat release in Section 4.3.

4.1 Largest upward displacement

The largest upward displacement will in the considered symmetrical cases occur along the z-axis. The case of an instantaneous point heat source is dealt with in Section 6.4 of [1]. The motion of a salt-water 'particle' is determined by the two velocity components from temperature and salt concentration. The largest upward displacement is determined by the point on the z-axis, where these two velocities balance each other.

4.1.1 Superposition

The velocity component $\vec{v}_T$ from the temperature field may be obtained from the previous solution by superposition. Let $Q(t)$ (W), $0 < t < \infty$, be any time-dependent heat release, and let $\vec{v}_T(x,z)|_{E_o=1}$ be the groundwater flow field at the considered time t_o for a *unit point* heat source, $E_o = 1$ (J), released $t = 0$.

The time-dependent heat source releases the heat $Q(t')dt'$ (J) in the small interval $t' < t < t' + dt'$. (Here, t' is an integration variable with the dimension of t, i.e. seconds.) This instantaneous heat source at $t = t'$ causes the flow field $\vec{v}_T(x,z)$ with E_o replaced by $Q(t')dt'$ and t_o by $t_o - t'$. The total flow field at the considered time t_o is obtained by superposition, i.e. by integration in t':

$$\vec{v}_T(x,z) = \int_0^{t_o} \vec{v}_T \Big|_{\{E_o=1, t_o \to t_o - t'\}} \cdot Q(t')dt' \tag{4.1}$$

The velocity along the z-axis at the considered time t_o is then:

$$v_{Tz}(0,z) = \int_0^{t_o} v_{Tz}(0,z)\Big|_{\{E_o=1, t_o\to t_o-t'\}} \cdot Q(t')dt' \tag{4.2}$$

4.1.2 Flow along the z-axis

The water flow is driven by $\vec{v}_T + \vec{v}_c$. The temperature component $\vec{v}_T$ is treated as time-independent, since the salt-induced flow has a much shorter time-scale than the change of the temperature T and the flow $\vec{v}_T$. See Section 3.6 in [1]. The basic assumption in order to get analytical formulas was to neglect the contribution from ∇P_c in expression (1:6.13) for $\vec{v}_c$:

$$\vec{v}_c' = -\nabla' P_c - c'\hat{z} \simeq -c'\hat{z} \tag{4.3}$$

The equation for the motion of a salt-water particle along the z'-axis is then according to (1:6.16):

$$\frac{dz'_m}{dt'} = v'_{Tz}(0, z'_m) - z'_m + z'_o \tag{4.4}$$

Here $z' = z'_m$ is the position of a particle that starts at z'_o at $t' = 0$. The formula is in dimensionless form. The length scale L_1 was equal to $\sqrt{4at_o}$. The corresponding formula with dimensions becomes ($z'_m = z_m/L_1$, $z'_o = z_o/L_1$, $t' = t/t_c$, $v'_{Tz} = v_{Tz}/v_{f1} = t_c v_{Tz}/L_1$):

$$\frac{dz_m}{dt} = v_{Tz}(0, z_m) - \frac{z_m - z_o}{t_c} \tag{4.5}$$

We must use this form since the superposition involves a time-dependent scale length $L_1 = \sqrt{4a(t_o - t')}$. The characteristic time t_c is given by (2.17). The considered particle starts at $(0, z_o)$:

$$z_m(0) = z_o \tag{4.6}$$

Eq. (4.5) with the above initial condition is a nonlinear first order differential equation.

It should be noted that we are using two time concepts here. The flow field from the time-dependent heat release $Q(t')$, $0 < t' < t_o$, is considered at a time t_o, while the time t in the equation above concerns the much faster process of salt-induced motion.

The velocity $v_{Tz}(0,z)$ depends on the considered heat source. We will have one expression for the exponentially decreasing point source in Section 4.2, and another one for the line source in Section 4.3. The differential equation may be integrated directly, when t is considered as a function of z_m. We have, as in (1:6.19), from (4.5-6):

$$t = t_c \cdot \int_{z_o}^{z_m} \frac{ds}{t_c \cdot v_{Tz}(0,s) - s + z_o} \tag{4.7}$$

It is straightforward to perform this integration numerically for any function $v_{Tz}(0,s)$. The time becomes infinite for a certain $z_m > z_o$, at which the denominator is zero. This z_m gives the largest upward displacement $z_{max}(z_o)$.

4.1.3 Buoyancy balance formula

The differential equation (4.4) describes the motion of a salt-water particle along the z-axis. There is a time-independent upward flow $v_T(0, z)$ due to the thermal buoyancy. The salt-water particle retains its original salt concentration at $z = z_o$. The downward salt-density force is given by $(z_m - z_o)/t_c$. It increases as the particle moves upwards. The two buoyancy forces from temperature and salt concentration will balance each other at a certain $z_m - z_o$:

$$v_{Tz}(0, z_m) = \frac{z_m - z_o}{t_c} \tag{4.8}$$

The particle velocity dz_m/dt is then zero according to (4.5).

This position gives the *largest upward displacement* $z_{max}(z_o)$ for a particle that starts at $z = z_o$ on the z-axis. We have the following general buoyancy balance formula, which gives for the largest upward displacement:

$$z_m - z_o = t_c \cdot v_{Tz}(0, z_m) \qquad z_m = z_{max}(z_o) \tag{4.9}$$

4.2 Point heat source

The point heat source considered in [1] released all heat E_o (J) instantaneously at $t = 0$. We now have an exponentially decreasing heat release at the point $(0, y_o, 0)$ with the decay time t_d:

$$Q(t) = \frac{E_o}{t_d} e^{-t/t_d} \qquad \text{(W)} \tag{4.10}$$

The total amount of released heat is still E_o:

$$\int_0^\infty Q(t)dt = E_o \qquad \text{(J)} \tag{4.11}$$

The case with several components with different decay times t_{dj} will also be considered:

$$Q(t) = E_o \sum_j \frac{\beta_j}{t_{dj}} e^{-t/t_{dj}} \tag{4.12}$$

Here, $\beta_j E_o$ denotes the total release with the decay time t_{dj}. The fractions β_j are positive and their sum is $+1$:

$$\beta_j > 0 \quad , \qquad \sum_j \beta_j = 1 \tag{4.13}$$

The total amount of released heat is then E_o.

4.2.1 Temperature-induced flow

The temperature flow component $v_{Tz}(x,z)$ for the instantaneous point source is given by (1:6.8) in [1]. The scale length L_1 will now depend on the integration variable t':

$$L_1 = \sqrt{4a\,(t_o - t')} \tag{4.14}$$

We have from (1:6.8) with $x' = 0$:

$$v'_{Tz}(0,z') = \frac{A_o}{2} \cdot \frac{1 - e^{-(z')^2}}{(z')^2} \qquad z' = \frac{z}{\sqrt{4a(t_o - t')}} \tag{4.15}$$

The dimensionless flow intensity factor A_o, taken for $E_o = 1$ and with t_o replaced by $t_o - t'$, is given by (1:6.5):

$$A_o|_{\{E_o=1, t_o \to t_o - t'\}} = \frac{\tilde{\alpha}}{\pi\sqrt{\pi}} \cdot \frac{1}{[4a\,(t_o - t')]^2} \cdot e^{-y_o^2/[4a(t_o - t')]} \tag{4.16}$$

Here we have introduced the notation:

$$\tilde{\alpha} = \frac{\alpha_T}{\alpha_c c_z^o C} \qquad (\mathrm{m}^4/\mathrm{J}) \tag{4.17}$$

This is a *buoyancy parameter* that is related to the balance between temperature and salt concentration buoyancy. The quantity $\tilde{\alpha}E_o$ has the dimension m^4, i.e. $\sqrt[4]{\tilde{\alpha}E_o} = \tilde{\ell}_o$ is a length. We have for this length:

$$\alpha_c c_z^o \cdot \tilde{\ell}_o = \alpha_T \cdot \frac{E_o}{C \cdot \tilde{\ell}_o^3} \qquad \tilde{\ell}_o = \sqrt[4]{\tilde{\alpha}E_o} \tag{4.18}$$

The right-hand side represents a thermal buoyancy force for the temperature $E_o/\left(C \cdot \tilde{\ell}_o^3\right)$, and the left-hand side the buoyancy from a salt gradient c_z^o over the length $\tilde{\ell}_o$.

The dimensionless velocity is to be multiplied by the velocity scale factor v_{f1}:

$$v_{Tz}(0,z) = v_{f1} \cdot v'_{Tz}(0,z') \qquad v_{f1} = \frac{L_1}{t_c} = \frac{\sqrt{4a\,(t_o - t')}}{t_c} \tag{4.19}$$

The total velocity is obtained with the superposition formula (4.2):

$$v_{Tz}(0,z) = \int_0^{t_o} \frac{\sqrt{4a\,(t_o - t')}}{t_c} \cdot v'_{Tz}(0,z')\bigg|_{\{E_o=1, t_o \to t_o - t'\}} \cdot \frac{E_o}{t_d} e^{-t'/t_d} dt' \tag{4.20}$$

Insertion of (4.15) and (4.16) gives:

$$v_{Tz}(0,z) = \frac{1}{t_c} \cdot \frac{1}{2\pi\sqrt{\pi}} \int_0^{t_o} \frac{\tilde{\alpha}E_o}{z^2\sqrt{4a\,(t_o - t')} \cdot t_d} \cdot e^{-y_o^2/[4a(t_o - t')]} \cdot$$

$$\cdot \left[1 - e^{-z^2/[4a(t_o - t')]}\right] \cdot e^{-t'/t_d} dt' \tag{4.21}$$

With the substitution $t_o - t' = t_d \cdot s^2$, we get the following expression for the velocity:

$$v_{Tz}(0,z) = \frac{1}{t_c} \cdot \frac{\tilde{\alpha} E_o}{\pi \sqrt{\pi} z^2 \sqrt{4at_d}} \cdot$$

$$\cdot \int_0^{\sqrt{t_o/t_d}} \left(e^{-y_o^2/(4at_d s^2)} - e^{-(y_o^2+z^2)/(4at_d s^2)} \right) \cdot e^{-t_o/t_d + s^2} ds \qquad (4.22)$$

The distance from the point source to the flow plane $y = 0$ is y_o. The *highest* velocities are obtained for $y_o = 0$:

$$v_{Tz}(0,z)|_{y_0=0} = \frac{1}{t_c} \cdot \frac{\tilde{\alpha} E_o}{\pi \sqrt{\pi} z^2 \sqrt{4at_d}} \cdot e^{-t_o/t_d} \cdot \int_0^{\sqrt{t_o/t_d}} e^{s^2} \cdot \left(1 - e^{-z^2/(4at_d s^2)}\right) ds \quad (4.23)$$

4.2.2 Largest upward displacement

The largest upward displacement is given by the solution of (4.9). With the velocity (4.22), this gives the equation for $z_{max}(z_o)$:

$$z_m^2 (z_m - z_o) = \frac{1}{\pi \sqrt{\pi}} \cdot \frac{\tilde{\alpha} E_o}{\sqrt{4at_d}} \cdot e^{-t_o/t_d} \cdot \int_0^{\sqrt{t_o/t_d}} e^{s^2} \left(e^{-y_o^2/(4at_d s^2)} - e^{-(y_o^2+z_m^2)/(4at_d s^2)} \right) ds$$

$$z_m = z_{max}(z_o) \qquad (4.24)$$

The dimensionless solution $z_m/\sqrt{4at_d}$ depends on the dimensionless parameters $z_o/\sqrt{4at_d}$, $\tilde{\alpha}E_o/(4at_d)^2$, t_o/t_d and $y_o/\sqrt{4at_d}$.

We are in particular interested in the case $z_o = 0$. The largest upward displacement is obtained for $y_o = 0$. We have in this case:

$$z_m^3 = \frac{1}{\pi \sqrt{\pi}} \cdot \frac{\tilde{\alpha} E_o}{\sqrt{4at_d}} \cdot e^{-t_o/t_d} \cdot \int_0^{\sqrt{t_o/t_d}} e^{s^2} \left(1 - e^{-z_m^2/(4at_d s^2)}\right) ds$$

$$z_m = z_{max}(0) \qquad (z_o = 0, \quad y_o = 0) \qquad (4.25)$$

The second factor of the integrand lies between 0 and 1:

$$0 \le 1 - e^{-z_m^2/(4at_d s^2)} < 1 \qquad (4.26)$$

This gives an *upper* limit on $z_{max}(0)$:

$$[z_{max}(0)]^3 \le \frac{1}{\pi \sqrt{\pi}} \cdot \frac{\tilde{\alpha} E_o}{\sqrt{4at_d}} \cdot e^{-t_o/t_d} \cdot \int_0^{\sqrt{t_o/t_d}} e^{s^2} ds \qquad (4.27)$$

This expression is our final formula to assess the largest upward displacement for a given t_o:

$$z_{max}(0) \le \frac{1}{\sqrt{\pi}} \sqrt[3]{\frac{\tilde{\alpha} E_o}{\sqrt{4at_d}} \cdot F\left(\sqrt{t_o/t_d}\right)} \qquad (4.28)$$

Here, the so-called Dawson integral, [2B], is introduced:

$$F(\tau) = e^{-\tau^2} \cdot \int_0^{\tau} e^{s^2} ds \qquad (4.29)$$

The integral is given in tables and diagrams in [2B].

The above formulas use the upper limit +1 of (4.26). For small $z_m = z_{max}(0)$ (compared to $\sqrt{4at_d}$), we can expect that the factor (4.26) in (4.25) gives a distinctly lower estimate than (4.28). But this result will be sufficient for our purposes, so we do not investigate this further.

The formula in [1] for $z_{max}(0)$, (1:6.38), contained the distance y_o to the flow plane in the denominator. It could not be used for small y_o. There was a singularity when the heat source lies in the flow plane $y = 0$. The singularity occurred, when all heat was released instantaneously. The singularity is removed, when the heat is released continuously. This is a gratifying improvement as we do not know, where a potential fracture plane lies. With this improved formula, *it does not matter* any more, where a fracture plane lies! The formula considers the worst case with the canisters lying directly in the fracture plane.

4.2.3 Dependence on t_o

The time t_o, at which the temperature field and the ensuing flow component $\vec{v}_T$ is taken, may be chosen at will. The t_o-dependence of $z_{max}(0)$ is determined by the Dawson integral $F(\tau)$, (4.28-29). A few values of $F(\tau)$ from [2B] are:

τ	0	0.2	0.5	0.75	0.924	1	1.25	1.5	2	3	5
$F(\tau)$	0	0.195	0.424	0.523	0.541	0.538	0.496	0.428	0.301	0.178	0.102

We have for small and large τ:

$$F(\tau) \simeq \tau - \frac{2}{3}\tau^3 \qquad 0 \le \tau < 0.5 \qquad (4.30)$$

$$F(\tau) \simeq \frac{1}{2\tau} \qquad \tau > 3 \qquad (4.31)$$

The function has a maximum, [2B]:

$$F_{max} = 0.541 \qquad \text{for} \quad \tau_{max} = 0.924 \qquad (4.32)$$

The largest upward displacement for *variable* t_o occurs for $\tau = \tau_{max}$ or $t_o = (0.924)^2 t_d = 0.854 t_d$. We get from (4.28):

$$z_{max}(0)|_{max t_o} \le \frac{1}{\sqrt{\pi}} \cdot \sqrt[3]{\frac{\tilde{\alpha} E_o}{\sqrt{4at_d}} \cdot F_{max}} \qquad (4.33)$$

This gives our *final* formula to assess the largest upward displacement from $z_o = 0$:

$$z_{max}(0)|_{max t_0} \le \frac{\sqrt[3]{F_{max}}}{\sqrt{\pi}} \cdot \sqrt[3]{\frac{\tilde{\alpha} E_o}{\sqrt{4at_d}}} \qquad \frac{\sqrt[3]{F_{max}}}{\sqrt{\pi}} = 0.46 \qquad (4.34)$$

The formula is valid for any t_o and y_o.

From the expansion (4.30) we have for small t_o:

$$z_{max}(0) \leq \frac{1}{\sqrt{\pi}} \cdot \sqrt[3]{\frac{\tilde{\alpha} E_o}{\sqrt{4at_d}} \cdot \sqrt{\frac{t_o}{t_d}} \left(1 - \frac{2t_o}{3t_d}\right)} \qquad t_o < t_d/4 \tag{4.35}$$

For large t_o, Eqs. (4.31) and (4.28) give:

$$z_{max}(0) \leq \frac{1}{\sqrt{\pi}} \sqrt[3]{\frac{\tilde{\alpha} E_o}{\sqrt{4at_d}} \cdot \frac{1}{2} \sqrt{\frac{t_d}{t_o}}} \quad t_o > 9t_d \tag{4.36}$$

The largest upward displacement decreases as $1/\sqrt[6]{t_o}$ as t_o increases. The decrease is slow. When the time t_o is increased by a factor hundred, then the displacement decreases by a factor two ($\sqrt[6]{100} \approx 2.2$).

4.2.4 Several decay components

The heat release with several decay components is given by (4.12). The decay time of component j is t_{dj} and its fraction of the total heat release is β_j. The solution for this case is obtained by a superposition, i.e. a sum over j. In the expression (4.22) for $v_{Tz}(0, z)$, E_o is replaced by $E_o \beta_j$ and t_d by t_{dj}, and the sum over the components j is performed. This summation is straightforward to perform for all formulas.

The formula (4.28) for the largest displacement for a given t_o ($y_o = 0$) becomes:

$$z_{max}(0) \leq \frac{1}{\sqrt{\pi}} \sqrt[3]{\tilde{\alpha} E_o \cdot \sum_j \frac{\beta_j}{\sqrt{4at_{dj}}} F\left(\sqrt{t_o/t_{dj}}\right)} \tag{4.37}$$

The largest value of F for variable t_o will be different for the different components. But an upper limit is:

$$z_{max}(0)|_{max t_o} \leq \frac{\sqrt[3]{F_{max}}}{\sqrt{\pi}} \cdot \sqrt[3]{\tilde{\alpha} E_o \sum_j \frac{\beta_j}{\sqrt{4at_{dj}}}} \tag{4.38}$$

4.3 Line heat source

The line heat source with all heat released instantaneously is dealt with in Chapter 2. We will now consider an exponentially decreasing heat release. The release of heat per unit length of the line source is $q(t)$ (W/m):

$$q(t) = \frac{E_o}{H_o t_d} e^{-t/t_d} \tag{4.39}$$

The total amount of released heat per unit length is E_o/H_o:

$$\int_o^\infty q(t)dt = \frac{E_o}{H_o} \tag{4.40}$$

4.3.1 Temperature-induced flow

The temperature-induced flow component $\vec{v}_T(x,z)$ for the instantaneous line heat source is given by (2.29). The dimensionless flow $v'_{Tz}(0,z')$ is given by (2.43) and the flow intensity A_1 by (2.11). Insertion in formula (4.2) gives in the same way as in Section 4.2.1:

$$v_{Tz}(0,z) = \frac{1}{t_c} \cdot \frac{1}{2\pi\sqrt{\pi}} \int_0^{t_o} \frac{\tilde{\alpha} E_o}{z H_o \sqrt{4a(t_o - t')} \cdot t_d} e^{-y_o^2/[4a(t_o-t')]} \cdot$$

$$\cdot v_a\left(z/\sqrt{4a(t_o - t')}\right) e^{-t'/t_d} dt' \qquad (z > 0) \tag{4.41}$$

Here, the function $v_a(z')$, which is related to $v^1_{Tz}(0,z')$, (2.48), is introduced:

$$v_a(z') = 1 - e^{-(z')^2} + \sqrt{\pi} z' \mathrm{erfc}(z') = z' \cdot v^1_{Tz}(0,z') \qquad (z' > 0) \tag{4.42}$$

Formulas (4.41) and (4.42) are only valid for positive z-values.

The above formula concerns the semi-infinite line heat source. The flow for the line heat source along $0 > z > -H_o$ is obtained by the superposition (2.6). The expression with z replaced by $z + H_o$ is to be subtracted from the above expression.

With the substitution $t_o - t' = t_d \cdot s^2$, we get the following expression for the velocity:

$$v_{Tz}(0,z) = \frac{1}{t_c} \cdot \frac{1}{\pi\sqrt{\pi}} \cdot \frac{\tilde{\alpha} E_o}{z H_o \sqrt{4at_d}} \cdot \int_0^{\sqrt{t_o/t_d}} e^{-y_o^2/(4at_d s^2)} \cdot v_a\left(\frac{z}{s\sqrt{4at_d}}\right) \cdot e^{-t_o/t_d + s^2} ds \tag{4.43}$$

The highest velocities are obtained for $y_o = 0$, i.e. when the line heat source lies in flow plane $y = 0$.

4.3.2 Largest upward displacement

The largest upward displacement $z_{max}(z_o)$ is given by the solution z_m of (4.9) with $v_{Tz}(0,z)$ given by the above expression for the semi-infinite line heat source:

$$z_m(z_m - z_o) = \frac{1}{\pi\sqrt{\pi}} \cdot \frac{\tilde{\alpha} E_o}{H_o \sqrt{4at_d}} \cdot$$

$$\cdot \int_0^{\sqrt{t_o/t_d}} e^{-y_o^2/(4at_d s^2)} \cdot v_a\left(\frac{z_m}{s\sqrt{4at_d}}\right) \cdot e^{-t_o/t_d + s^2} ds \tag{4.44}$$

The dimensionless solution $z_m/\sqrt{4at_d}$ depends on the dimensionless variables $z_o/\sqrt{4at_d}$, $\tilde{\alpha} E_o / \left[H_o \cdot (4at_d)^{3/2}\right]$, t_o/t_d and $y_o/\sqrt{4at_d}$.

In the important case $y_o = 0$ and $z_o = 0$ we have:

$$z_m^2 = \frac{1}{\pi\sqrt{\pi}} \cdot \frac{\tilde{\alpha} E_o}{H_o \sqrt{4at_d}} \cdot \int_0^{\sqrt{t_o/t_d}} v_a\left(\frac{z_m}{s\sqrt{4at_d}}\right) \cdot e^{-t_o/t_d + s^2} ds$$

$$z_m = z_{max}(0) \tag{4.45}$$

The behaviour of the function $v_a(z')$ for positive z' is of interest. We have from (4.42):

$$v_a(0) = 0 \qquad v_a(\infty) = 1 \tag{4.46}$$

$$\frac{dv_a}{dz'} = \sqrt{\pi} \cdot \mathrm{erfc}(z') \tag{4.47}$$

The function increases monotonously with decreasing derivative from $v_a(0) = 0$ to $v_a(\infty) = 1$. A series expansion gives for small z':

$$v_a(z') \simeq \sqrt{\pi} z' - (z')^2 \qquad |z'| < 0.5 \tag{4.48}$$

An asymptotic expansion of erfc(z') for large z' gives, [2C]:

$$v_a(z') \simeq 1 - \frac{1}{2(z')^2} e^{-(z')^2} \qquad z' > 1.5 \tag{4.49}$$

A few values of $v_a(z')$ and the two approximations are:

z'	0	0.25	0.5	0.75	1	1.25	1.5	1.75	2
$v_a(z')$	0	0.381	0.646	0.814	0.911	0.961	0.985	0.995	0.998
(4.48)	0	0.381	0.636	0.767	-	-	-	-	-
(4.49)	-	-	-	-	-	0.933	0.977	0.992	0.998

The function $v_a(z')$ in Eq. (4.45), which gives $z_{max}(0)$, lies between 0 and 1. We get an *upper limit* for $z_{max}(0)$, if $v_a(z')$ is replaced by its largest value +1. This gives:

$$z_{max}(0) \leq \frac{1}{\pi^{3/4}} \cdot \sqrt{\frac{\tilde{\alpha} E_o}{H_o \sqrt{4 a t_d}} \cdot F\left(\sqrt{t_o/t_d}\right)} \tag{4.50}$$

Here, $F(\tau)$ is Dawson's integral (4.29):

$$F(\tau) = e^{-\tau^2} \cdot \int_0^{\tau} e^{s^2} ds. \tag{4.51}$$

4.3.3 Dependence on t_o

The dependence of $z_{max}(0)$ on t_o is, as in the very similar formulas in Section 4.2.3 for the point heat source, determined by $F(\sqrt{t_o/t_d})$.

The largest upward displacement for variable t_o occurs for $\sqrt{t_o/t_d} = \tau_{max}$, Eq. (4.32), or $t_o = 0.854 t_d$. We have as in (4.33):

$$z_{max}(0)|_{max t_o} \leq \frac{\sqrt{F_{max}}}{\pi^{3/4}} \cdot \sqrt{\frac{\tilde{\alpha} E_o}{H_o \sqrt{4 a t_d}}} \qquad \frac{\sqrt{F_{max}}}{\pi^{3/4}} = 0.31 \tag{4.52}$$

This important formula is valid for any t_o and y_o.

From the expansion (4.30) we have for small t_o:

$$z_{max}(0) \leq \frac{1}{\pi^{3/4}} \cdot \sqrt{\frac{\tilde{\alpha} E_o}{H_o \sqrt{4 a t_d}} \sqrt{\frac{t_o}{t_d}} \left(1 - \frac{2 t_o}{3 t_d}\right)} \qquad t_o < t_d/4 \tag{4.53}$$

For large t_o, we have with equation (4.31):

$$z_{max}(0) \leq \frac{1}{\pi^{3/4}}\sqrt{\frac{\tilde{\alpha}E_o}{H_o\sqrt{4at_d}} \cdot \frac{1}{2}\sqrt{\frac{t_d}{t_o}}} \qquad t_o > 9t_d \tag{4.54}$$

The largest upward displacement decreases quite slowly as $1/\sqrt[4]{t_o}$ as t_o increases. When t_o is increased by a factor hundred, then the displacement decreases by a factor 3 ($\sqrt[4]{100} \simeq 3.2$).

4.3.4 Several decay components

In the case of several decay components, we have as in Section (4.2.4) from (4.50) by superposition:

$$z_{max}(0) \leq \frac{1}{\pi^{3/4}} \cdot \sqrt{\frac{\tilde{\alpha}E_o}{H_o} \cdot \sum_j \frac{\beta_j}{\sqrt{4at_{dj}}} F\left(\sqrt{t_o/t_{dj}}\right)} \tag{4.55}$$

An upper limit for variable t_o is as in (4.38):

$$z_{max}(0)|_{max t_o} \leq \frac{\sqrt{F_{max}}}{\pi^{3/4}} \cdot \sqrt{\frac{\tilde{\alpha}E_o}{H_o} \cdot \sum_j \frac{\beta_j}{\sqrt{4at_{dj}}}} \tag{4.56}$$

4.3.5 Inclined fracture plane

As in [1], we have considered a *vertical* fracture plane. The necessary modifications, when the plane is inclined an angle ϕ_c, are discussed briefly in Section 3.1 in [1].

The gravity force is reduced by the factor $\cos(\phi_c)$:

$$g \rightarrow g \cdot \cos(\phi_c) \tag{4.57}$$

Let z_v denote the vertical z-axis, while z is the vertical coordinate *along* the inclined plane. Then we have

$$z_v = z \cdot \cos(\phi_c) \tag{4.58}$$

The salt gradient along z is reduced by the factor $\cos(\phi_c)$:

$$c_z^o \rightarrow c_z^o \cdot \cos(\phi_c) \tag{4.59}$$

It should be kept in mind that c_z^o is the vertical salt gradient. The buoyancy factor (4.17) contains c_z^o, so it is modified in the following way:

$$\tilde{\alpha} \rightarrow \tilde{\alpha} \cdot \frac{1}{\cos(\phi_c)} \tag{4.60}$$

For the time-scale t_c, (2.17), we get with the substitutions (4.57) and (4.59):

$$t_c \rightarrow t_c \cdot \frac{1}{\cos^2(\phi_c)} \tag{4.61}$$

In the basic formula (4.52), we get a factor $\cos(\phi_c)$ from (4.58) and a factor $1/\sqrt{\cos(\phi_c)}$ from (4.60). For an inclined fracture plane formula (4.52) becomes:

$$z_{max}\Big|_{maxt_o} = \sqrt{\cos(\phi_c)} \cdot 0.31\sqrt{\frac{\tilde{\alpha}E_o}{H_o\sqrt{4at_d}}} \tag{4.62}$$

The formula (4.52) concerns the case when the borehole lies in the fracture plane. When the plane is inclined, the distances between the vertical line heat source and the plane will increase, which means that the driving temperature decreases. This will further diminish the largest upward flow.

Thus, the vertical plane will always give the largest upward displacement. It is the worst case.

Chapter 5

Three-dimensional groundwater flow

The studies have this far concerned two-dimensional groundwater flow in a fracture plane surrounded by impermeable rock. We will now consider another idealized case. The rock is considered as a *homogeneous* porous medium. The groundwater flow becomes three-dimensional. We will only study the analytical formulas, which give the largest upward displacement. The heat release is from the repository is as before modelled by a point source or a line source, which is either instantaneous or exponentially decreasing with time. The three-dimensional case of this chapter without any salt effects, i.e. the thermal part, has been studied by Hodgkinson [3] and Robinson [4].

5.1 Instantaneous point source

We first consider the simplest case of an instantaneous point source. The heat E_o (J) is released at (0,0,0) at $t = 0$.

5.1.1 Temperature field

The excess temperature field is given by (1:4.4):

$$T''(x, y, z, t) = \frac{E_o}{C(4\pi at)^{3/2}} \cdot e^{-\left(x^2+y^2+z^2\right)/(4at)} \tag{5.1}$$

This temperature field is considered at a time t_o. The scale length L_1 is as usual equal to $\sqrt{4at_o}$. The dimensionless excess temperature is, following Section 2.6 in [1]:

$$T'(x', y', z') = A_2 \cdot e^{-(r')^2} \tag{5.2}$$

$$r' = \sqrt{(x')^2 + (y')^2 + (z')^2} \tag{5.3}$$

$$x' = \frac{x}{\sqrt{4at_o}} \qquad y' = \frac{y}{\sqrt{4at_o}} \qquad z' = \frac{z}{\sqrt{4at_o}} \tag{5.4}$$

The dimensionless temperature amplitude becomes:

$$A_2 = \frac{1}{T_1} \cdot \frac{E_o}{C\,(4\pi a t_o)^{3/2}} \qquad \frac{1}{T_1} = \frac{\alpha_T}{\alpha_c c_z^o \sqrt{4 a t_o}} \tag{5.5}$$

or

$$A_2 = \frac{1}{\pi\sqrt{\pi}} \cdot \frac{\tilde{\alpha} E_o}{(4 a t_o)^2} \tag{5.6}$$

Here, $\tilde{\alpha}$ is given by (4.17).

The dimensionless pressure $P'_T(x, y, z)$ satisfies equation (1:3.40). Dropping primes, we have:

$$\nabla^2 P_T - \frac{\partial T}{\partial z} = 0 \tag{5.7}$$

Here, ∇^2 is the Laplace operator in *three* dimensions. The dimensionless temperature-induced flow is, (1:3.40):

$$\vec{v}_T = -\nabla P_T + T\hat{z} \tag{5.8}$$

5.1.2 Flow for $\rho = \rho(r)$

The temperature (5.2) depends on the radius r only: $T = T(r)$. As in Section 3.2 in [1], we first consider the general case with a density that only depends on r: $\rho = \rho(r)$.

Let P be the pressure and $\vec{v}$ the ensuing groundwater flow. Then we have the equations (1:3.9-10):

$$\nabla^2 P + \frac{\partial \rho}{\partial z} = 0 \qquad \rho = \rho(r) \tag{5.9}$$

$$\vec{v} = -\nabla P - \rho\hat{z} \tag{5.10}$$

As in Section 3.2.2 in [1], we consider first the simpler equation:

$$\nabla^2 U + \rho = 0 \tag{5.11}$$

The pressure P is obtained by derivation with respect to z:

$$P = \frac{\partial U}{\partial z} \tag{5.12}$$

In the case $\rho = \rho(r)$, the solution U of (5.11) depends on r only. We have for $U = U(r)$:

$$\frac{1}{r^2}\frac{d}{dr}\left(r^2 \frac{dU}{dr}\right) + \rho(r) = 0 \tag{5.13}$$

$$r^2 \frac{dU}{dr} = B_1 - \int_0^r s^2 \rho(s) ds \tag{5.14}$$

The integration constant B_1 is zero, since the solution does not have any singularity at $r = 0$. So we have:

$$\frac{dU}{dr} = -\frac{1}{r^2}\int_0^r s^2 \rho(s) ds \tag{5.15}$$

The pressure P becomes:

$$P = \frac{\partial}{\partial z}[U(r)] = \frac{dU}{dr} \cdot \frac{\partial r}{\partial z} = \frac{dU}{dr} \cdot \frac{z}{r} \tag{5.16}$$

or

$$P = -\frac{z}{r^3} \int_0^r s^2 \rho(s) ds \qquad r = \sqrt{x^2 + y^2 + z^2} \tag{5.17}$$

The dimensionless groundwater flow $\vec{v}$ is given by (5.10):

$$\vec{v} = \nabla \left(\frac{z}{r^3} \int_0^r s^2 \rho(s) ds \right) - \rho(r) \hat{z} \tag{5.18}$$

For the x-component we have:

$$v_x = \frac{\partial}{\partial x} \left(\frac{z}{r^3} \int_0^r s^2 \rho(s) ds \right) = z \cdot \left(\frac{-3}{r^4} \cdot \int_0^r s^2 \rho(s) ds + \frac{1}{r^3} \cdot r^2 \rho(r) \right) \cdot \frac{\partial (r)}{\partial x} =$$

$$= z \cdot \left(\frac{1}{r^4} \left[-s^3 \rho(s) \right]_0^r + \frac{1}{r^4} \int_0^r s^3 \frac{d\rho}{ds} ds + \frac{\rho(r)}{r} \right) \cdot \frac{x}{r} \tag{5.19}$$

or

$$v_x = \frac{xz}{r^5} \int_0^r s^3 \frac{d\rho}{ds} ds \tag{5.20}$$

There is an analogue expression for v_y. The expression for v_z may after similar calculations involving partial integration be written in the following way:

$$v_z = -\frac{2}{3} \rho(r) + \frac{3z^2 - r^2}{3r^5} \cdot \int_0^r s^3 \frac{d\rho}{ds} ds \tag{5.21}$$

The general expression for the flow from a density distribution $\rho = \rho(r)$ is now:

$$\vec{v} = -\frac{2}{3} \rho(r) \hat{z} + \left(3xz, 3yz, 2z^2 - x^2 - y^2 \right) \frac{1}{r^5} \cdot \frac{1}{3} \int_0^r s^3 \frac{d\rho}{ds} ds \tag{5.22}$$

This expression is the three-dimensional analogue of (1:3.23-25).

The flow $\vec{v}$ consists of a downward component $2\rho(r)/3$ in the $(-\hat{z})$-direction. The first factor of the second part is actually a three-dimensional dipole field:

$$\left(\frac{3xz}{r^5}, \frac{3yz}{r^5}, \frac{2z^2 - x^2 - y^2}{r^5} \right) = \nabla \left(\frac{-z}{r^3} \right) \tag{5.23}$$

The two-dimensional analogue is discussed in Section 3.2.3 in [1]. The dipole field (5.23) is multiplied by the last factor, i.e. by the integral of $s^3/3 \cdot d\rho/ds$.

5.1.3 Temperature-induced flow

For the dimensionless temperature-induced flow we have from (5.7), (5.9) and (5.2):

$$\rho(r) = -A_2 \cdot e^{-r^2} \tag{5.24}$$

The general formula (5.22) gives:

$$\vec{v}_T = A_2 \left[\frac{2}{3} e^{-r^2} \cdot \hat{z} + \left(3xz, 3yz, 2z^2 - x^2 - y^2 \right) \frac{1}{r^5} \cdot \frac{2}{3} \int_0^r s^4 \cdot e^{-s^2} ds \right] \tag{5.25}$$

The integral is determined by partial integrations:

$$\int_0^r s^4 e^{-s^2} ds = \frac{3\sqrt{\pi}}{8} \operatorname{erf}(r) - \left(\frac{r^3}{2} + \frac{3r}{4} \right) e^{-r^2} \tag{5.26}$$

Here, $\operatorname{erf}(r)$ is the error function:

$$\operatorname{erf}(r) = 1 - \operatorname{erfc}(r) = \frac{2}{\sqrt{\pi}} \int_0^r e^{-s^2} ds \tag{5.27}$$

From the above equations we have:

$$\vec{v}_T = A_2 \left[\frac{2}{3} e^{-r^2} \cdot \hat{z} + \left(3xz, 3yz, 2z^2 - x^2 - y^2 \right) \frac{1}{r^5} \cdot f_2(r) \right] \tag{5.28}$$

$$f_2(r) = \frac{\sqrt{\pi}}{4} \operatorname{erf}(r) - \left(\frac{r^3}{3} + \frac{r}{2} \right) e^{-r^2} \tag{5.29}$$

The flow along the z-axis is of particular interest. We have for $x = 0$ and $y = 0$ ($v_{Tx} = v_{Ty} = 0$):

$$v_{Tz}(0,0,z) = \frac{A_2}{z^3} \cdot \left(\frac{\sqrt{\pi}}{2} \operatorname{erf}(z) - z\, e^{-z^2} \right) \tag{5.30}$$

The above formulas are in *dimensionless* form. In order to get the real velocity, we must multiply by the velocity scale factor $v_{f1} = \sqrt{4at_o}/t_c$ and replace z by $z/\sqrt{4at_o}$. The velocity along the z-axis is then:

$$v_{Tz}(0,0,z) = \frac{\sqrt{4at_o}}{t_c} \cdot \frac{\tilde{\alpha} E_o}{\pi\sqrt{\pi}\,(4at_o)^2} \cdot \frac{\left(\sqrt{4at_o}\right)^3}{z^3} \cdot \frac{\sqrt{\pi}}{2} \cdot v_b\left(z/\sqrt{4at_o} \right) \tag{5.31}$$

or

$$v_{Tz}(0,0,z) = \frac{1}{t_c} \cdot \frac{\tilde{\alpha} E_o}{2\pi z^3} \cdot v_b\left(z/\sqrt{4at_o} \right) \tag{5.32}$$

Here, the function $v_b(z')$ is given by:

$$v_b(z') = \operatorname{erf}(z') - \frac{2z'}{\sqrt{\pi}} e^{-(z')^2} \tag{5.33}$$

For $v_b(z')$ we have:

$$v_b(0) = 0 \qquad v_b(\infty) = 1 \qquad \frac{dv_b}{dz'} = \frac{4(z')^2}{\sqrt{\pi}} e^{-(z')^2} \tag{5.34}$$

$$0 \leq v_b(z') < 1 \quad z' \geq 0 \tag{5.35}$$

$$v_b(z') \simeq \frac{4}{3\sqrt{\pi}} (z')^3 \qquad |z'| \leq 0.5 \tag{5.36}$$

5.1.4 Largest upward displacement

The largest upward displacement is, with the approximation (4.3), given by the buoyancy balance (4.8):

$$v_{Tz}(0,0,z_m) = \frac{z_m - z_o}{t_c} \tag{5.37}$$

or, inserting (5.32):

$$z_m^3 (z_m - z_o) = \frac{\tilde{\alpha} E_o}{2\pi} \cdot v_b\left(z_m/\sqrt{4at_o}\right) \qquad z_m = z_{max}(z_o) \tag{5.38}$$

Eqs.(5.34) and (5.35) show that the function $v_b(z')$ is smaller than $+1$. So we have for $z_o = 0$:

$$z_{max}(0) \leq \sqrt[4]{\frac{\tilde{\alpha} E_o}{2\pi}} \tag{5.39}$$

This estimate is valid for *any* t_o (and for any y_o).

For small z', expansion (5.36) is valid. Then we get for $z_o = 0$:

$$z_m^4 \simeq \frac{\tilde{\alpha} E_o}{2\pi} \cdot \frac{4}{3\sqrt{\pi}} \cdot \left(\frac{z_m}{\sqrt{4at_o}}\right)^3 \qquad \left(\frac{z_m}{\sqrt{4at_o}} \leq 0.5\right) \tag{5.40}$$

or

$$z_{max}(0) = \frac{2}{3\pi\sqrt{\pi}} \cdot \frac{\tilde{\alpha} E_o}{(4at_o)^{3/2}} \qquad \left(z_{max}(0) \leq \sqrt{at_o}\right) \tag{5.41}$$

5.2 Instantaneous line source

We consider a semi-infinite line heat source along the negative z-axis $(0,0,z)$, $0 > z > -\infty$. The heat release at $t = 0$ is E_o/H_o (J/m).

5.2.1 Temperature field

The excess temperature is given by (2.5) with $y_o = 0$:

$$T''(x,y,z,t) = \frac{E_o}{CH_o 8\pi at} \cdot e^{-(x^2+y^2)/(4at)} \cdot \operatorname{erfc}\left(\frac{z}{\sqrt{4at}}\right) \tag{5.42}$$

The dimensionless temperature at the chosen time t_o becomes, in analogy with the similar two-dimensional case of Section 2.1, Eqs. (2.8-12):

$$T'(x',y',z') = A_3 \cdot e^{-(x')^2-(y')^2} \cdot \frac{\sqrt{\pi}}{2} \operatorname{erfc}(z') \tag{5.43}$$

The dimensionless temperature amplitude A_3 is:

$$A_3 = \frac{1}{\pi\sqrt{\pi}} \cdot \frac{\tilde{\alpha} E_o}{H_o (4at_o)^{3/2}} \tag{5.44}$$

The derivative of T' with respect to z' becomes:

$$\frac{\partial T'}{\partial z'} = -A_3 \cdot e^{-(x')^2-(y')^2-(z')^2} \tag{5.45}$$

5.2.2 Groundwater flow

The dimensionless pressure $P_T' = P_T$ satisfies equation (5.7). Insertion of (5.45) gives:

$$\nabla^2 P_T + A_3 \cdot e^{-r^2} = 0 \tag{5.46}$$

This turns out to be our equation for U in Section 5.1.2. The pressure depends on r only: $P_T = P_T(r)$. So we have:

$$\frac{1}{r^2}\frac{d}{dr}\left(r^2 \frac{dP_T}{dr}\right) + A_3\, e^{-r^2} = 0 \tag{5.47}$$

We have as in (5.15):

$$\frac{dP_T}{dr} = -\frac{A_3}{r^2}\int_0^r s^2 e^{-s^2} ds =$$

$$= -\frac{A_3\sqrt{\pi}}{4r^2}\left[\operatorname{erf}(r) - \frac{2r}{\sqrt{\pi}}e^{-r^2}\right] \tag{5.48}$$

The dimensionless, temperature-induced groundwater flow becomes:

$$\vec{v}_T = -\nabla P_T + T\hat{z} = \frac{A_3\sqrt{\pi}}{4r^2}\left[\operatorname{erf}(r) - \frac{2r}{\sqrt{\pi}}e^{-r^2}\right] \cdot \nabla(r) + T\hat{z} \tag{5.49}$$

or

$$\vec{v}_T = \frac{A_3\sqrt{\pi}}{4r^2}\left[\operatorname{erf}(r) - \frac{2r}{\sqrt{\pi}}e^{-r^2}\right] \cdot \hat{r} + A_3 \cdot e^{-x^2-y^2} \cdot \frac{\sqrt{\pi}}{2}\operatorname{erfc}(z)\hat{z} \tag{5.50}$$

$$\hat{r} = \left(\frac{x}{r}, \frac{y}{r}, \frac{z}{r}\right)$$

The upward flow along the z-axis becomes ($x = 0, y = 0$):

$$v_{Tz}(0,0,z) = A_3 \cdot \frac{\sqrt{\pi}}{4z^2}\left[\operatorname{erf}(z) - \frac{2z}{\sqrt{\pi}}e^{-z^2} + 2z^2 \operatorname{erfc}(z)\right] \tag{5.51}$$

The above equations are all in *dimensionless* form. The real velocity becomes as in (5.31):

$$v_{Tz}(0,0,z) = \frac{\sqrt{4at_o}}{t_c} \cdot \frac{1}{\pi\sqrt{\pi}} \cdot \frac{\tilde{\alpha}E_o}{H_o\,(4at_o)^{3/2}} \cdot \frac{\sqrt{\pi}}{4} \cdot \frac{4at_o}{z^2} \cdot v_c\left(z/\sqrt{4at_o}\right) \tag{5.52}$$

or

$$v_{Tz}(0,0,z) = \frac{1}{t_c} \cdot \frac{1}{4\pi} \cdot \frac{\tilde{\alpha}E_o}{H_o z^2} \cdot v_c\left(z/\sqrt{4at_o}\right) \tag{5.53}$$

Here, the following function is introduced:

$$v_c(z') = \operatorname{erf}(z') - \frac{2z'}{\sqrt{\pi}}e^{-(z')^2} + 2(z')^2 \operatorname{erfc}(z') \tag{5.54}$$

We have for $v_c(z')$:

$$v_c(0) = 0 \qquad v_c(\infty) = 1 \tag{5.55}$$

$$\frac{dv_c}{dz'} = 4z' \operatorname{erfc}(z') > 0 \qquad z' > 0 \tag{5.56}$$

$$0 \le v_c(z') \le 1 \quad \text{for} \quad 0 \le z' \le \infty \tag{5.57}$$

5.2.3 Largest upward displacement

The buoyancy balance equation (4.8) with the velocity (5.53) gives the largest upward displacement $z_{max}(z_o)$ as the solution of:

$$z_m^2\left(z_m - z_o\right) = \frac{\tilde{\alpha} E_o}{4\pi H_o} \cdot v_c\left(z_m/\sqrt{4at_o}\right) \qquad z_{max}(z_o) = z_m \tag{5.58}$$

We are in particular interested in the solution for $z_o = 0$:

$$z_m = \sqrt[3]{\frac{\tilde{\alpha} E_o}{4\pi H_o} \cdot v_c\left(z_m/\sqrt{4at_o}\right)} \qquad z_m = z_{max}(0) \tag{5.59}$$

The function $v_c(z')$ is smaller than $+1$ for positive z', Eq.(5.57). We have the following *final formula* to assess the largest upward displacement from an instantaneous line heat source in a homogeneous porous medium:

$$z_{max}(0) \leq \sqrt[3]{\frac{\tilde{\alpha} E_o}{4\pi H_o}} \tag{5.60}$$

The formula does not contain the time t_o, so it is valid for *any* t_o. In the two-dimensional case, there is a singularity for $t_o = 0$, Eq. (2.63). This problem does not occur for three-dimensional groundwater flow. The formula concerns a semi-infinite line source, but it is of course also valid for any line source of finite length.

5.3 Exponentially decreasing point source

The largest upward displacement is obtained, when all heat is released instantaneously at $t = 0$ and $y = 0$. In the case of two-dimensional groundwater flow in a fracture plane, the maximum became infinite for $t_o = 0$. This singularity was removed, when exponentially decreasing heat release was considered.

Formulas (5.39) and (5.60) show that this singularity problem with respect to t_o does not exist in the case of three-dimensional groundwater flow in a homogeneous porous medium. There is not the same need to consider exponentially decreasing heat release. But for the sake of completeness, we will give the formulas in these cases also for the point and line heat sources.

We consider an exponentially decreasing point heat source at $(0,0,0)$. The rate of heat release $Q(t)$ is given by (4.10):

$$Q(t) = \frac{E_o}{t_d} \cdot e^{-t/t_d} \qquad \text{(W)} \tag{5.61}$$

5.3.1 Groundwater flow

The corresponding case for two-dimensional groundwater flow is dealt with in Section 4.2.1. The solution is obtained by integration over $0 \leq t' \leq t_o$ of the flow from the instantaneous point heat source. Here, the three-dimensional solution (5.32) is to be used. The time t_o is to be replaced by $t_o - t'$ and E_o by $Q(t')dt'$. We get by integration of (5.32) multiplied $Q(t')dt'$:

$$v_{Tz}(0,0,z) = \frac{1}{t_c} \cdot \frac{\tilde{\alpha}}{2\pi z^3} \cdot \int_0^{t_o} v_b\left(z/\sqrt{4a(t_o - t')}\right) \cdot \frac{E_o}{t_d} e^{-t'/t_d} dt' \tag{5.62}$$

With the substitution $t_o - t' = t_d \cdot s^2$ we get:

$$v_{Tz}(0,0,z) = \frac{1}{t_c} \cdot \frac{\tilde{\alpha} E_o}{\pi z^3} \cdot \int_0^{\sqrt{t_o/t_d}} v_b\left(\frac{z}{s\sqrt{4at_d}}\right) \cdot e^{-t_o/t_d + s^2} \cdot s\, ds \tag{5.63}$$

5.3.2 Largest upward displacement

The largest upward displacement is given by the solution of the buoyancy balance (4.8):

$$z_m^3(z_m - z_o) = \frac{\tilde{\alpha} E_o}{\pi} \cdot \int_0^{\sqrt{t_o/t_d}} v_b\left(\frac{z_m}{s\sqrt{4at_d}}\right) \cdot e^{-t_o/t_d + s^2} \cdot s\, ds \tag{5.64}$$

$$z_m = z_{max}(z_o)$$

This equation has to be solved numerically.

The function $v_b(z')$ is smaller than $+1$, (5.35). For $z_o = 0$, this gives the following estimate for $z_m = z_{max}(0)$:

$$z_m^4 \leq \frac{\tilde{\alpha} E_o}{\pi} \cdot \int_0^{\sqrt{t_o/t_d}} 1 \cdot e^{-t_o/t_d + s^2} \cdot s\, ds = \frac{\tilde{\alpha} E_o}{2\pi}\left(1 - e^{-t_o/t_d}\right) \tag{5.65}$$

or

$$z_{max}(0) \leq \sqrt[4]{\frac{\tilde{\alpha} E_o}{2\pi}\left(1 - e^{-t_o/t_d}\right)} \tag{5.66}$$

In the limit $t_o = \infty$, we recover the basic formula (5.39).

5.4 Exponentially decreasing line source

The heat release of the exponentially decreasing line heat source is given by (4.39):

$$q(t) = \frac{E_o}{H_o t_d} e^{-t/t_d} \qquad \text{W/m} \tag{5.67}$$

5.4.1 Groundwater flow

The corresponding two-dimensional case is dealt with in Section 4.3.1. The velocity (5.53) is to be used. The time t_o is replaced by $t_o - t'$ and E_o/H_o by $q(t')\,dt'$. Integration in t' gives:

$$v_{Tz}(0,0,z) = \frac{1}{t_c} \cdot \frac{\tilde{\alpha}}{4\pi z^2} \cdot \int_0^{t_o} v_c\left(z/\sqrt{4a\,(t_o - t')}\right) \cdot \frac{E_o}{H_o t_d} e^{-t'/t_d} dt' \tag{5.68}$$

With the substitution $t_o - t' = t_d \cdot s^2$, we get

$$v_{Tz}(0,0,z) = \frac{1}{t_c} \cdot \frac{\tilde{\alpha} E_o}{2\pi z^2 H_o} \cdot \int_0^{\sqrt{t_o/t_d}} v_c\left(z/\left[s\sqrt{4at_d}\right]\right) \cdot e^{-t_o/t_d + s^2} \cdot s\, ds \tag{5.69}$$

The function $v_c(z')$ is given by (5.54).

5.4.2 Largest upward displacement

The largest upward displacement is determined from the buoyancy balance (4.8):

$$z_m^2(z_m - z_o) = \frac{\tilde{\alpha} E_o}{2\pi H_o} \cdot \int_0^{\sqrt{t_o/t_d}} v_c\left(z/\left[z\sqrt{4at_d}\right]\right) \cdot e^{-t_o/t_d+s^2} \cdot s\,ds \tag{5.70}$$

$$z_m = z_{max}(z_o)$$

This equation has to be solved numerically.

The function $v_c(z')$ is smaller than $+1$, Eq. (5.57). For $z_o = 0$, this gives the following estimate for $z_m = z_{max}(0)$:

$$z_m^3 \leq \frac{\tilde{\alpha} E_o}{2\pi H_o} \cdot \int_0^{\sqrt{t_o/t_d}} 1 \cdot e^{-t_o/t_d+s^2} \cdot s\,ds = \frac{\tilde{\alpha} E_o}{4\pi H_o}\left(1 - e^{t_o/t_d}\right) \tag{5.71}$$

or

$$z_{max}(0) \leq \sqrt[3]{\frac{\tilde{\alpha} E_o}{4\pi H_o}\left(1 - e^{-t_o/t_d}\right)} \tag{5.72}$$

In the limit $t_o = \infty$, we obtain the basic formula (5.60).

Chapter 6

Largest upward displacement

A number of formulas for the largest upward displacement of groundwater from the top of the nuclear waste repository has been derived. In Section 6.1, a survey of formulas is given. In Section 6.2, the formulas are applied to the SKB concept shown in Figure 1.1.

The important question of sensitivity of the parameters is discussed in Section 6.3.

The formulas concern a single borehole or a single point heat source. The effect of influence between boreholes is studied in Section 6.4. It is shown that the influence may be neglected for the planned spacing $D = 500$ m between the boreholes.

6.1 Survey of formulas

A number of formulas for the largest upward displacement $z_{max}(0)$ have been derived. They always give an *upper limit* under the stated conditions. The formulas are normally more correct for large values of $z_{max}(0)$, while they often overestimate the upward displacement for small $z_{max}(0)$. But the formulas are always on the safe side.

All formulas contain the buoyancy parameter $\tilde{\alpha}$, (4.17):

$$\tilde{\alpha} = \frac{\alpha_T}{\alpha_c c_z^o C} \qquad (\mathrm{m}^4/\mathrm{J}) \tag{6.1}$$

The total heat release of the point or line source is E_o (J). The quantity $\tilde{\alpha}E_o$, which occurs in all formulas, has the dimension m^4.

The first study [1] and Chapters 2 to 4 deal with the case of **two-dimensional** groundwater flow in a fracture plane.

For an *instantaneous point heat source*, Eqs. (6.38-39) in [1] read:

$$z_{max}(0) = 0.34 \cdot \sqrt[3]{\frac{\tilde{\alpha}E_o}{y_o}} \tag{6.2}$$

This is the largest upward displacement (for any time t_o), when the distance to the flow plane is y_o. For an *instantaneous line heat source*. Eqs. (2.65-66) read:

$$z_{max}(0) = 0.20 \cdot \sqrt{\frac{\tilde{\alpha}E_o}{H_o y_o}} \tag{6.3}$$

For an *exponentially decreasing point heat source*, Eq. (4.34) reads:

$$z_{max}(0) = 0.46 \cdot \sqrt[3]{\frac{\tilde{\alpha} E_o}{\sqrt{4at_d}}} \tag{6.4}$$

The formula concerns the worst case $y_o = 0$, but it is also valid as an upper estimate for *any* value of the distance y_o to the fracture plane. Here, t_d (s) is the decay time, and a (m^2/s) the thermal diffusivity. The quantity $\sqrt{4at_d}$ has the dimension of a length.

For an *exponentially decreasing line heat source*, Eq. (4.52) reads:

$$z_{max}(0) = 0.31 \cdot \sqrt{\frac{\tilde{\alpha} E_o}{H_o\sqrt{4at_d}}} \tag{6.5}$$

The formula concerns the worst case $y_o = 0$, but it is as (6.4) valid for *any* y_o. Formula (6.5) concerns a semi-infinite line source. It gives an upper limit for any line source of finite length H_o. The semi-infinite approximation gives a negligible overestimation in our applications ($H_o \simeq 2000$ m). The exponential decay may involve *several decay times*, t_{dj}. Eq. (4.56) reads:

$$z_{max}(0) = 0.31 \cdot \sqrt{\frac{\tilde{\alpha} E_o}{H_o} \cdot \sum_j \frac{\beta_j}{\sqrt{4at_{dj}}}} \tag{6.6}$$

Here, $\beta_j E_o$ is the total amount of released heat with the decay time t_{dj}.

In Chapter 5, the ground is treated as a homogeneous porous medium. The groundwater flow is **three-dimensional**.

For an instantaneous *point heat source*, Eq.(5.39) reads:

$$z_{max}(0) = \sqrt[4]{\frac{\tilde{\alpha} E_o}{2\pi}} \tag{6.7}$$

For an instantaneous *line heat source*, Eq.(5.60) reads:

$$z_{max}(0) = \sqrt[3]{\frac{\tilde{\alpha} E_o}{4\pi H_o}} \tag{6.8}$$

The above two formulas for the three-dimensional case concern the instantaneous heat source with all heat released at $t = 0$. This is the worst case, so the formulas are also valid (as an upper estimate) for any exponentially decreasing heat release.

6.2 Application to SKB repository

In the numerical application of the formulas to the SKB repository, the same data as in [1] are used. The data (1:3.55) concern granitic rock with a salt concentration gradient of 2% per 1000 m. The data of Section 6.6 are also used. The considered 300 canisters release totally the heat $E_o = 0.32$ TWh with a main decay component $t_d = 46$ years. We have from (1:6.52-55) and (1:3.55):

$$\tilde{\alpha} = \frac{\alpha_T}{\alpha_c c_z^o C} = 6.43 \cdot 10^{-6} \text{ m}^4/\text{J} \qquad E_o = 1.16 \cdot 10^{15} \text{ J} \qquad H_o = 2000 \text{ m} \tag{6.9}$$

$$y_o = 100 \text{ m} \qquad t_d = 46 \text{ years} \qquad a = 1.62 \cdot 10^{-6} \text{ m}^2/\text{s} \tag{6.10}$$

This gives:

$$\tilde{\alpha} \cdot E_o = 7.46 \cdot 10^9 \text{ m}^4 \qquad \sqrt{4at_d} = 97 \text{ m} \tag{6.11}$$

Formula (6.2) for the instantaneous point heat source with flow in a fracture plane lying 100 m away gives:

$$z_{max}(0) = 0.34 \cdot \sqrt[3]{\frac{7.46 \cdot 10^9}{100}} = 143 \text{ m} \tag{6.12}$$

This was given in [1], (1:6.56). Formula (6.3) for the instantaneous line heat source gives:

$$z_{max}(0) = 0.20 \cdot \sqrt{\frac{7.46 \cdot 10^9}{2000 \cdot 100}} = 39 \text{ m} \tag{6.13}$$

The spreading of the heat release along the borehole over 2000 m reduces the largest upward displacement from the top of the line heat source considerably ($39/143 = 0.27$).

Formula (6.4) for an exponentially decreasing point heat source gives:

$$z_{max}(0) = 0.46 \cdot \sqrt[3]{\frac{7.46 \cdot 10^9}{97}} = 196 \text{ m} \tag{6.14}$$

Here, the fracture plane may go directly through the point source ($y_o = 0$). Formula (6.5) for an exponentially decreasing line heat source gives:

$$z_{max}(0) = 0.31 \cdot \sqrt{\frac{7.46 \cdot 10^9}{2000 \cdot 97}} = 61 \text{ m} \tag{6.15}$$

We see again that line source gives a considerably reduction of $z_{max}(0)$ compared to the point source ($61/196=0.31$). The value 61 m concerns the worst case, when the line source lies directly in the fracture plane ($y_o = 0$).

The exponentially decreasing heat release contains in reality different decay times. The two main components are according to (1:6.52-53):

$$t_{d1} = 46 \text{ years} \qquad \beta_1 = 0.75 \tag{6.16}$$

$$t_{d2} = 780 \text{ years} \qquad \beta_2 = 0.25 \tag{6.17}$$

Formula (6.6) gives for this case:

$$z_{max}(0) = 0.31 \cdot \sqrt{\frac{7.46 \cdot 10^9}{2000} \cdot \left(\frac{0.75}{97} + \frac{0.25}{97 \cdot \sqrt{780/46}} \right)} = 55 \text{ m} \tag{6.18}$$

The use of two decay components reduces the value by 10%. It is for our purpose sufficient to use the main decay time (46 years).

The last two formulas (6.7) and (6.8) concern the case, when the rock is treated as a homogeneous porous medium with three-dimensional groundwater flow. Formula (6.7) for the point heat source gives:

$$z_{max}(0) = \sqrt[4]{\frac{7.46 \cdot 10^9}{2\pi}} = 186 \text{ m} \tag{6.19}$$

Formula (6.8) for the line heat source gives:

$$z_{max}(0) = \sqrt[3]{\frac{7.46 \cdot 10^9}{4\pi \cdot 2000}} = 67 \text{ m} \tag{6.20}$$

These two values concern the instantaneous heat source. An exponential decrease would give smaller values. The values are to be compared with (6.12) and (6.13). But the values are not directly comparable, since the values 143 and 39 m concern a fracture at a distance of 100 m, while the values 186 and 67 m concern the three-dimensional porous medium with direct contact between the heat sources and the groundwater.

The SKB concept concerns a line heat source with an exponentially decreasing heat release. Formula (6.5) is therefore the one to use. The **final assessment** for the largest upward displacement from the top of the canisters in a borehole is then for the assumed data:

$$\boxed{z_{max}(0) \simeq 60 \text{ m}} \tag{6.21}$$

This value concerns a single borehole. The influence between boreholes is discussed in Section 6.4.

6.3 Sensitivity to parameter variations

The main formula for the largest upward displacement is (6.5). We have, inserting (6.1):

$$z_{max}(0) = 0.31 \cdot \sqrt{\frac{\alpha_T E_o}{\alpha_c c_z^o C H_o \sqrt{4at_d}}} \tag{6.22}$$

The formula contains the following quantities:

- Total amount of released heat E_o (J)
- Main decay time t_d (s)
- Thermal diffusivity a (m^2/s) and volumetric heat capacity C (J/m^3K) of the rock
- Salt concentration gradient c_z^o ($(kg_s/kg_w)/m$)
- Thermal expansion coefficient α_T ($1/°C$) and relative density increase with salt concentration α_c ($1/(kg_s/kg_w)$)

The sensitivity to parameter variations is reasonably modest due to the square root:

$$\sqrt{2} = 1.4 \qquad \sqrt{10} = 3.2 \tag{6.23}$$

So a change of α_T, E_o, α_c, c_z^o, C, H_o, $\sqrt{a}$ or $\sqrt{t_d}$ by a factor 2 will change $z_{max}(0)$, by some 40%, while a change by a factor 10 changes $z_{max}(0)$ by a factor 3.

The quantities that *do not enter* into the formula are quite noteworthy. The formula is valid as an upper estimate for any position of the fracture plane. The hydraulic conductivity of the fracture plane does not enter. So this very uncertain (and spatially variable) quantity does not matter either. We believe that the formula gives the order of magnitude of the largest upward flow for **any system of fracture planes** of large extensions in all directions.

The time t_o, at which the temperature field is used, does not enter either, since we have considered the largest value for variable t_o.

6.4 Influence between boreholes

The formulas and the above figures concern a single line heat source. The SKB repository consists of some twenty boreholes drilled in a quadratic pattern with a spacing D. See Figure 1.1. The distance D is in the reference case:

$$D = 500 \text{ m} \tag{6.24}$$

This is a rather large distance compared to the range of the buoyancy flow, so we expect that the influence between the line heat sources is modest.

In order to investigate this, we consider the case of Chapter 2. The line sources release all heat at $t = 0$. The case of several boreholes is dealt with in Section 2.2.5. There are N boreholes, where borehole j lies along (x_j, y_j, z). The groundwater flow plane lies as usual at $y = 0$ (Case A in Figure 6.1).

The formula to determine the largest upward displacement is given by the largest solution z_m of (2.74) for different x'-values. We consider the case of 5x4 ($N = 20$) boreholes. See Figure 6.1.

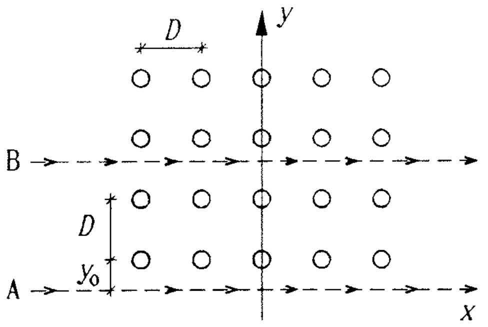

Figure 6.1. Considered 5x4 boreholes with the fracture plane at $y = 0$ (case A) or at $y = 2D$ (case B).

The data (6.9-10) and (6.24) are used. The largest upward flow of the single line source occurs for $\sqrt{4at_o} = y_o\sqrt{2}$ in (2.65) and for $\sqrt{4at_o} = y_o$ in (2.67). We will here calculate the solution for some different values of $\sqrt{4at_o}$.

Eq. (2.74) is to be solved for the borehole configuration of Figure 6.1. We have chosen the configuration so that it is symmetrical with respect to $x = 0$. The maximum (2.75) will occur for $x' = 0$. The case $N = 1$ is the reference case of a single borehole. The result is given in Table 6.1 and Figure 6.2.

$\sqrt{4at_o}$ (m)	50	100	200	500	1000	10000
t_o (years)	12	49	195	1200	4900	490000
$z_{max}(0)$ $N = 1$	4.15	19.45	11.19	2.28	0.59	0.006
$z_{max}(0)$ $N = 5 \times 4$	4.15	19.67	11.38	5.06	4.03	0.12

Table 6.1. Numerically calculated $z_{max}(0)$ for the case of a single borehole and a configuration of 5×4 boreholes. Case A with fracture plane at $y = 0$.

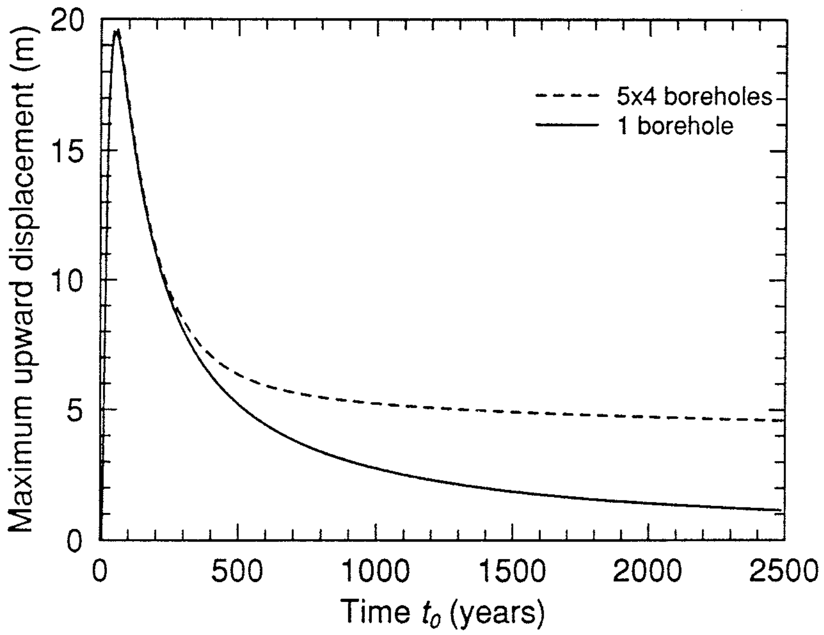

Figure 6.2. Maximum upward displacement for a single borehole and the considered case with 5x4 boreholes (D=500 m). Data according to (6.9-10). Fracture position A.

We can see from figure 6.2 that the maximum upward displacement in the fracture reaches a maximum of about 20 m for $t_0 \approx 50$ years, after which it gradually decreases to a value of about 5 m after 2500 years. During the first few hundred years there is little difference between the 5x4 configuration and the single borehole. This is just what we can expect, since the single borehole and the closest borehole of the 5x4 configuration are located at the same distance (100 m) from the point $x' = 0$ in the fracture. Other boreholes in the 5x4 configuration are found at a distance of at least 510 m from the point of maximum upward displacement in the fracture. The heat from these boreholes will start to influence the considered point after about 400 years.

It may be noted that formula (6.3) gives $z_{max}(0) = 39$ m, Eq. (6.13), and not 20 m. This discrepancy is due to the fact that A_1 is quite small here ($A_1 = 0.25$). Formula

(2.63), which gives a smaller value, is applicable. Eq. (6.3) overestimates $z_{max}(0)$ in this case.

The maximum upward displacement will depend on the distance D between the boreholes, since this also determines the distance between the boreholes and the considered point in the fracture. See Figure 6.3 where some different borehole spacings are considered.

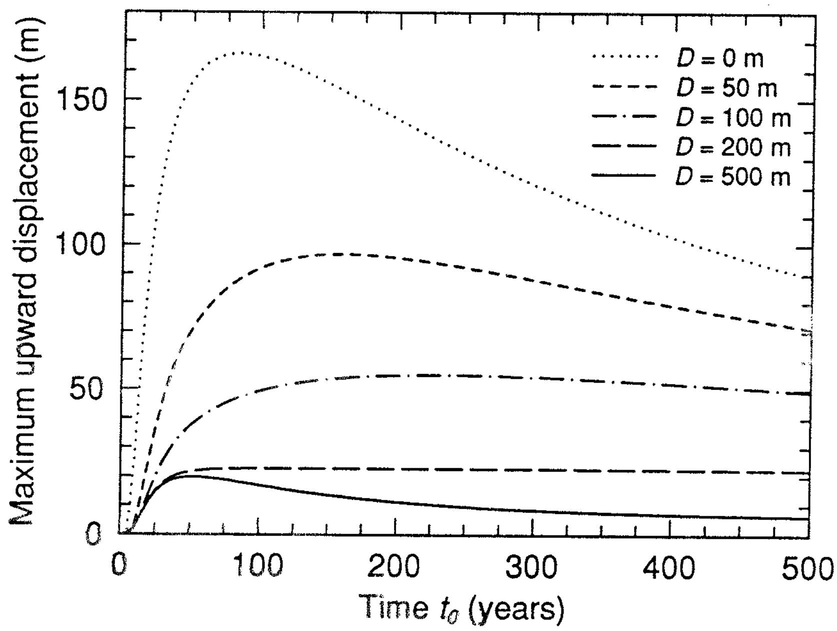

Figure 6.3. Maximum upward displacement for the considered case with 5x4 boreholes as a function of the chosen time t_0 for some different borehole spacings D. Data according to (6.9-10). Fracture position A.

The worst case is obtained for a borehole spacing D equal to zero, which practically means that all canisters are placed in the same enlarged borehole. The maximum upward displacement is then 165 m. For larger values of the borehole spacing, the maximum upward displacement rapidly becomes smaller, until reaches the value of the single borehole at $D \approx 200 - 300$ m. We see that the distance between the boreholes does not matter at all as long as it exceeds, say, 200 m.

Finally, let us consider a case where the fracture plane cuts through the center of the repository with a minimum of 100 m between the fracture and a row of boreholes. The position of the fracture is shown as case B in Figure 6.1. Figure 6.4 shows the result of the calculation.

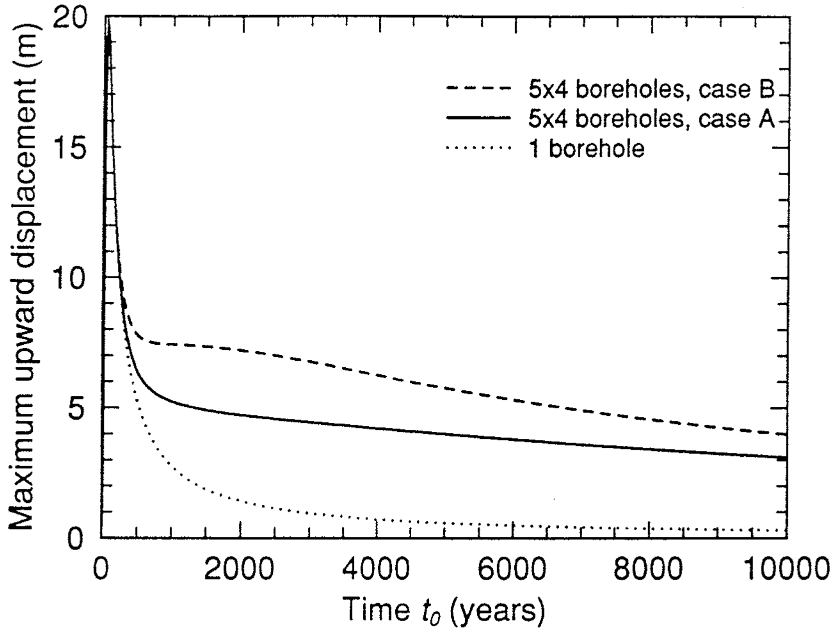

Figure 6.4. Maximum upward displacement for a single borehole and the borehole configuration with 5x4 boreholes (D = 500 m). The two positions of the fracture plane are shown as case A and B in Figure 6.1. Other data according to (6.9-10).

The behavior is the same as for the original case of Figure 6.1 for the first 500 years. The maximum value of the upward displacement attained after about 50 years is not changed.

Chapter 7

Survey of the analyses in the study

This study and the preceding one, Ref. 1, contain quite a lot of material, and many different tools of analyses are used. A survey of the line of thought and the main analyses and results is therefore presented in this chapter. The result of the first study, which is presented in a similar survey in Chapter 7 of Ref. 1, are included in a somewhat condensed form.

The study has two objectives. The first one is to gain understanding and insight into the coupled processes for heat, salt and groundwater with buoyancy due to both temperature and salt density variations. The second objective is to assess the largest upward displacement of groundwater from the canister region. In particular, we have endeavored to establish explicit formulas for the largest upward displacement of groundwater from the top of the canister row in a borehole. The released heat and the location of the canisters deep below the ground surface are given. By assumption, there is an increase downwards of the salt concentration in the undisturbed groundwater. The groundwater flow is analysed for two extreme cases. In the first case, the groundwater flow is confined to a single vertical crack or fracture plane. In the second case, the rock is considered as a homogeneous porous medium. The temperature process is three-dimensional, while the groundwater and salt flow processes are two-dimensional in the first case. In the second case, all three processes are three-dimensional.

The general governing equations for water, salt and heat are discussed in Chapter 2 in the first study, Ref. 1. The convective heat flow can be neglected in the present application with very small groundwater flows. The thermal process is then governed by pure heat conduction and by the prescribed heat sources from the canisters. This leads to the important simplification that the thermal process is independent of the groundwater and salt process.

A major assumption is the use of Boussinesq's approximation with constant water viscosity μ_{w0} and constant water density ρ_{w0} except in the buoyancy term, for which the density $\rho_w(T,c)$ in linearized using a constant thermal expansion coefficient α_T and a corresponding coefficient α_c for the variation with salt concentration. Salt dispersion and diffusion are neglected. This means that the salt is just displaced convectively with the moving groundwater. The processes take place far below the ground surface, which lies some 2 km above, so the upper boundary lies virtually at infinity. All quantities – temperature T, pressure P and salt concentration c – tend to undisturbed values far away from the canister region.

The undisturbed salt concentration $c_0(z)$ and water density increase downwards. A constant salt gradient c_z^0 ($kg_s/kg_w m$) is used. There is an undisturbed situation with a temperature $T_0(z)$ and a pressure $P_0(z)$. The deviations from equilibrium, or excess variables, for temperature, salt concentration and pressure are denoted T'', c'' and P'', respectively. The equations are transformed to a dimensionless form in Section 2.6 in Ref. 1 using scale factors L_1, $t_1 = t_c, T_1, c_1$ and P_1. The governing equations for the *dimensionless excess variables* T', c' and P' become, (2.46-51) in Ref. 1:

$$(\nabla')^2 P' + \frac{\partial c'}{\partial z'} - \frac{\partial T'}{\partial z'} = 0 \tag{7.1}$$

$$\frac{\partial c'}{\partial t'} + \nabla' \cdot \left[(-z' + c')\,\vec{v}_f'\right] = 0 \tag{7.2}$$

$$\vec{v}_f' = -\nabla' P' - c'\hat{z} + T'\hat{z} \tag{7.3}$$

$$c'\,|_{t=0} = 0 \qquad T' \quad \text{given independently} \tag{7.4}$$

The first equation (7.1) determines the pressure P' due to the dimensionless excess density distribution $\rho' = c' - T'$. The third equation gives, according to Darcy's law, the filtration velocity with which the salt is moved convectively in accordance with equation (7.2). The dimensionless salt concentration, $\tilde{c} = -z' + c'$, contains an undisturbed part $-z'$, with unit gradient in the dimensionless formulation, and an excess part c'. The value of $\tilde{c}$ is constant for a salt-groundwater 'particle' when it moves around with the velocity field $\vec{v}_f'$.

An important result, which is a consequence of the previous assumptions, is that the dimensionless equations (7.1-4) do not contain *any intrinsic parameters.* The only parameters to occur in our total process come from the scale factors and the parameters of the dimensionless temperature T'. Another important result of the dimensionless formulation is the scale factor for the time t_c ($t' = t/t_c$):

$$t_c = \frac{V_p \mu_{w0}}{k g \rho_{w0} \alpha_c c_z^0} \tag{7.5}$$

In the two-dimensional case, k/V_p is replaced by k^c/V_p^c, Eq. (3.4) in Ref. 1. This time gives a *characteristic time-scale* for flow induced by salt variations. It is noteworthy that t_c depends on salt parameters (α_c, c_z^0) and intrinsic permeability k, but it is independent of the thermal properties.

The dimensionless groundwater flow, (7.3), is according to (7.1) driven by the density $\rho' = c' - T'$, i.e. by one salt and one temperature component. These two parts will be calculated separately:

$$(\nabla')^2 P_T' - \frac{\partial T'}{\partial z'} = 0 \qquad \vec{v}_T' = -\nabla' P_T' + T'\hat{z} \tag{7.6}$$

$$(\nabla')^2 P_c' + \frac{\partial c'}{\partial z'} = 0 \qquad \vec{v}_c' = -\nabla' P_c' - c'\hat{z} \tag{7.7}$$

$$\vec{v}_f' = \vec{v}_T' + \vec{v}_c' \tag{7.8}$$

Equations (7.6) and (7.7) are of Poisson's type. The pressures P'_T and P'_c at any particular time t are determined by the source term, i.e. by the temperature field T' and the salt concentration field c' at that time. From the solutions we get the total groundwater flow $\vec{v}'_f$ according to (7.8) and (7.6-7). This flow field displaces the salt according to Eq. (7.2).

The salt process will be solved numerically with calculations in a sequence of time-steps. At each time-step, equations (7.6) and (7.7) are solved. The salt is then displaced to new positions at next time-step, and so on.

The temperature field T' is the primary driving force for the groundwater and salt processes. As the salt concentration field is displaced from its original stable values at $t = 0$, it induces a salt buoyancy component $\vec{v}_c$, which adds to $\vec{v}_T$. The intrinsic time-scales of these two processes are very different. It is shown in section 3.6 of Ref. 1 that the time-scale of the salt-induced buoyancy, t_c, lies in the range 16 hours to 90 days, while a characteristic time for variations of the thermal process is many years. This means that the salt-buoyancy process is virtually a steady-state one, which will change to new virtual steady-state conditions following the slowly varying temperature field.

We are interested in the largest upward displacement of groundwater from the canister region during a very long period (say 10 000 years), until all heat has been released and the driving excess temperature field has disappeared through thermal diffusion. It is a very cumbersome computational task to follow this whole process. However, our aim is only to assess the *largest* upward displacement, which should occur for some intermediate time, when the temperature field has so to speak its strongest effect. A considerable simplification is to use this particular temperature field only. Then we have to calculate the process for a time period of, say, $5 \cdot t_c$ only.

We proceed as follows. The temperature field is considered at a time t_0. We use this 'frozen' temperature field $T(x, y, z, t_0)$, and calculate the process (7.1-7.4) for this time-independent temperature. The salt concentration starts with the undisturbed linear values at $t = 0$. For each choice of t_0, we will obtain a largest upward displacement. Then we calculate the maximum of this largest displacement, when t_0 is varied. This maximum gives our largest upward displacement valid for any time. The difference between this assessment and the value from a more elaborate solution of the original problem should be insignificant.

The heat from the canisters is released with an exponentially decreasing effect. The main decay time, $t_d = 46$ years, accounts for 75% of the total heat E_0. A reasonable simplification, valid after say 100 years, is to release all heat instantaneously at $t = 0$. This simplification was made in the first study. The finite extension of the line heat source was also neglected. All heat E_0 was released at $t = 0$ at a single point. Thus, the case of an instantaneous point heat source was considered. The groundwater and salt flow process was confined to a fracture plane which lay at the distance y_0 from the point heat source. The final formula to assess the largest upward flow from the center became:

$$z\big|_{\text{max upward}} = 0.34 \cdot \sqrt[3]{\frac{\tilde{\alpha} E_0}{y_0}} \tag{7.9}$$

Here, $\tilde{\alpha}$ is the important buoyancy flow parameter, which accounts for coupled thermal and salt buoyancy:

$$\tilde{\alpha} = \frac{\alpha_T}{\alpha_c c_z^0 C} \tag{7.10}$$

This formula gave with SKB-data an upward displacement of 143 m for $y_0 = 100$.

The distance y_0 is unknown. A considerable flaw for the otherwise quite handy formula (7.9) is that the displacement becomes infinite for $y_0 = 0$. This problem is removed when we consider the exponentially decreasing heat release with its 'softer' driving temperature field.

The first extension of the previous study is to consider a line heat source, Chapter 2. The heat release is still instantaneous, and the groundwater and salt process is two-dimensional in a vertical fracture plane at a distance y_0 from the line heat source, which lies along the negative z-axis. The line heat source is quite long: $H_0 = 2000$ m. It may be considered as semi-infinite ($H_0 = \infty$), since we are interested in the process in a region of a few hundred meters around the top of the canister row.

The temperature field, which is considered at a time t_0, is discussed in Section 2.1. The scale length for the coordinates is $L_1 = \sqrt{4at_0}$, Eq. (2.8). The dimensionless temperature field becomes, (2.10):

$$T'(x', z') = A_1 \cdot e^{-(x')^2} \cdot \int_{z'}^{\infty} e^{-u^2} du \tag{7.11}$$

The last factor is essentially the complementary error function. The dimensionless temperature amplitude A_1, (2.11), involves $\tilde{\alpha}E_0/H$, $4at_0$ and y_0. Our problem is defined by equation (7.1-4) and (7.11). A gratifying fact, which is a consequence of the previous assumptions and analyses, is that the problem contains a *single* dimensionless parameter A_1 only.

Eq. (7.1) is, as in the first study, divided into the two parts (7.6) and (7.7). The temperature-induced flow, Eq. (7.6) with T' given by (7.11), is solved analytically in Section 2.2. The dimensionless velocity $\vec{v}_T'$ is given by (2.29).

The remaining problem for the salt and groundwater is defined by Eqs. (7.7), (7.8), (7.2) and the initial condition $c' = 0$ for $t' = 0$, (7.4). This part is solved numerically, Ch. 3.

A particular numerical technique has been developed. See Ch. 5 in Ref. 1. The numerical problem is solved for time-step after time-step. A particle-tracking technique is used. The particle (i, j) with a constant salt concentration $\tilde{c}_{ij} = -z_{ij}' + c_{ij}'$ is displaced during the time-step in accordance with the total velocity $\vec{v}_T' + \vec{v}_c'$. We obtain the salt concentration at the next time-step.

The main problem is to calculate $\vec{v}_c'$ at each time-step. We have to solve the Poisson equation (7.7). The solution to a Poisson equation is analytically given by certain integrals of the source term ($\partial c'/\partial z$ in (7.7)). The integral for $\vec{v}_c'$ is given by (5.3) in Ref. 1. The main problem in the model is to evaluate the double integral for $\vec{v}_c'$, when c' is known numerically for the moving particles $(x_{ij}(t), z_{ij}(t))$. The integral is transformed from the (x', z')-plane to the $(x', \tilde{c})$-plane. This very particular method facilitates the calculations considerably. The double-sum is approximated by a Riemann sum based on the positions and salt concentrations of the particles.

Problems for the modelling technique are discussed in Section 3.3. The particles accumulate in certain areas and separate in others. This problem is solved by insertion and removal of particles. The $\tilde{c}$-curves may lie very close to each other in certain areas. A particle may then be removed, if two curves come too close to each other at a point. A new problem compared to the previous case in Ref. 1 is that the flow velocity $\vec{v}_T'$ is quite large in the vicinity of the line heat source.

The computed groundwater and salt process is shown in Figs. 3.3-6 for $A_1 = 0.1$, 1, 10 and 30, respectively. The largest upward displacement for different A_1 is given in Table 3.1. These numerical values are compared with values from our approximate formulas, which are discussed below.

The largest upward displacement occurs due to symmetry for the particles (water + salt) that flow along the z-axis. Let $z_m(t', z_0)$ denote the particle that starts at $z_m = z_0$ at $t = 0$ (z_m and z_0 are dimensionless). We have the following equation for z_m, Eq. (7.8):

$$\frac{dz_m}{dt'} = v'_{Tz}(0, z_m) + v'_{cz}(0, z_m, t') \tag{7.12}$$

The temperature-induced velocity is known analytically, Eq. (2.43). For the salt-induced velocity we have for the z-component, Eq. (7.7):

$$v'_{cz} = -\frac{\partial P'_c}{\partial z'} - (z_m - z_0) \tag{7.13}$$

Here we have used the fact that $\tilde{c} = -z' + c'$ is constant for a given particle:

$$\tilde{c}\,|_t = \tilde{c}|_{t=0} \Leftrightarrow -z_m + c' = -z_0 + 0 \Leftrightarrow c' = z_m - z_0 \tag{7.14}$$

Equations (7.12-13) are exact. The problem is that we do not know P'_c, since the salt pressure component is obtained in the numerical calculation.

The approximate formulas are all based on the assumption that the salt pressure term $-\partial P'_c/\partial z'$ is not strongly dominating in (7.12-13). An approximation is then to *neglect this term.* The temperature-induced velocity $v'_{Tz}(0, z_m)$ decreases, when $z_m > 0$ increases, while the salt-concentration term $v'_{cz} \simeq -(z_m - z_0)$ increases in magnitude. At a certain point, which is approached asymptotically, when t' tends to infinity, they will balance each other. This buoyancy balance with upward thermal buoyancy and counteracting salt-density buoyancy determines the largest upward displacement $z'_{max}(z_0)$. We have in dimensionless form:

$$v'_{Tz}(0, z_m) = z_m - z_0 \qquad z_m = z'_{max}(z_0) \tag{7.15}$$

The corresponding equation in dimensional form is, (4.8):

$$v_{Tz}(0, z_m) = \frac{z_m - z_0}{t_c} \qquad z_m = z_{max}(z_0) \tag{7.16}$$

We are in particular interested in the largest upward displacement $z_{max}(0)$ for the particle that starts at $z_0 = 0$. All formulas to assess the largest upward displacement originate from the solution of (7.15) or (7.16) with the appropriate temperature-induced velocity.

Formula (7.15) is applied for the instantaneous line heat source in Section 2.2.3. The velocity $v'_{Tz}(0, z_m)$ is given by (2.43). The solution is illustrated graphically in Fig. 2.2 for different z_0 and A_1. The main result is, (2.52):

$$z'_{max}(0) = \sqrt{A_1/2} \tag{7.17}$$

This approximation and another one valid for small A_1 are compared to result from the numerical model in Table 3.1. The agreement is quite good. The corresponding formula for $z_{max}(0)$ (m) is Eq. (2.62). The value depends on the chosen time t_0. The final step is to consider the maximum with respect to t_0. This gives the following formula for the instantaneous line heat source, (2.65-66):

$$z|_{\text{max upward}} \simeq 0.20 \cdot \sqrt{\frac{\tilde{\alpha}E_0}{H_0 y_0}} \tag{7.18}$$

The formulas (7.9) and (7.18) for the largest upward displacement for a point and a line heat source are tested against the numerical model in the first study and in this study, respectively. The agreement is quite satisfactory for our purpose of assessment. The approximation to obtain assessment formulas is used in the rest of the study without further tests against numerical calculations.

In order to remove the flaw with the distance to the fracture plane, y_0, in the denominator of (7.17), we have to consider the exponentially decaying heat release. All heat cannot be released instantaneously.

The flow component $\vec{v}_T$ for any time-dependent heat release is obtained by a superposition integral from the solution for an instantaneous heat source. See Eq. (4.1).

The case of a point heat source with exponentially decaying heat release, (4.10), is considered in Section 4.2. We need the flow $v_{Tz}(0, z)$. The expression in dimensional form is given by (4.21). The equation for $z_m = z_{max}(z_0)$ is then given by (7.16) or (4.24). The equation involves z_0, $\tilde{\alpha}E_0$, t_0, t_d and y_0. The worst case occurs when the heat source lies directly in the fracture plane: $y_0 = 0$. The equation for $z_{max}(0)$ is then given by (4.25). Eq. (4.28) is an upper estimate. Finally, the maximum with respect to t_0 is determined. Eq. (4.34) gives the largest upward displacement for an exponentially decaying point heat source:

$$z|_{\text{max upward}} \simeq 0.46 \cdot \sqrt[3]{\frac{\tilde{\alpha}E_0}{\sqrt{4at_d}}} \tag{7.19}$$

The corresponding analysis for the line heat source is presented in Section 4.3. Eq. (4.52) is our main formula (0.1) for the largest upward displacement from an exponentially decaying line heat source:

$$z|_{\text{max upward}} \simeq 0.31 \cdot \sqrt{\frac{\tilde{\alpha}E_0}{H_0\sqrt{4at_d}}} \tag{7.20}$$

The fracture plane may lie anywhere.

The case, when the rock is considered as a *homogeneous porous medium* is treated in Chapter 5. The groundwater and salt flow process is now three-dimensional. (The problem with an unknown distance y_0 to a fracture plane disappears.)

The case with an instantaneous point heat source is discussed in Section 5.1. The dimensionless temperature field is given by (5.2). The corresponding temperature-flow $\vec{v}_T$ is calculated in Sections 5.1.2-3. The expression for $v_{Tz}(0, 0, z_m)$ is given by (5.32-33). Insertion of this in Eq. (7.16) gives $z_{max}(0)$ and, with a few estimates, the largest upward displacement, (5.39):

$$z|_{\text{max upward}} \simeq \sqrt[4]{\frac{\tilde{\alpha}E_0}{2\pi}} \tag{7.21}$$

The corresponding analysis for the instantaneous line heat source is given in Section 5.2. The dimensionless temperature field is given by (5.43), and the temperature flow $\vec{v}_T$, Eq. (5.50), is calculated in Section 5.2.2. The flow along the z-axis $v_{Tz}(0, 0, z_m)$ to be used in Eq. (7.16) is here given by (5.51). The final formula for the largest upward displacement is, (5.60):

$$z|_{\text{max upward}} \simeq \sqrt[3]{\frac{\tilde{\alpha} E_0}{4\pi H_0}} \tag{7.22}$$

This is our main formula, (0.2), for the case of homogeneous porous rock.

The expressions for exponentially decaying point and line heat sources are indicated in Section 5.3 and 5.4. The formulas become more complicated. However, the formulas (7.22) and (7.21) are sufficient for our purpose.

Section 6.1 gives a survey of the formulas for largest upward displacement, and these are applied to the SKB repository in Section 6.2. It is shown that the effect of the second decay component (t_{d2} = 780 years) is quite small.

The important question of sensitivity to parameter variations is discussed in Section 6.3.

All formulas concern a single line heat source or borehole. The question of influence between the boreholes is discussed in Section 6.4. It is shown that, for the SKB data, this influence can be neglected, since the largest upward displace due to a certain borehole occurs before the influence from adjacent boreholes becomes significant.

The analyses and final formulas of this study are based on a number of *assumptions*. A few of these are *not fulfilled* for the real process, but the discussion below will show that the results still are valid. The unfulfilled assumptions are:

- constant increase c_z^0 of salt concentration
- constant α_T
- constant viscosity
- constant permeability of fracture plane and of homogeneous rock in the case of three-dimensional ground water flow

The assumption of a constant salt increase is a simplification, but we see from the sensitive analysis in Section 6.3, that a change by a factor 10, results in a change of $\sqrt{10} \simeq 3.2$ only for $z_{max}(0)$. This assumption is therefore not a critical one, as long as there is a clear increase downwards.

The thermal expansivity α_T varies a factor 5 from T = 15 °C to T = 100 °C. See Section 3.5 in Ref. 1. The use of an intermediate value gives a variation of some 50% in the main formula (0.1), but the real error in an assessment should be even smaller. The use of a constant, intermediate α_T will certainly deform the flow pattern somewhat but the error should only be some 25% or less.

The viscosity of groundwater varies a factor 4 between 15 °C and 100 °C. Here, the argument used for α_T is valid. But the water viscosity does not enter into the formulas (0.1) and (0.2). Therefore, it should not matter much, if it is variable.

The permeability of a fracture plane or a more or less homogeneously fractured rock is certainly not constant in any real case. But the permeability does not enter into the formulas for largest upward displacement. This factor cancels in the buoyancy balance formula between v_T and v_c. The permeability enters into the time t_c, (7.5), so it influences the time-scale to attain steady-state conditions for the salt-induced process.

Nomenclature

The nomenclature of [1], pp. 66-67, is used. A few new notations have been added. An equation in the initial study [1] is referenced by putting 1: before the equation number. As an example, a reference to Eq. (2.13) of the initial study will be written as Eq. (1:2.13).

$a = \lambda/C$	thermal diffusivity of the ground	(m^2/s)
A_o	dimensionless temperature amplitude, Eq. (1:6.5)	(-)
A_1	dimensionless temperature amplitude for the line heat source, Eq. (2.11)	(-)
A_2	dimensionless temperature amplitude for the point heat source with 3-dimensional groundwater flow, Eq. (5.6)	(-)
A_3	dimensionless temperature amplitude for the line heat source with 3-dimensional groundwater flow, Eq. (5.44)	
B	width of fracture zone	(m)
c	salt concentration	(kg_s/kg_w)
c'	dimensionless excess salt concentration	(-)
c''	excess salt concentration	(kg_s/kg_w)
$\tilde{c} = -z' + c'$	dimensionless total salt concentration	(-)
$c_o(z)$	undisturbed salt concentration	(kg_s/kg_w)
$c_o^z = -dc_o/dz$	salt concentration gradient	($kg_s/kg_w m$)
c_1	scale factor for salt concentration	(kg_s/kg_w)
C	volumetric heat capacity of the ground	(J/m^3K)
d	fracture width	(m)
D	spacing between boreholes	(m)
E_{can}	total heat release from a canister	(J)
E_o	total heat release from the point source	(J)
f_ρ	radial density function, Eq. (1:3.25)	(-)
F	Dawson's integral, Eq. (4.29)	(-)
$g = 9.81$	standard gravity	(m/s^2)
h	heat source	(W/m^3)
H_o	length of line heat source	(m)
$H_o' = H_o/L_1$	dimensionless length of line heat source	(-)
k	intrinsic permeability	(m^2)
k^c	intrinsic permeability of fracture zone	(m^3)
L_1	scale factor for length coordinates	(m)
P	groundwater pressure	(Pa)
P'	dimensionless excess pressure	(-)
P''	excess pressure	(Pa)
P_1	scale factor for pressure	(Pa)
P_c, P_T	dimensionless salt and temperature components of the pressure	(-)

$\vec{q}_w = (q_{wx}, q_{wy}, q_{wz})$	volumetric groundwater flow	$(\mathrm{m}_w^3/\mathrm{m}^2\mathrm{s})$
$\vec{q}_w^{\,c}$	volumetric groundwater flow in fracture plane or fracture zone	$(\mathrm{m}_w^3/\mathrm{ms})$
$q(t)$	heat release rate per unit length of line heat source	(W/m)
$Q(t)$	heat release rate from a point source	(W)
Q_o	rate of heat release	(W)
$Q_{o,can}$	initial rate of heat release from a canister	(W)
$r = \sqrt{x^2 + z^2}$	radial distance in flow plane	(m)
r'	dimensionless radial distance	(m)
r_1	radial length	(m)
t	time	(s)
t'	dimensionless time	(-)
t_o	time at which the temperature field is taken, see Section 1:6.1	(s)
t_c	characteristic time-scale, scale factor for time	(s)
t_d	decay time for heat source, Eq. (1:4.11)	(s)
t_{dj}	decay time of heat release component j	(s)
t_T	characteristic time-scale for temperature field, Eq. (1:3.60)	(s)
T	temperature in the ground	(°C)
T'	dimensionless excess temperature	(-)
T''	excess temperature	(°C)
T_o	undisturbed ground temperature	(°C)
T_1	scale factor for temperature	(°C)
T^c	temperature in fracture plane	(°C)
T^c_{int}	integral of the temperature over the fracture plane, Eq. (1:4.3)	(m^2°C)
U	solution to Eq. (1:3.14)	(-)
$\vec{v}_f$	filtration velocity	(m/s)
$\vec{v}'_f$	dimensionless filtration velocity	(-)
$\vec{v}^{\,1}_T$	flow field for line heat source, Eq. (2.30)	(-)
$v_a(z')$	Eq. (4.42)	(-)
$v_b(z')$	Eq. (5.33)	(-)
$v_c(z')$	Eq. (5.54)	(-)
v_{f1}	scale factor for filtration velocity	(m/s)
v_c, v_T	dimensionless salt and temperature components of filtration velocity	(-)
V_p	pore volume	$(\mathrm{m}_w^3/\mathrm{m}^3)$
V_p^c	pore volume of fracture zone	$(\mathrm{m}_w^3/\mathrm{m}^2)$
x, y	horizontal coordinates	(m)
x', y'	dimensionless horizontal coordinates	(-)
y_o	distance from heat source to flow plane	(m)
z	vertical coordinate	(m)
$\hat{z}$	vertical unit vector pointing upwards	(-)
z'	dimensionless vertical coordinate	(-)

$z_m(t', z_o)$	particle motion along the z'-axis	(-)
$z'_{max}(z_o)$	maximal dimensionless upward displacement	(-)
$z_{max}(z_o)$	maximal upward displacement	(m)
z_o	dimensionless starting point on the z'-axis	(-)
α_c	relative density increase with salt concentration, Eq. (1:2.30)	$(1/(kg_s/kg_w))$
α_T	thermal expansion coefficient, Eq. (1:2.30)	(1/°C)
$\tilde{\alpha} = \alpha_T / (\alpha_c c_z^o C)$	buoyancy parameter	m^4/J
β_j	fraction of total heat release by component j	(-)
λ	thermal conductivity of the ground	(W/mK)
μ_w	dynamic viscosity of water	(kg/ms)
ρ_w	density of water	(kg/m^3)
$\rho' = c' - T'$	dimensionless excess density	(-)
ρ''	excess water density, Eq. (1:2.26)	(kg/m^3)
ϕ_c	angle between the z-axis and fracture plane	(rad)
ψ	stream function, Eqs. (2.35, 2.37)	(-)
$\nabla = \left(\frac{\partial}{\partial x}, \frac{\partial}{\partial y}, \frac{\partial}{\partial z}\right)$	gradient operator	(m^{-1})
$\nabla' = \left(\frac{\partial}{\partial x'}, \frac{\partial}{\partial y'}, \frac{\partial}{\partial z'}\right)$	dimensionless gradient operator	(-)

Here, m_w^3 denotes cubic meter of water, kg_s kilogram of dissolved salt and kg_w kilogram of water including the dissolved salt. The prime $'$, which denotes dimensionless excess variables, is sometimes suppressed for convenience. In particular, it should be noted that the following variables are *dimensionless*:

$$\tilde{c} \quad P_c \quad P_T \quad v_c \quad v_T \quad z_o \quad z_m(t', z_o)$$

References

1. Claesson, J., 1992, Buoyancy Flow in Fractured Rock with a Salt Gradient in the Groundwater - An initial study, Technical Report 92-05, SKB, Stockholm.

2. Abramowitz, M., I.A. Stegun, 1964, Handbook of Mathematical Functions, National Bureau of Standards, Washington DC. (Dover Paperback, N.Y. 1970). A: Ch. 5, Eq. 5.1.11. B: Ch. 7, Figure 7.2, Table 7.5, Eq. 7.1.17. C: Ch. 7, Eq. 7.1.23.

3. Hodgkinson, D.P., 1980, A Mathematical Model for Hydrothermal Convection around a Radioactive Waste Depository in Hard Rock, Annals of Nuclear Energy, Vol. 7, pp. 313-334, Pergamon Press.

4. Robinson, P.C., 1980, A Mathematical Model of Convection around a Cylindrical Repository, Report, Theoretical Physics Division, Atomic Energy Research Establishment (AERE), Harwell, Didcot, Oxon OX11 ORA, U.S.A.

5. Probert, T., 1993, Buoyancy Flow in Fractured Rock with a Salt Gradient in the Groundwater - Manual for Computer Codes, Dept. Mathematical Physics, Lund University, Sweden.

List of SKB reports

Annual Reports

1977-78
TR 121
KBS Technical Reports 1 – 120
Summaries
Stockholm, May 1979

1979
TR 79-28
The KBS Annual Report 1979
KBS Technical Reports 79-01 – 79-27
Summaries
Stockholm, March 1980

1980
TR 80-26
The KBS Annual Report 1980
KBS Technical Reports 80-01 – 80-25
Summaries
Stockholm, March 1981

1981
TR 81-17
The KBS Annual Report 1981
KBS Technical Reports 81-01 – 81-16
Summaries
Stockholm, April 1982

1982
TR 82-28
The KBS Annual Report 1982
KBS Technical Reports 82-01 – 82-27
Summaries
Stockholm, July 1983

1983
TR 83-77
The KBS Annual Report 1983
KBS Technical Reports 83-01 – 83-76
Summaries
Stockholm, June 1984

1984
TR 85-01
Annual Research and Development Report 1984
Including Summaries of Technical Reports Issued during 1984. (Technical Reports 84-01 – 84-19)
Stockholm, June 1985

1985
TR 85-20
Annual Research and Development Report 1985
Including Summaries of Technical Reports Issued during 1985. (Technical Reports 85-01 – 85-19)
Stockholm, May 1986

1986
TR 86-31
SKB Annual Report 1986
Including Summaries of Technical Reports Issued during 1986
Stockholm, May 1987

1987
TR 87-33
SKB Annual Report 1987
Including Summaries of Technical Reports Issued during 1987
Stockholm, May 1988

1988
TR 88-32
SKB Annual Report 1988
Including Summaries of Technical Reports Issued during 1988
Stockholm, May 1989

1989
TR 89-40
SKB Annual Report 1989
Including Summaries of Technical Reports Issued during 1989
Stockholm, May 1990

1990
TR 90-46
SKB Annual Report 1990
Including Summaries of Technical Reports Issued during 1990
Stockholm, May 1991

1991
TR 91-64
SKB Annual Report 1991
Including Summaries of Technical Reports Issued during 1991
Stockholm, April 1992

Technical Reports
List of SKB Technical Reports 1992

TR 92-01
GEOTAB. Overview
Ebbe Eriksson[1], Bertil Johansson[2], Margareta Gerlach[3], Stefan Magnusson[2], Ann-Chatrin Nilsson[4], Stefan Sehlstedt[3], Tomas Stark[1]
[1]SGAB, [2]ERGODATA AB, [3]MRM Konsult AB
[4]KTH
January 1992

TR 92-02
Sternö study site. Scope of activities and main results
Kaj Ahlbom[1], Jan-Erik Andersson[2], Rune Nordqvist[2], Christer Ljunggren[3], Sven Tirén[2], Clifford Voss[4]
[1]Conterra AB, [2]Geosigma AB, [3]Renco AB,
[4]U.S. Geological Survey
January 1992

TR 92-03
Numerical groundwater flow calculations at the Finnsjön study site – extended regional area
Björn Lindbom, Anders Boghammar
Kemakta Consultants Co, Stockholm
March 1992

TR 92-04
Low temperature creep of copper intended for nuclear waste containers
P J Henderson, J-O Österberg, B Ivarsson
Swedish Institute for Metals Research, Stockholm
March 1992

TR 92-05
Boyancy flow in fractured rock with a salt gradient in the groundwater – An initital study
Johan Claesson
Department of Building Physics, Lund University, Sweden
February 1992

TR 92-06
Characterization of nearfield rock – A basis for comparison of repository concepts
Roland Pusch, Harald Hökmark
Clay Technology AB and Lund University of Technology
December 1991

TR 92-07
Discrete fracture modelling of the Finnsjön rock mass: Phase 2
J E Geier, C-L Axelsson, L Hässler,
A Benabderrahmane
Golden Geosystem AB, Uppsala, Sweden
April 1992

TR 92-08
Statistical inference and comparison of stochastic models for the hydraulic conductivity at the Finnsjön site
Sven Norman
Starprog AB
April 1992

TR 92-09
Description of the transport mechanisms and pathways in the far field of a KBS-3 type repository
Mark Elert[1], Ivars Neretnieks[2], Nils Kjellbert[3], Anders Ström[3]
[1]Kemakta Konsult AB
[2]Royal Institute of Technology
[3]Swedish Nuclear Fuel and Waste Management Co
April 1992

TR 92-10
Description of groundwater chemical data in the SKB database GEOTAB prior to 1990
Sif Laurent[1], Stefan Magnusson[2],
Ann-Chatrin Nilsson[3]
[1]IVL, Stockholm
[2]Ergodata AB, Göteborg
[3]Dept. of Inorg. Chemistry, KTH, Stockholm
April 1992

TR 92-11
Numerical groundwter flow calculations at the Finnsjön study site – the influence of the regional gradient
Björn Lindbom, Anders Boghammar
Kemakta Consultants Co., Stockholm, Sweden
April 1992

TR 92-12
HYDRASTAR – a code for stochastic simulation of groundwater flow
Sven Norman
Abraxas Konsult
May 1992

TR 92-13
Radionuclide solubilities to be used in SKB 91
Jordi Bruno[1], Patrik Sellin[2]
[1]MBT, Barcelona Spain
[2]SKB, Stockholm, Sweden
June 1992

TR 92-14
Numerical calculations on heterogeneity of groundwater flow
Sven Follin
Department of Land and Water Resources, Royal Institute of Technology
June 1992

TR 92-15
Kamlunge study site. Scope of activities and main results
Kaj Ahlbom[1], Jan-Erik Andersson[2], Peter Andersson[2], Thomas Ittner[2], Christer Ljunggren[3], Sven Tirén[2]
[1]Conterra AB
[2]Geosigma AB
[3]Renco AB
May 1992

TR 92-16
Equipment for deployment of canisters with spent nuclear fuel and bentonite buffer in horisontal holes
Vesa Henttonen, Miko Suikki
JP-Engineering Oy, Raisio, Finland
June 1992

TR 92-17
The implication of fractal dimension in hydrogeology and rock mechanics Version 1.1
W Dershowitz[1], K Redus[1], P Wallmann[1], P LaPointe[1], C-L Axelsson[2]
[1]Golder Associates Inc., Seattle, Washington, USA
[2]Golder Associates Geosystem AB, Uppsala, Sweden
February 1992

TR 92-18
Stochastic continuum simulation of mass arrival using a synthetic data set. The effect of hard and soft conditioning
Kung Chen Shan[1], Wen Xian Huan[1], Vladimir Cvetkovic[1], Anders Winberg[2]
[1] Royal Institute of Technology, Stockholm
[2] Conterra AB, Gothenburg
June 1992

TR 92-19
Partitioning and transmutation. A review of the current state of the art
Mats Skålberg, Jan-Olov Liljenzin
Department of Nuclear Chemistry, Chalmers University of Technology
October 1992

TR 92-20
SKB 91
Final disposal of spent nuclear fuel. Importance of the bedrock for safety
SKB
May 1992

TR 92-21
The Protogine Zone. Geology and mobility during the last 1.5 Ga
Per-Gunnar Andréasson, Agnes Rodhe
September 1992

TR 92-22
Klipperås study site. Scope of activities and main results
Kaj Ahlbom[1], Jan-Erik Andersson[2], Peter Andersson[2], Tomas Ittner[2], Christer Ljunggren[3], Sven Tirén[2]
[1]Conterra AB
[2]Geosigma AB
[3]Renco AB
September 1992

TR 92-23
Bedrock stability in Southeastern Sweden. Evidence from fracturing in the Ordovician limestones of Northern Öland
Alan Geoffrey Milnes[1], David G Gee[2]
[1]Geological and Environmental Assessments (GEA), Zürich, Switzerland
[2]Geologiska Institutionen, Lund, Sweden
September 1992

TR 92-24
Plan 92
Costs for management of the radioactive waste from nuclear power production
Swedish Nuclear Fuel and Waste Management Co
June 1992

TR 92-25
Gabbro as a host rock for a nuclear waste repository
Kaj Ahlbom[1], Bengt Leijon[1], Magnus Liedholm[2], John Smellie[1]
[1]Conterra AB
[2]VBB VIAK
September 1992

TR 92-26
Copper canisters for nuclear high level waste disposal. Corrosion aspects
Lars Werme, Patrik Sellin, Nils Kjellbert
Swedish Nuclear Fuel and Waste Management Co, Stockholm, Sweden
October 1992

TR 92-27
Thermo-mechanical FE-analysis of butt-welding of a Cu-Fe canister for spent nuclear fuel
B L Josefson[1], L Karlsson[2], L-E Lindgren[2], M Jonsson[2]
[1]Chalmers University of Technology, Göteborg, Sweden
[2]Division of Computer Aided Design, Luleå University of Technology, Luleå, Sweden
October 1992

TR 92-28
A rock mechanics study of Fracture Zone 2 at the Finnsjön site
Bengt Leijon[1], Christer Ljunggren[2]
[1]Conterra AB
[2]Renco AB
January 1992

TR 92-29
Release calculations in a repository of the very long tunnel type
L Romero, L Moreno, I Neretnieks
Department of Chemical Engineering,
Royal Institute of Technology, Stockholm, Sweden
November 1992

TR 92-30
Interaction between rock, bentonite buffer and canister. FEM calculations of some mechanical effects on the canister in different disposal concepts
Lennart Börgesson
Clay Technology AB, Lund Sweden
July 1992

TR 92-31
The Äspö Hard Rock Laboratory: Final evaluation of the hydrogeochemical pre-investigations in relation to existing geologic and hydraulic conditions
John Smellie[1], Marcus Laaksoharju[2]
[1]Conterra AB, Uppsala, Sweden
[2]GeoPoint AB, Stockholm, Sweden
November 1992

TR 92-32
Äspö Hard Rock Laboratory: Evaluation of the combined longterm pumping and tracer test (LPT2) in borehole KAS06
Ingvar Rhén[1] (ed.), Urban Svensson[2] (ed.), Jan-Erik Andersson[3], Peter Andersson[3], Carl-Olof Eriksson[3], Erik Gustafsson[3], Thomas Ittner[3], Rune Nordqvist[3]
[1]VBB VIAK AB
[2]Computer-aided Fluid Engineering
[3]Geosigma AB
November 1992

TR 92-33
Finnsjö Study site. Scope of activities and main results
Kaj Ahlbom[1], Jan-Erik Andersson[2], Peter Andersson[2], Thomas Ittner[2], Christer Ljunggren[3], Sven Tirén[2]
[1]Conterra AB
[2]Geosigma AB
[3]Renco AB
December 1992

TR 92-34
Sensitivity study of rock mass response to glaciation at Finnsjön, Central Sweden
Jan Israelsson[1], Lars Rosengren[1], Ove Stephansson[2]
[1]Itasca Geomekanik AB, Falun, Sweden
[2]Royal Institute of Technology, Dept. of Engineering Geology, Stockholm, Sweden
November 1992

TR 92-35
Calibration and validation of a stochastic continuum model using the Finnsjön Dipole Tracer Test. A contribution to INTRAVAL Phase 2
Kung Chen Shan[1], Vladimir Cvetkovic[1], Anders Winberg[2]
[1]Royal Institute of Technology, Stockholm
[2]Conterra AB, Göteborg
December 1992

TR 92-36
Numerical simulation of double-packer tests in heterogeneous media
Sven Follin
Department of Engineering Geology, Lund University, Lund, Sweden
December 1992

TR 92-37

Thermodynamic modelling of bentonite-groundwater interaction and implications for near field chemistry in a repository for spent fuel

Hans Wanner, Paul Wersin, Nicolas Sierro
MBT Umwelttechnik AG, Zürich, Switzerland
November 1992

TR 92-38

Climatic changes and uplift patterns – past, present and future

S Björck, N-O Svensson
Department of Quaternary Geology,
University of Lund
November 1992

TR 92-39

Characterization of crystalline rocks in deep boreholes. The Kola, Krivoy Rog and Tyrnauz boreholes

NEDRA
December 1992

TR 92-40

PASS – Project on Alternative Systems Study. Performance assessment of bentonite clay barrier in three repository concepts: VDH, KBS-3 and VLH

Roland Pusch, Lennart Börgesson
Clay Technology AB, Lund
December 1992